SIMPLE MATHEMATICAL MODELS OF SOCIAL BEHAVIOR

A Dissertation

Presented to the Faculty of the Graduate School

of Cornell University

in Partial Fulfillment of the Requirements for the Degree of

Doctor of Philosophy

by

Seth Austin Marvel

May 2011

SIMPLE MATHEMATICAL MODELS

OF SOCIAL BEHAVIOR

Seth Austin Marvel, Ph.D.

Cornell University 2011

We present and analyze minimal models for three social phenomena: the development of two-sided conflicts, interactions between conformists and contrarians, and pair formation between individuals seeking mates. In all three cases, the phenomena can be viewed as processes occurring on the node or edge values of a graph with fixed topology. Together, these three case studies illustrate that mathematical analysis of simple models may give us mechanistic insight into how real social systems behave.

BIOGRAPHICAL SKETCH

Seth Marvel received a Bachelor of Science degree in Chemical Physics from Rice University in 2005. His mathematical coursework included topology, algebra, real and complex analysis, differential equations, differential geometry, combinatorics, and mathematical logic. He graduated with the highest GPA in the Rice Class of 2005. His undergraduate summer appointments had a strong biological component, including research positions at Baylor College of Medicine and the FAS Center for Systems Biology at Harvard University.

Following graduation, he was recruited by Nobel Laureate Richard Smalley to work as a research associate at what is now the Smalley Institute for Nanoscale Science and Technology. There he developed mathematical models and built electronic equipment for the study of dielectric response and dielectrophoretic manipulation of nanotubes. These contributions helped to establish the study of electronic properties of carbon based materials as a core research area in the lab.

In 2006, Seth started his graduate studies at Cornell University as an NSF-IGERT Fellow in Nonlinear Systems. His coursework centered around nonlinear dynamics, networks, probability theory, perturbation, computational methods, and algorithms. In late 2008, he joined an NSF-funded research group led by Steve Strogatz, Kevin Tang and Eric Friedman, which studied dynamics of decentralized networks and peer-to-peer systems using multiscale analytical and computational methods. He also served as an instructor for a course on computer networks and as a session chair for an international conference on mathematical psychology. While at Cornell, he has published in *Physical Review Letters* and *Proceedings of the National Academy of Sciences*, and his research has been featured in *Scientific American* and *The Los Angeles Times*. He currently has an Erdös number of 3.

ACKNOWLEDGEMENTS

It would be an understatement to say that I've written this section several times over. And it would be an overstatement to say that even now I know how I should write it. The simple truth is that there have been a great many people who have done me a great many favors that have allowed me to be where I am now and I will probably never be able to repay or even adequately thank them all. But here I will do my best to show my gratitude for their kindness.

Without question, the single most critical person to my success at Cornell has been Steve Strogatz. Several years before coming to Cornell, I asked for and was given his book *Nonlinear Dynamics and Chaos* as a Christmas present from my parents. I arrived at Cornell a devoted fan of his approach to teaching, but thought it was unlikely that I would have the opportunity to work with him. True to form, he was overwhelmed with interest from other students, and had no openings for the first year and half that I was at Cornell. However he finally agreed to be a member on my special committee, and several months later he took me as his student. Our first project together was on coupled oscillator dynamics; it gave me a foothold as an aspiring researcher and taught me my first lessons about how to publish a scientific paper.

As we waded deeper into research together, he arranged meetings with Jon Kleinberg, and the three of us worked together on systems of structural balance. My meetings with Steve and Jon were invaluable—their conversations gave me an insider's perspective of the academic world and taught me the proper conventions for reporting my work. Steve and Jon also drew many of their friends into our research—Rennie Mirollo, Bobby Kleinberg, Hyunsuk Hong, and others—and these often made fundamental contributions to the problems we were studying.

While we researched together, Steve served as a teacher to me on many levels.

He spent countless hours helping me refine the clarity of my writing, and his candid feedback was invaluable in shaping me into a clearer thinker and communicator. At the same time, he also introduced me to the field of dynamical systems through courses that he taught himself, books and articles he loaned to me, and many meetings with me in his office. I found all of these crucial in learning the subject, and I feel profoundly privileged to have been able to study under his careful guidance.

Combined with this, Steve also gave me the freedom to study many other areas, both inside and outside applied mathematics, even sending me on one occasion to conferences in cognitive science and mathematical psychology because he knew these were areas that interested me. These were gifts of love from a mentor to his student, and I will forever be grateful for his use of academic freedom as a tool for developing me as a scientist. In all, Steve has been to me an incredible teacher, a humbling advocate, and most of all, an unconditional friend. It has been a terrific honor to work with him and call myself his student.

While Steve made significant investments in me, he was not the only one. Jon Kleinberg also gave a great deal of his time and ideas to the projects that we worked on together. He and Bobby Kleinberg made many of the key discoveries, and Jon alone made several critical connections between problems that we faced in our research and existing literature. I am extremely grateful for Jon's involvement as an unofficial co-advisor for much of the time that I was working with Steve, and for his intellectual contributions that went well beyond this co-advising role.

At the same time, there were many others that made contributions that also deserve recognition. For example, Bobby Kleinberg was responsible for a fair amount of the math behind the continuous balance paper, and his help was fundamental in helping us resolve the central problem in an elegant way. It was a pleasure and

joy to work with him as this paper took shape. I also greatly enjoyed meeting Rennie Mirollo on his trip to Ithaca. Through his notes, he taught me much of what I know about Lie group action and provided a great deal of the mathematical material in our paper together on Möbius group action. Additionally, working with Hyunsuk Hong was an uplifting experience. Her creativity for presenting results in the simplest possible way often challenged me to improve my own ways of explaining mathematics, and I greatly appreciated the cheerful spirit that she brought to our collaboration.

While at Cornell, I was exceptionally fortunate to be supported by the main grant (NSF Grant CISE-0835706) of the computational-analytic group headed by Eric Friedman, Kevin Tang, and Steve Strogatz. In our group meetings, Eric and Kevin were warm and encouraging, and their insightful questions and comments often influenced the research course we took moving forward. I also owe Kevin for providing me with a teaching assistantship in Fall 2008, a critical window of time in my graduate career where no other funding seemed to be available. As well as supporting me, this position gave me valuable classroom experience in teaching that was useful when I later was looking for postdoctoral positions.

With respect to the postdoctoral search itself, I am also profoundly indebted to Steve, Jon and Kevin for the innumerable letters that they sent out on my behalf. Their endorsement was of course the reason that I received any offers at all, but I still wish this had not been such a burden on them. There is simply no way that I can thank them enough for what they did.

I am also grateful for the support of David Delchamps for my graduate application years ago when I applied to Cornell. Without his interest, it is hard to say where I would have ended up. Moreover, I was elated that he was willing to serve on my special committee, and I have enjoyed hearing his thoughts and feedback

at the key milestones of my time at Cornell.

Over the years at Cornell, I have come to value the friendship of many of the students in the Center for Applied Mathematics, including especially Tim Novikoff, Joel Nishimura, and Diarmuid Cahalane. We four braved a selection process to determine which students would work with Steve, and oddly the sense of competition drew us closer to each other. I have also enjoyed the friendship of many others, both inside and outside the Center for Applied Math, including (but certainly not limited to) Leif Ristroph, Johan Ugander, Erik Martens, Lauren Childs, Christian Kuehn, Sasha Gutfraind, Philipp Meerkamp, Sam Arbesman, Sharon Gerbode, Bryan Daniels, Dan Romero, June Andrews, Rocio Ruelas, Rachel Ferst, Sarah Iams, Chris Scheper, Scott Clark, Katie Sullivan and Maarika Teose.

Last, but far from least, I would like to thank my parents, Elaine and Steve Marvel. They have shown me unconditional love and encouragement despite the uncertainty in my trajectory, and I am grateful for this beyond what words can express. Their patience as I followed my heart has meant the world to me, and I will treasure their support wherever my scientific curiosity leads.

In humble gratitude,

Seth

TABLE OF CONTENTS

CHAPTER 1

INTRODUCTION

In the following chapters, we study how local behavior relates to global behavior for several models of social behavior. Although we will be focused primarily on mathematical questions, these local-to-global relationships might be useful for experiments and correlative studies on real social systems. In particular, they may be helpful for understanding the mechanisms giving rise to complex observed behaviors that are not easily resolved by traditional statistical techniques.

In addition, from a mathematical perspective, all the models we study take the form of graphs with dynamically changing node or edge attributes. Hence the techniques we use to analyze them may be useful for analyzing other model systems with similar sociological relevance.

More broadly, our research here falls within a growing body of work on the mathematical study of social dynamics. For physicists, a recent review of the relevant physics literature is given by Castellano et al. [13]. For those from other backgrounds, references range from the ground-breaking tome of Wasserman and Faust [82] to smaller and more modern books like *Social Dynamics* by Durlauf and Young [21].

Readers wanting to know more about social networks might take a look at the recent textbooks, *Networks, Crowds, and Markets* by Easley and Kleinberg [25] and *Networks: An Introduction* by Newman [56], although older reviews such as "Exploring complex networks" by Strogatz [71] and "The structure and function of complex networks" by Newman [55] still remain classic reading in the field.

1.1 Two-sided conflict per structural balance theory

We begin our study of social behavior in Chapter 2 with the consideration of two-sided conflicts. In human populations, such conflicts appear in many contexts, including warfare, religious controversies, competition between groups of companies, two-party political systems, and divided juries. One mechanism for the development of these two-faction states is given by a framework from social psychology known as *structural balance theory*. In its mathematical form, as it was first described by Frank Harary, it considers a population coarsely modeled as a signed graph, with positive edges denoting friendly relationships and negative edges denoting unfriendly ones. It starts from the assumption that cycles in the graph with an even number of unfriendly edges are stable in time (or "balanced") whereas cycles with an odd number of unfriendly edges are comparatively short-lived ("unbalanced"). The rationale is essentially an extension of the logic of friendship that "the enemy of my enemy is my friend," "the enemy of my friend is my enemy," and so on.

Harary proved that the nodes of any signed graph containing only balanced cycles can be partitioned into two factions such that all edges between the sides are unfriendly and all edges internal to either side are friendly. These maximally balanced signings may be thought of as the global minima in a landscape of signings of the underlying graph, where landscape elevation (or energy) is identified with the number of unbalanced triangles in the signing. When the underlying graph is complete, this landscape also has metastable states, or *jammed states* as they are called in the literature on structural balance.

In Chapter 2, we find a strict upper bound on the energy of a jammed state. Interestingly, it is easy to show that this strict upper bound is an upper bound

but significantly harder to show that it is strict. The networks that we use to prove the latter—that is the jammed states with the maximum allowed unbalanced triangles—are in fact modified Paley graphs. Additionally, we prove that any signed network can be partitioned into a set of balanced cliques (to be defined later), and we find empirically that commonly encountered jammed states have a relatively small number of such cliques. Finally, we show that the more cliques a jammed state has, the higher is its allowed range of energies.

We then analyze a *continuous* model of structural balance, showing that it is free of the metastable states of the discrete model. Our results for this second model include a closed-form solution of the model system and a proof that initial states drawn from a continuous distribution evolve to a two-faction state with probability one. This proof constitutes the first demonstration in literature than any dynamical system of structural balance actually achieves structural balance.

1.2 Conformists and contrarians per coupled oscillators

In Chapter 3, we consider a coupled oscillator model for how idealized conformists and contrarians in a population may interact. The mathematical structure for this model is reminiscent of the original coupled oscillator model proposed by Yoshiki Kuramoto, which consisted only of a population of free-running phases with all-to-all sinusoidal coupling:

$$\frac{d\phi_j}{dt} = \omega_j + \frac{K}{N}\sum_{k=1}^{N}\sin(\phi_k - \phi_j) \qquad \text{for } j = 1, \ldots, N. \tag{1.1}$$

Here the phase of the kth oscillator is denoted by ϕ_j and its natural frequency by ω_j. N is the number of oscillators, and K is their coupling strength. The ω_j's are generally assumed to be distributed according to a unimodal density $g(\omega)$. The

sine terms drive the system toward synchrony, while the variance in the ω_j's has a desynchronizing effect.

Our work starts with a demonstration that for a particular system involving *identical* coupled oscillators (all ω_j's equal), the N-dimensional phase space can be foliated into three-dimensional leaves. This result resolves several problems that had remained open in the literature on coupled oscillators for over fifteen years. In the course of demonstrating our result, we make an intriguing connection to pure mathematics: under a change of variables, the general equation of motion for identical coupled oscillators can be reexpressed as the group action of the Möbius group, the same group responsible for transformations between circles and lines in the complex plane.

We then move on to consider a simple application of these results to a model of conformists and contrarians (which we assume for simplicity are sinusoidally coupled to each other). In this model, conformists are assigned a positive coupling constant K_1 and contrarians a negative coupling constant K_2. Fixed point and stability analysis of this model suggest (loosely speaking) that when conformists are more intense or more numerous, contrarians generally tend to be more cohesive. Additionally the analysis implies that when the average of all the coupling constants is less than zero, complete asynchrony is stable.

In the final section of Chapter 3, we prove that this condition in fact holds for an *arbitrary* distribution of coupling constants. This may have implications for biological systems that need to remain at least somewhat asychronous for sustainable functioning (e.g. large-scale electical activity in the brain, mating patterns in certain species, mitosis in certain cell populations).

1.3 Pair formation per randomized greedy matching

Finally in Chapter 4, we consider pair formation between adjacent nodes on a network. This has at least one obvious sociological interpretation: monogamous mating. We first look at pair formation along a simple path of n nodes via a randomized selection of edges. The most natural "greedy" algorithms for this leave isolated nodes. A natural question is therefore what is the expected fraction of remaining unpaired nodes (out of n) in the limit of large n?

We discuss the fragmented literature from separate fields on this problem. For example, in computer science, it is known as randomized greedy matching on a path. In physics it is one-dimensional random sequential absorption (or, more exotically, the density of bosons in a TonksGirardeau gas). In material science it is the one-dimensional sphere packing problem or dimer filling on a one-dimensional lattice. We conclude this discussion with a demonstration of the historical result (first given by the Nobel Laureate chemist Paul Flory) that the expected fraction of unpaired nodes is in fact e^{-2}.

We then move on to consider the modestly more realistic case of pair formation on a two-dimensional grid. We start by outlining a new model for matching that handles regular network topologies in a more analytically tractable manner than traditional algorithms. This model also has a new feature inspired by real social systems: it allows for the assignment of a quality factor to each node which influences which matches that node may form.

Our mathematical analysis of this model involves a demonstration that a large number of the interesting quantities of the model can be easily estimated by hand. This has the advantage of simplicity over methods of truncation common in statis-

tical physics literature. We conclude by evaluating the accuracy of our estimates with Monte Carlo simulations, and by proving an upper bound on the grid for the fraction of unpaired nodes obtained by any model of pair formation using only a single quality factor.

CHAPTER 2

TWO-SIDED CONFLICT [1]

In Section 2.1 of this chapter, we model a close-knit community of friends and enemies as a complete graph with positive and negative signs on its edges. A framework from social psychology called *structural balance theory* proposes that certain sign patterns on the graph are more stable than others. This notion of social "balance" allows us to define an energy landscape for such networks. However its structure is complex: numerical experiments reveal a landscape dimpled with local minima at widely varying elevations. We derive rigorous bounds on the energies of these local minima and prove that they have a modular structure that can be used to classify them.

In Section 2.2, we consider a continuous model of structural balance theory given by the dynamical system $\dot{X} = X^2$, where X is a matrix of the friendliness or unfriendliness between pairs of nodes in the network and the overdot represents differentiation by time. Krzysztof Kułakowski, the first to propose this model, performed simulations that suggested only two types of behavior are possible for this system: either all relationships become friendly, or two hostile factions emerge. We prove that for generic initial conditions, these are indeed the only possible outcomes. Our analysis yields a closed-form expression for faction membership as a function of the initial conditions, and implies that the initial amount of friendliness in large social networks (started from random initial conditions) determines whether they will end up in intractable conflict or global harmony.

[1] Much of the material in this chapter is drawn from S. A. Marvel, S. H. Strogatz, and J. M. Kleinberg. Energy landscape of social balance. *Physical Review Letters*, 103:198701, 2009. and S. Marvel, J. M. Kleinberg, R. D. Kleinberg, and S. H. Strogatz. Continuous-time model of structural balance. *Proceedings of the National Academy of Sciences*, 108:1771, 2011.

2.1 Discrete structural balance

The shifting of alliances and rivalries in a social group can be viewed as arising from an energy minimization process. For example, suppose you have two friends who happen to detest each other. The resulting awkwardness often resolves itself in one of two ways: either you drop one of your friends, or they find a way to reconcile. In such scenarios, the overall social stress corresponds to a kind of energy that relaxes over time as relationships switch from hostility to friendship or vice versa.

This notion, now known as balance theory, was first articulated by Heider [38, 39] and has since been applied in fields ranging from anthropology to political science [77, 53]. Cartwright and Harary converted Heider's conceptual framework to a graph-theoretic model and characterized the global minima of the social energy landscape [12]. Their tidy analysis gave no hint that the energy landscape was anything more complicated than a series of equally deep wells, each achieving the minimum possible energy. Recently, however, Antal, Krapivsky and Redner [5] observed that the energy landscape also contains local minima, which they called *jammed states*.

Jammed states are important to understand because they can trap a system as it moves down the energy landscape. Yet little is known about their allowed energies, their structure, or how they depend on the size of the network. Even the maximum possible energy of a jammed state is not obvious: a simple argument (see below) shows that jammed states cannot be located more than halfway up the energy spectrum, but it is hard to see whether this upper bound can be achieved.

In this section we prove that for arbitrarily large networks, there do indeed exist jammed states all the way up to the midpoint energy using a construction based

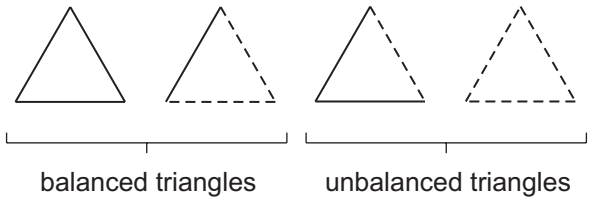

Figure 2.1: Socially balanced and unbalanced configurations of a triangle. Solid edges represent friendly (+) relationships, and dashed edges hostile (−) relationships.

on highly symmetric structures first discovered by Paley in his work on orthogonal matrices [62]. We also show that jammed states have a natural modular structure. This allows us to organize the jammed states encountered by simulation and to explain why high-energy jammed states must be structurally more complex than low-energy ones.

More broadly, our work here is part of a growing line of research that employs tools from physics to analyze models of complex social systems [4, 18, 55]. Theories of signed social networks form an appealing domain for such techniques, as they are naturally cast in the framework of energy minimization.

We begin by modeling a fully connected social network as a signed complete graph on n nodes. Each edge $\{i, j\}$ of the network is labeled with either a plus or minus sign, denoted by s_{ij}, corresponding to feelings of friendship or animosity between the nodes i and j.

Up to node permutation, there are four possible signings of a triangle (Fig. 2.1). We view the two triangles with an odd number of plus edges as balanced configurations, since both satisfy the adages that "the enemy of my enemy is my friend," "the friend of my enemy is my enemy," and so on. Since the two triangles with an even number of plus edges break with this logic of friendship, we consider them

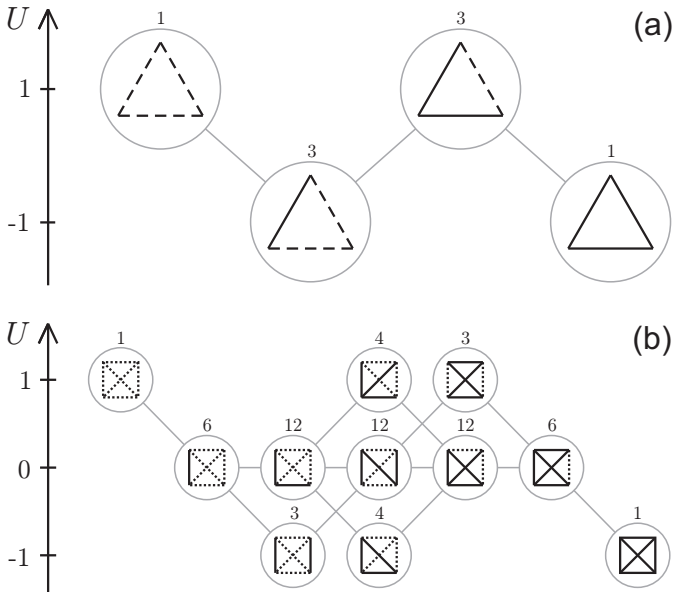

Figure 2.2: The energy landscapes of signed complete social networks on (a) 3 and (b) 4 nodes. For simplicity, each set of sign configurations identical up to node permutation is represented by a single configuration; the number above each configuration indicates its multiplicity. Lines between circles join networks differing by a single sign flip. No jammed states occur for these small networks; they appear only when $n = 6$ or $n \geq 8$. Strict jammed states occur when $n = 9$ and $n \geq 11$ [5].

unbalanced.

The product of the edge signs is positive for a balanced triangle and negative for an unbalanced triangle. If we sum the negative of these products and divide by the total number of triangles, we obtain a quantity U that represents the elevation, or potential energy, of a social network above the domain of all its possible sign configurations (Fig. 2.2). Explicitly,

$$U = -\frac{1}{\binom{n}{3}} \sum s_{ij} s_{jk} s_{ik} \tag{2.1}$$

where the sum is over all triangles $\{i, j, k\}$ of the network.

The configuration in which all node pairs are friends has the lowest possible energy: $U = -1$. Hence, no additional structure is necessary to define the global

minima; they are just the sign configurations for which $U = -1$. Cartwright and Harary [12] identified all such ground states, finding that they consist of two warring factions: internally friendly cliques with only antagonistic edges between them. (The all-friends configuration represents the extreme in which one clique is the empty set.)

To define the concept of a local minimum, however, we need to specify what it means for two states to be adjacent. The most natural choice is to define two sign configurations to be adjacent if each can be reached from the other by a single sign flip. Then a jammed state, as defined by Antal et al., is a sign configuration for which all adjacent sign configurations have higher energy [5]. Here, however, we will slightly vary their terminology by calling this a 'strict jammed state,' reserving the term 'jammed state' for the weaker concept of a sign configuration with no adjacent sign configurations of lower energy.

Our first result is that jammed states cannot have energies above zero. To see this, note that every edge of a jammed state takes part in at least as many balanced triangles as unbalanced triangles. It is therefore found in $(n-2)/2$ unbalanced triangles if n is even and $(n-3)/2$ unbalanced triangles if n is odd. Thus, summing over all edges and dividing by three to avoid triple counting yields $U \leq -\frac{1}{3}\binom{n}{2}\left[\left(n-2-\frac{n-2}{2}\right)-\frac{n-2}{2}\right]/\binom{n}{3} = 0$ if n is even and $U \leq -(n-2)^{-1}$ if n is odd.

Are there jammed states that achieve this upper bound on U? One possible way to address this question is through computational searches. For example, suppose that from a random initial configuration, we select and switch single signs uniformly at random from the set of unbalanced edges (an edge is defined as unbalanced if more than half the triangles that include it are unbalanced). We continue switching

signs until the network reaches a local minimum of U. Extensive searches of this form reveal only two small examples of zero-energy jammed states: a configuration on 6 nodes, consisting of a 5-cycle of positive edges and all other edges negative, and a more complex configuration on 10 nodes. Even on 10 nodes, only about 7 in 10^8 searches end up at zero-energy jammed states, and no such states were found on larger numbers of nodes. The failure of this approach to produce even moderately-sized examples is consistent with findings of Antal et al. [5], who showed that such local search methods reach jammed states with a probability that decreases to 0 extremely rapidly as a function of the network size n.

With only these data, the chances of finding a larger collection of jammed states at $U = 0$ may seem slim. However, we now show how an infinite collection of zero-energy jammed states can be identified through a direct combinatorial construction. This construction is motivated by the two small examples found through computational searches: when we re-examined the zero-energy jammed states on 6 and 10 nodes, we noticed that the positive edges formed so-called Paley graphs [10] on 5 and 9 nodes. This beautiful connection turns out to be general: a family of arbitrarily large jammed states with $U = 0$ may be derived from the undirected Paley graphs.

Briefly, an undirected Paley graph P_q can be constructed on a set of q nodes, where q is a prime of the form $q = 4k+1$ for some integer k. To do so, we index the nodes with the integers $0, \ldots, q-1$ and then connect each v and w in this node set with an edge if there is an x in $\{0, \ldots, q-1\}$ such that $(v - w) \bmod q = x^2 \bmod q$. To construct the jammed state with $U = 0$ from P_q, we give plus signs to the edges of P_q and minus signs to the edges of its complement. We then add a node v_n, where $n = q + 1$, and link it to all nodes of P_q with negative edges. (Paley graphs

also exist if q is a prime power, but then one needs to work over the finite field of order q.)

We now show that this new signed complete graph has zero energy. Clearly, this is equivalent to the condition that each edge is in exactly $\frac{n-2}{2}$ balanced triangles. To check the latter claim, we make use of two known properties of Paley graphs: (i) P_q is $2k$-regular, and (ii) for any two nodes v and w of P_q, there are k nodes adjacent to v but not w, and k nodes adjacent to w but not v [10].

Now, if $\{v, w\}$ is a negative edge in P_q, then it forms balanced triangles with all nodes x in P_q that are linked by a positive edge to exactly one of v or w. By property (ii), there are $2k = \frac{q-1}{2} = \frac{n-2}{2}$ such nodes, so $\{v, w\}$ is in exactly $\frac{n-2}{2}$ balanced triangles. Similarly, if $\{v, w\}$ is a positive edge in P_q, then it forms unbalanced triangles with all nodes x of P_q that are linked via a positive edge to exactly one of v or w. Again, these nodes account for $2k = \frac{n-2}{2}$ unbalanced triangles, so $\{v, w\}$ is in exactly $\frac{n-2}{2}$ balanced triangles. Finally, since P_q is $2k$-regular, there are exactly $2k$ nodes in P_q adjacent via positive edges to each node w of P_q. Hence, each negative edge $\{v_n, w\}$ is also in exactly $\frac{n-2}{2}$ balanced triangles.

The above construction is related to a result by Seidel regarding two-graphs [68]. Using the theory of two-graphs, one can also construct infinite families of strict jammed states that approach $U = 0$ from below as n grows large. Such constructions can be carried out using bilinear forms modulo 2 [68], and projective planes in finite vector spaces [76].

Given the conceptual complexity of these constructions of high-energy jammed states, and the computational difficulty in finding such states via search, it is natural to ask why it is harder to construct jammed states closer to $U = 0$ than at

lower energies. We now explain this by formulating a measure of the complexity of different jammed states. This will establish a precise sense in which higher-energy jammed states are structurally more complex than lower-energy jammed states, through a result showing that every signed complete graph has a natural decomposition into internally balanced modules.

The statement of this *edge balance decomposition* is as follows. Consider the subgraph K consisting of all nodes in the network, together with those edges that appear only in balanced triangles. Then (i) K is a union of disjoint cliques $\{C_a\}$ (possibly including single-node cliques), and (ii) for every pair of cliques C_a and C_b, every edge between C_a and C_b is involved in the same number of balanced triangles. In the spirit of (i), we call each clique of the partition a *balanced clique*.

To prove part (i) of the decomposition, one can show that if some connected component of K is not a clique, then this component contains edges $\{i, j\}$ and $\{i, k\}$ sharing a node i that are both found only in balanced triangles, and such that $\{j, k\}$ is in at least one unbalanced triangle (involving a fourth node ℓ). But then the set of four nodes $\{i, j, k, \ell\}$ would have three of its four triangles balanced, which is not possible for any sign pattern.

To prove part (ii) of the decomposition, one can show that if there were cliques C_a and C_b such that two different edges between them were involved in different numbers of unbalanced triangles, then there would be two such edges $\{i, j\}$ and $\{i, k\}$ sharing a node i in C_a, such that for some other node ℓ, the triangle $\{i, j, \ell\}$ is balanced but the triangle $\{i, k, \ell\}$ is not. But since $\{j, k\}$ is inside the clique C_b, all the triangles involving it are balanced, and so the four-node set $\{i, j, k, \ell\}$ would have three of its four triangles balanced, which again is not possible for any sign pattern.

We now return to the question that we posed above: why is it harder to construct jammed states near $U = 0$ than at substantially lower energies? We can close in on an elementary answer by computing an upper bound on the allowed energy of a jammed state as a function of the number of balanced cliques it contains. We find that as the energy approaches $U = 0$ from below, the number of cliques in the decomposition must grow unboundedly in n, the number of nodes in the network.

First observe that for a fixed number of balanced cliques m, the fewest number of edges are in balanced cliques—and hence the most edges are available for inclusion in unbalanced triangles—when the n nodes of the network are equally distributed among the m balanced cliques. We can verify this using Lagrange multipliers: we seek to minimize $\sum_i \binom{c_i}{2}$ relative to the constraints $\sum_i c_i = n$, $c_i > 0$, where c_i is the number of nodes in the ith balanced clique. This implies $\frac{d}{dc_i}\binom{c_i}{2} = \lambda$ for all c_i, where λ is some constant. The derivative of the gamma function extension of $\binom{c_i}{2}$ is monotone increasing on $c_i > 0$, so we invert it to find all c_i equal to the same function of λ.

Hence, no jammed state with n nodes and m balanced cliques can have greater energy than one in which the nodes are equidistributed among the balanced cliques and each edge spanning two balanced cliques participates in $\frac{n-2}{2}$ unbalanced triangles. This implies an upper bound on U of

$$U_n^{UB}(m) = -1 + 2\frac{\frac{1}{3}\binom{m}{2}(\frac{n}{m})^2\frac{n-2}{2}}{\binom{n}{3}} = -\frac{n-m}{m(n-1)}. \tag{2.2}$$

For example, $\lim_{n\to\infty} U_n^{UB}(3) = -1/3$, whereas the corresponding tight upper bound (also verified by Lagrange multipliers) is $\lim_{n\to\infty} U = -\lim_{n\to\infty}[(\binom{n}{2} - (\frac{n}{3})^3) - (\frac{n}{3})^3]/\binom{n}{3} = -5/9$.

We can see directly from Eq. (2.2) that as we approach $U = 0$ from below,

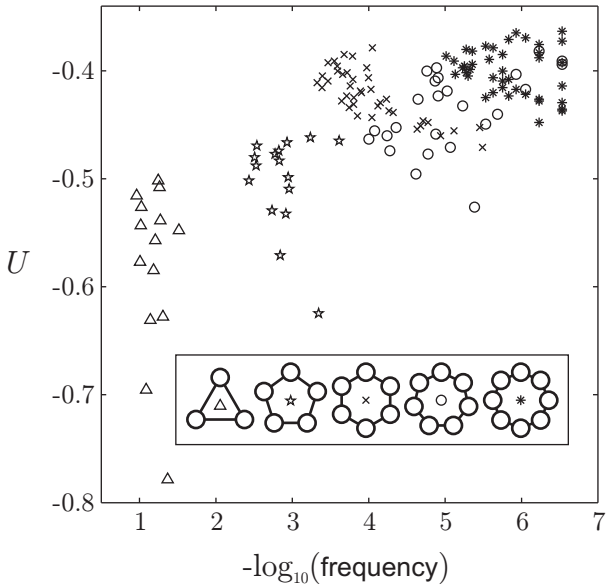

Figure 2.3: Jammed states for networks with $n = 26$ nodes, distinguished according to their energy, frequency of occurrence, and clique structure. The different data symbols show the number of balanced cliques in a given state (see inset for key). We find that jammed states with higher energies are not only rarer (as shown by Antal et al. [5]), but also more structurally complex, as measured by their number of balanced cliques. To find these states, we evolved 10^8 social networks to energy minima via the Markov process described in the text, assuming that each edge was initially unfriendly. For simplicity, only jammed states with eight or fewer balanced cliques are shown (these comprised $> 99.99\%$ of all jammed states found). Jammed states with two and four balanced cliques are impossible. Analogous distributions for other n and other initial sign patterns are similar, and increasing the number of trial networks does not significantly change the distribution.

jammed states with n nodes and m or fewer balanced cliques no longer appear above $U_n^{UB}(m)$. In other words, jammed states disappear as the energy is raised in order of least to greatest complexity. Finally, at $U = 0$, the condition $U_n^{UB}(m) = 0$ implies that $m = n$, as we would expect since every edge must be in exactly $\frac{n-2}{2}$ balanced triangles.

In addition to illuminating a fundamental progression within the energy spectrum of the jammed states, the edge balance decomposition also provides a partition of the set of $2^{\binom{n}{2}}$ possible sign configurations which proves useful for classi-

fying jammed states. Consistent with Antal et al. [5], our numerical simulations of small networks (generally $n < 2^{10}$) turned up an enormous number of three-clique jammed states. Less frequently, we encountered jammed states with five, six and seven cliques, and rarely did we find jammed states with more than seven cliques (Fig. 2.3). This numerical evidence leads us to suspect that the most common jammed states found in sign patterns arising from local search have only a few balanced cliques and hence would be easily classified by the edge balance decomposition. (That said, it is possible to *construct* strict jammed states with m balanced cliques for all odd m in the large-n limit; whether such a construction exists for even $m > 6$ remains open.)

In future work, it could be interesting to explore the model above using tools from other parts of physics, such as spin glasses [29, 16], generalized Ising models [85], and Z_2 gauge theories [28]. For example, the social balance model that we've considered here may be viewed as a generalized Ising model [85, 28] on the complete graph, and is similar to spin-glass models [29] where nodes in a network are likewise joined by edges of mixed signs, and U measures the average frustration of the system. This line of work includes results on spin-glass systems with three-way interactions [31], such as occur in Eq. (2.1). One potential obstacle to making this link is that in spin-glass models, adjacency between configurations is defined by changes in the signs of nodes (due to spin flips) while edge signs remain fixed; whereas here it is the signs of edges that vary as one moves across the landscape. This could possibly be addressed using transformations that interchange the roles of nodes and edges; however, when the complete graph is transformed in this way, the resulting network has a complex structure that may render analysis difficult.

Taken together, the results presented here yield a first look at the energy land-

scape for completely connected social networks in which opportunities for greater relational consistency and cooperation are the driving forces for change. For now, our understanding of the landscape is confined to a few results about its local and global minima. The challenge for the future is to understand its large-scale structure, perhaps even including a characterization of the pathways leading out of the deepest minima—those corresponding to the most entrenched conflict—and toward states of reconciliation.

2.2 Continuous structural balance

The dynamical system that we want to study in this section is best understood as an outgrowth of structural balance theory [82]. So let's begin with a brief review of what this theory says.

Consider three individuals: Anna, Bill and Carl, and suppose that Bill and Carl are friends with Anna, but are unfriendly with each other. If the sentiment in the relationships is strong enough, Bill may try to strengthen his friendship with Anna by encouraging her to turn against Carl, and Carl might likewise try to convince Anna to terminate her friendship with Bill. Anna, for her own part, may try to bring Bill and Carl together so they can reconcile and become friends. In abstract terms, relationship triangles containing exactly two friendships are prone to transition to triangles with either one or three friendships.

Alternately, suppose that Anna, Bill and Carl all view each other as rivals. In many such situations, there are incentives for the two people in the weakest rivalry to cooperate and form a working friendship or alliance against the third. In these cases, a single friendship may be prone to appear in a relationship triangle that

initially has none.

These two thought experiments suggest a notion of stability, or balance, that can be traced back to the work of Heider [38]. Heider's theory was expanded into a graph-theoretic framework by Cartwright and Harary [12], who considered graphs on n nodes (representing people, countries or corporations) with edges signed either positive ($+$) to denote friendship or negative ($-$) to denote rivalry. If a social network feels the proper social stresses (those felt by Anna, Bill and Carl in the examples above), then Cartwright and Harary's theory predicts that in steady state the triangles in the graph should contain an odd number of positive edges—in other words, three positive edges or one positive edge and two negative edges. We refer to such triangles as *balanced*, and triangles with an even number of positive edges as *unbalanced*. Finally, we call a graph *complete* if it contains edges between all pairs of nodes, and we say that a complete graph with signs on its edges is *balanced* if all its triangles are balanced. (All graphs in this chapter will be complete.)

As it turns out, these local notions of balance theory are closely related to the global structure of two opposing factions. In particular, suppose that the nodes of a complete graph are partitioned into two factions such that all edges inside each faction are positive and all edges between nodes in opposite factions are negative. (One of these factions may be empty, in which case the other faction includes all the nodes in the graph, and consequently all edges of the network are positive.) Note that this network must be balanced, since each triangle either has all three members in the same faction (yielding three positive edges) or has two members in one faction and the third member in the other faction (yielding one positive edge and two negative ones). In fact, a stronger and less obvious statement is

true: any balanced graph can be partitioned into two factions in this way, with one faction possibly empty [12]. As a result, when we speak of balanced graphs, we can equivalently speak of networks with this type of two-faction structure.

Structural balance is a static theory—it posits what a "stable" signing of a social network should look like. However its underlying motivation is dynamic, based on how unbalanced triangles ought to resolve to balanced ones. This situation has led naturally to a search for a full dynamic theory of structural balance. Yet finding systems that reliably guide networks to balance has proved a challenge in itself.

A first exploration of this issue was conducted by Antal et al. [5] who considered a family of discrete-time models. In one of the main models of this family, an edge of the graph is examined in each time step, and its sign is flipped if this produces more balanced triangles than unbalanced ones. While a balanced graph is a stable point for these discrete dynamics, it turns out that many unbalanced graphs called *jammed states* are as well [5, 50].

Thus, the natural problem became to identify and rigorously analyze a simple system that could progress to balanced graphs from generic initial configurations. A novel approach to this problem was taken by Kułakowski, Gawroński, and Gronek [45], who proposed a continuous-time model for structural balance. They represented the state of a completely connected social network using a real symmetric $n \times n$ matrix X whose entry x_{ij} represents the strength of the friendliness or unfriendliness between nodes i and j (a positive value denotes a friendly relationship and a negative value an unfriendly one). Note that for a given X, there is a signed complete graph with edge signs equal to the signs of the corresponding elements x_{ij} in X. We will call X balanced if this associated signed complete graph

is balanced.

Kułakowski et al. considered variations on the following basic differential equation, which they proposed as a dynamical system governing the evolution of the relationships over time:

$$\frac{dX}{dt} = X^2. \tag{2.3}$$

Remarkably, simulations showed that for essentially any initial $X(0)$, the system reached a balanced pattern of edge signs in finite time.

Writing Eq. (2.3) directly in terms of the entries x_{ij} gives a sense for why this differential equation should promote balance:

$$\frac{dx_{ij}}{dt} = \sum_k x_{ik}x_{kj}. \tag{2.4}$$

Notice that x_{ij} is being pushed in a positive or negative direction based on the relationships that i and j have with k: if x_{ik} and x_{kj} have the same sign, their product guides the value of x_{ij} in the positive direction, while if x_{ik} and x_{kj} have opposite signs, their product guides the value of x_{ij} in the negative direction. In each case, this is the direction required to balance the triangle $\{i, j, k\}$. Note also that Eq. (2.4) applies for the case that $i = j$. While this case is harder to interpret, the monotonic increase of x_{ii} implied by Eq. (2.4) might be viewed in psychological terms as an increase of self-approval or self-confidence as i becomes more resolute in its opinions about others in the network.

For a network with just three nodes, it can be easily proved that a variant of these dynamics generically balances the single triangle in this network; such a

three-node analysis has been given by Kułakowski et al. [45], and we describe a short proof in Appendix A. What is much less clear, however, is how the system should behave with a larger number of nodes, when the effects governing any one edge $\{i, j\}$ are summed over all nodes k to produce a single aggregate effect on x_{ij}.

It has therefore been an open problem to prove that Eq. (2.4) or any of the related systems studied by Kułakowski et al. will bring a generic initial matrix $X(0)$ to a balanced state. It has also been an open problem to characterize the structure of the balanced state that arises as a function of the starting state $X(0)$.

We resolve these two open problems. We first show that for a random initial matrix (drawn from any absolutely continuous distribution), the system reaches a balanced matrix in finite time with a probability converging to 1 in the number of nodes n. In addition, we provide a closed-form expression for this balanced matrix in terms of the initial one; essentially, we discover that the system of differential equations serves to "collapse" the starting matrix to a nearby rank-one matrix. We also characterize additional aspects of the process, giving for example a description of an "exceptional" set of matrices of probability measure converging to 0 in n for which the dynamics are not necessarily guaranteed to produce a balanced state.

We then analyze the solutions of the system for classes of random matrices in the large-n limit—in particular, we consider the case in which each unique matrix entry is drawn independently from a distribution with bounded support that is symmetric about a number μ (the mean value of the initial friendliness among the nodes). In this case, we find a transition in the solution as μ varies: when $\mu > 0$, the system evolves to an all-positive sign pattern, whereas when $\mu \leq 0$, the system evolves to a state in which the network is divided evenly into two all-positive cliques connected entirely by negative edges. We end by discussing some implications of

the model and the associated transition between harmony and conflict, including an evaluation of the model on empirical data and some potential connections to research on reconciliation in social psychology.

Behavior of the Model: Evolution to a Balanced State

Suppose we randomly select the $x_{ij}(0)$'s from a continuous distribution on the real line. Then the $x_{ij}(t)$'s found by numerical integration generally sort themselves in finite time into the sign pattern of two feuding factions. To reformulate this observation as a precise statement and explain why the behavior holds so pervasively, we now solve Eq. (2.3) explicitly.

Solution to the model. The initial matrix $X(0)$ is real and symmetric by assumption, so we can write it as $QD(0)Q^T$ where $D(0)$ is the diagonal matrix with the eigenvalues of $X(0)$, denoted $\lambda_1 \geq \lambda_2 \geq \cdots \geq \lambda_n$, as diagonal entries ordered from largest to smallest, and Q is the orthogonal matrix with the corresponding eigenvectors of $X(0)$, denoted $\omega_1, \omega_2, \ldots, \omega_n$, as columns. The superscript T signifies transposition.

The differential equation Eq. (2.3) is a special case of a general family of equations known as *matrix Riccati equations* [2]. The analysis of the full family is complicated and not fully resolved, but we now show that the special case of concern to us, Eq. (2.3), has an explicit solution with a form that exposes its connections to structural balance. We proceed as follows. First, we observe that by separation of variables, the solution of the single-variable differential equation $\dot{x} = x^2$ (overdot representing differentiation by time) with initial condition $x(0) = \lambda_k$ is

$$\ell_k(t) = \frac{\lambda_k}{1 - \lambda_k t}. \tag{2.5}$$

Therefore the diagonal matrix $D(t) = \text{diag}(\ell_1(t), \ell_2(t), \ldots, \ell_n(t))$ is the solution of Eq. (2.3) for the initial condition $X(0) = \text{diag}(\lambda_1, \lambda_2, \ldots, \lambda_n)$.

Moreover $Y(t) = QD(t)Q^T$ is also a solution of Eq. (2.3) since $\dot{Y} = Q\dot{D}Q^T = Q(D^2)Q^T = (QDQ^T)^2 = Y^2$. But $Y(t)$ has the same initial condition as $X(t)$ in our original problem: $Y(0) = QD(0)Q^T = X(0)$. So by uniqueness, $Y(t) = QD(t)Q^T$ must be the solution we seek.

Our solution $X(t)$ can also be written in a different way to mimic the solution of the one-dimensional equation $\dot{x} = x^2$. Since $x_{ij}(t) = \sum_{k=1}^n q_{ik}\ell_k(t)q_{jk}$, where q_{ij} is the (i,j)th entry of Q, we can expand the denominators of the $\ell_k(t)$ functions in powers of t to rewrite $X(t)$ as $X(0) + X(0)^2 t + X(0)^3 t^2 + \cdots$, or more concisely,

$$X(t) = X(0)[I - tX(0)]^{-1}. \tag{2.6}$$

(Note that the matrices $X(0)$ and $[I - X(0)t]^{-1}$ commute.) This equation is valid when t is less than the radius of convergence of every λ_k, that is when $t < 1/\lambda_1$ (assuming $\lambda_1 > 0$).

Finally we note that the above method of solving Eq. (2.3) contains a reduction of the number of dynamical variables of the system from $\binom{n+1}{2}$ to n. The $\binom{n}{2}$ constants of motion generated by this reduction are just the off-diagonal elements of $Q^T X(t) Q = D(t)$, or $\sum_{k=1}^n \sum_{\ell=1}^n q_{ki} x_{k\ell}(t) q_{\ell j} = 0$ for all $1 \le i < j \le n$. Furthermore, the procedure for reducing $X(t)$ can be easily generalized to any system of the form $\dot{X} = f(X)$ where f is a polynomial of X.

Behavior of the solution. Let's now examine the behavior of our solution $X(t)$ to see why in the typical case it splits into two factions in finite time. It turns out that this is the guaranteed outcome if the following three conditions hold (and as we will see below, they hold with probability converging to 1 as n goes to infinity):

1. $\lambda_1 > 0$,
2. $\lambda_1 \neq \lambda_2$ (and hence $\lambda_1 > \lambda_2$), and
3. all components of ω_1 are nonzero.

To see why these conditions imply a split into two factions, observe from Eq. (2.5) that each $\ell_k(t)$ diverges to infinity at $t = 1/\lambda_k$. Since $x_{ij}(t) = \sum_{k=1}^{n} q_{ik}\ell_k(t)q_{jk}$, all x_{ij}'s diverge to infinity when the ℓ_k with the smallest positive $1/\lambda_k$ does. Under the first and second conditions, this ℓ_k is ℓ_1, so the blow-up time t^* of Eq. (2.3) must be $1/\lambda_1$. To show that the nodes are partitioned into two factions as $X(t)$ approaches t^*, let $\overline{X}(t) = X(t)/||X(t)||$ on the half-open interval $[0, t^*)$, where $||X(t)||$ denotes the Frobenius norm of X. The matrix $\overline{X}(t)$ has the sign pattern of $X(t)$, and as t approaches t^* it converges to the rank-one matrix

$$X^* = Q \operatorname{diag}(1, 0, 0, \ldots, 0)\, Q^T = \omega_1 \omega_1^T. \tag{2.7}$$

Now let ω_{1k} denote the value of the kth coordinate of ω_1, and let $S = \{k : \omega_{1k} > 0\}$ and $T = \{k : \omega_{1k} < 0\}$. Then S and T partition the node indices $1, 2, \ldots, n$ by our condition that ω_1 has no zero components. From Eq. (2.7), this partition must correspond to two cliques of friends joined by a complete bipartite graph of unfriendly ties.

The three conditions. We now return to the three conditions above. We first show that the second and third hold with probability 1. We then show that the first condition holds with probability converging to 1 as n goes to infinity. Lastly, we analyze the behavior of the system in the unlikely event that the first condition does not hold. The fact that the conjunction of all three conditions holds with probability converging to 1 as n grows large justifies our earlier claim that the behavior described above holds for almost all choices of initial conditions.

First we show why the second and third conditions hold with probability 1 so long as the (joint) distribution from which $X(0)$ is drawn is absolutely continuous with respect to Lebesgue measure—in other words, assigns probability zero to any set of matrices whose Lebesgue measure is zero. Our arguments below make use of the following two basic facts:

i. the set of zeros of a nontrivial multivariate polynomial has Lebesgue measure zero, and

ii. the existence of a common root of two univariate polynomials P and Q is equivalent to the vanishing of a multivariate polynomial in the coefficients of P and Q (specifically, it is equivalent to the vanishing of the determinant of the Sylvester matrix of P and Q, also called the *resultant* of P and Q).

To show that $\lambda_1 \neq \lambda_2$ with probability 1, let P denote the characteristic polynomial of $X(0)$, and let Q denote the derivative of P. Then $X(0)$ has a repeated eigenvalue if and only if P has a repeated root, which it does if and only if P and Q have a common root. This condition is equivalent to the vanishing of the resultant of P and Q, which is a multivariate polynomial in the entries of $X(0)$. The polynomial cannot be zero everywhere, because there is at least one symmetric

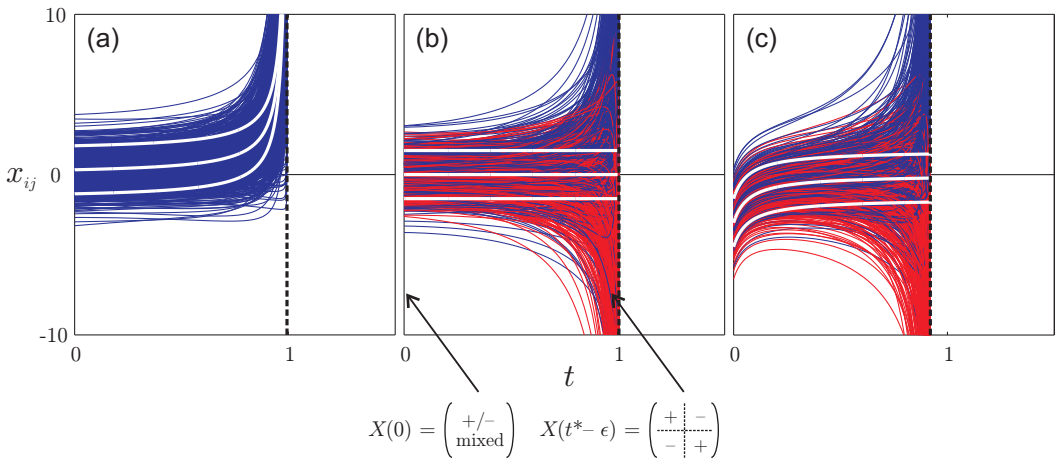

Figure 2.4: Representative large-n plots of the model for (a) $\mu > 0$ ($\mu = 3/10$ in the plot shown), (b) $\mu = 0$, and (c) $\mu < 0$ ($\mu = -3$ in the plot shown). For all three plots, $\sigma = 1$ and $n = 90$. To reduce image complexity, only one randomly sampled fifth of the trajectories is included. In the second plot, t^* denotes the time at which the system diverges, and ϵ denotes a sufficiently small displacement. The white curves superimposed on the three plots are the large-n trajectories $x_{ij}(t) = x_{ij}(0) - \mu + \mu/(1 - \mu nct)$ for $x_{ij}(0) = \mu, \mu \pm 3\sigma/2$, where c represents a rescaling of time. Since we want to fix the blow-up time t^* near 1 and since $ct^* = 1/\lambda_1$ as found in the text, we choose $c = 1/(\mu n + \nu - \mu + \sigma^2/\mu)$ for (a) and $c = 1/(2\sigma\sqrt{n})$ for (b) and (c) using estimates of λ_1 taken from Ref. [32]. The black dotted lines mark the blow-up times $t^* = 1/(c\lambda_1)$.

matrix that does not have a repeated eigenvalue. So the set of matrices having a repeated eigenvalue has Lebesgue measure zero.

Similarly, to show that all components of ω_1 are nonzero, let P denote the characteristic polynomial of $X(0)$ and P_i the characteristic polynomial of the $(n-1) \times (n-1)$ submatrix $X_i(0)$ obtained by deleting the ith row and ith column of $X(0)$. It is easy to check that if any eigenvector of $X(0)$ has a zero in its ith component, then the vector obtained by deleting that component is an eigenvector of $X_i(0)$ with the same eigenvalue. Consequently, P and P_i must have a common root, implying that the resultant of P and P_i vanishes. This resultant is once again a multivariate polynomial in the entries of $X(0)$, and once again it must be nonzero somewhere because there is at least one symmetric matrix whose eigenvectors all

have nonzero entries. Hence, the set of matrices having an eigenvector with zero in its ith component has Lebesgue measure zero.

Finally, to determine the likelihood of the first condition, we first must say a bit more about the way that $X(0)$ is selected. Suppose that the off-diagonal $x_{ij}(0)$'s are drawn randomly from a common distribution F and the on-diagonal $x_{ii}(0)$'s are drawn randomly from a common distribution G. All selections are independent for $i \leq j$. (For $i > j$, we let $x_{ij}(0) = x_{ji}(0)$, so that $X(0)$ is symmetric.) For this construction of $X(0)$, Arnold [6] has shown that with the remarkably weak additional assumption that F has a finite second moment, Wigner's semicircle law holds in probability as n grows to infinity. This in turn implies that $\lambda_1 > 0$ in probability in the same limit.

Moreover, suppose we are in the low-probability case that $\lambda_1 \leq 0$. In this case, the analysis above shows that all the functions $\ell_i(t)$ converge to 0 as $t \to \infty$. Thus, $\lim_{t\to\infty} D(t) = 0$, and since $X(t) = QD(t)Q^T$, we also have $\lim_{t\to\infty} X(t) = 0$.

Although the entries of $X(t)$ converge to zero when $\lambda_1 \leq 0$, one might still want to know if the sign pattern of $X(t)$ is eventually constant (i.e., remains unchanged for all t above some threshold value) and, if so, what determines this sign pattern. It is possible to answer this question, again assuming the second and third conditions. By expanding the function $\ell_i(t) = \lambda_i/(1 - \lambda_i t)$ in powers of $u = 1/t$, we obtain the asymptotic series

$$\ell_i(t) = -u - u^2\lambda_i^{-1} - O(u^3), \tag{2.8}$$

which implies

$$X(t) = QD(t)Q^T = -uI - u^2X(0)^{-1} - O(u^3). \tag{2.9}$$

In the limit of small u, the leading order term of the diagonal entries of $X(t)$ is the linear term, which has negative sign. For the off-diagonal entries of $X(t)$, the leading-order term as u tends to zero is the quadratic term, whose sign matches the sign of the corresponding off-diagonal entry of the matrix $-X(0)^{-1}$.

Behavior of the Model: From Factions to Unification

The analysis in the previous subsection tells us how to find both the blow-up time t^* and final sign configuration of a network if we know its initial state $X(0)$. However we might also want to know whether we can characterize the behavior of $X(t)$ in the large-n limit in terms of statistical parameters of $X(0)$. This could, for example, help us forecast the behavior of groups of individuals when collecting complete relationship-level data is not feasible. Clearly if the underlying network is a complete graph, it is not realistic to consider n that are too large, but we find fortunately in simulations that the asymptotic behavior we will derive in this section becomes apparent even for moderate values of n (less than 100). As a result, these large-n results are perhaps most usefully viewed as an approximate guide to what happens in medium-sized groups that are large enough to show predictable collective behavior but for which a completely connected set of relationships is still feasible to maintain.

In this section, we show that there is a transition from final states consisting of two factions to final states consisting of all positive relations as the "mean friendliness" of $X(0)$ (the mean of the distributions used to generate the off-diagonal

entries of $X(0)$) is increased from negative to positive values. This is consistent with the numerical simulations shown in Fig. 2.4; as noted above, the asymptotic behavior we are studying is already clear in these simulations, which are performed for $n = 90$.

Before discussing the details, we describe how $X(0)$ is selected in this section. We start by adopting the procedure of Füredi and Komlós [32]: the elements $x_{ij}(0)$ are drawn independently from distributions F_{ij} with zero mass outside of $[-K, K]$. The off-diagonal F_{ij}'s have a common expectation μ and finite variance σ^2, while the on-diagonal F_{ii}'s have a common expectation ν and variance τ^2. In addition, we require that each off-diagonal distribution F_{ij} be symmetric about μ. Random matrix models of this type have attracted considerable recent interest (see e.g. Refs. [81, 75]), but we need only the basic results of Füredi and Komlós [32] for our purposes, and so we use these in the development below. We consider the three cases of positive, zero and negative μ.

Case 1: $\mu > 0$**.** The results of Füredi and Komlós [32] show that when $\mu > 0$, the deviation of ω_1 from $(1, 1, \ldots, 1)/\sqrt{n}$ vanishes in probability in the large-n limit. Hence the final state of the system consists of one large clique of friends containing all but at most a vanishing fraction of the nodes. Moreover, by assuming a bound on σ we can strengthen this statement further: if $\sigma < \mu/2$, then the findings of Füredi and Komlós imply that the final state consists of a single clique of friends, with no negative edges. These observations are consistent with the representative numerical trial shown in Fig. 2.4a. Moreover, Füredi and Komlós show that the asymptotic behavior of λ_1 grows like $\mu n + O(1)$, and hence the blow-up time scales like $1/(\mu n)$.

We can gain insight into the behavior of the system for small t using an informal Taylor series calculation: if we rescale time in Eq. (2.3) by inserting a $1/n$ before the summation, compute the Taylor expansion of $x_{ij}(t)$ term-by-term and then take the expectation of each term, we obtain the geometric series $x(t) = \mu + \mu^2 t + \mu^3 t^2 + \cdots$, or

$$x(t) = \frac{\mu}{1 - \mu t}. \tag{2.10}$$

With significantly more work, it can be proved that every trajectory $x_{ij}(t)$ has this time dependence on $[0, 1/K)$ in the large-n limit with probability 1 (see Appendix A), so we may write

$$\lim_{n\to\infty} x_{ij}(t) = x_{ij}(0) - \mu + \frac{\mu}{1 - \mu t} \quad \text{with prob. 1} \tag{2.11}$$

for all t in $[0, 1/K)$. Observe that this limit has a blow-up time t^* of $1/\mu$. Since our rescaling of time represents a zooming in or magnification of time by a factor of n, this t^* corresponds to a blow-up time asymptotic to $1/(\mu n)$ for the unrescaled system, consistent with the results of Füredi and Komlós.

Case 2: $\mu = 0$. In the event that the network starts from a mean friendliness of zero, numerical experiments indicate that the system ends up with two factions of equal size in the large-n limit (Fig. 2.4b). We now prove this to be the case. For the remainder of this discussion, we will abbreviate $X(0)$ as A and $x_{ij}(0)$ as a_{ij}.

Since the off-diagonal entries of A have symmetric distributions by assumption, we have for any off-diagonal a_{ij} and any interval S_{ij} on the real line that $P(a_{ij} \in$

$S_{ij}) = P(-a_{ij} \in S_{ij})$. Now let D be a diagonal matrix with some sequence of $+1$ and -1 along its diagonal (where the ith diagonal entry is denoted by d_i). Then the random matrices A and $B = DAD$ are identically distributed, as we will now show.

To say that A and B are identically distributed means that for every Borel set of matrices S, $P(A \in S) = P(B \in S)$. To prove this, it suffices to consider the case in which S is a product of intervals S_{ij}, since these product sets generate the Borel sigma-algebra. The entries of A are independent, so $P(A \in S) = \Pi_{i \leq j} P(a_{ij} \in S_{ij})$. Similarly, $P(B \in S) = \Pi_{i \leq j} P(d_i a_{ij} d_j \in S_{ij})$. By the symmetry of the off-diagonal distributions, $\Pi_{i \leq j} P(a_{ij} \in S_{ij}) = \Pi_{i \leq j} P(d_i a_{ij} d_j \in S_{ij})$, which gives us $P(A \in S) = P(B \in S)$ as desired. (Note that when $i = j$, the factor $d_i d_j$ is 1 so the on-diagonal distributions need not be symmetric.)

Now consider the set S of matrices with an ω_1 consisting of all positive components. The above demonstration implies that the probability of choosing an A in this set is the same as choosing an A such that B is in this set. Regarding the later event, $A(D\omega_i) = \lambda_i(D\omega_i)$ implies $B\omega_i = \lambda_i \omega_i$, so the λ_1 eigenvector of the A used to compute B is $D\omega_1$. This demonstrates that all sign patterns for the components of ω_1 are equally likely. In other words, the distribution of the number of positive components in ω_1 is the binomial distribution $B(n, 1/2)$ and the fraction of positive components in ω_1 converges (in several senses) to $1/2$ as n grows large.

Additionally, we can consider how λ_1 varies with n in the case that $\mu = 0$ to determine when the blow-up will occur. Füredi and Komlós [32] found for this case that $\lambda_1 \in 2\sigma\sqrt{n} + O(n^{1/3} \log n)$ with probability tending to 1, so with probability tending to 1 the blow-up time shrinks to zero like $1/\sqrt{n}$, an order of $\sqrt{n}$ slower

than in the $\mu > 0$ case.

Case 3: $\mu < 0$**.** For this final case, Füredi and Komlós [32] found that $\lambda_1 < 2\sigma\sqrt{n} + O(n^{1/3}\log n)$ with probability tending to 1. The semicircle law gives a lower bound: $\lambda_1 > 2\sigma\sqrt{n} + o(\sqrt{n})$ in probability. So the blow-up time goes to zero like $1/\sqrt{n}$ in the unrescaled system.

Note also that if we define a new matrix $C = -A$ where A is now the initial matrix $X(0)$ of Case 3, then C satisfies the condition of Case 1, $\mu > 0$. Thus the distance between the top eigenvector of C and $(1, 1, \ldots, 1)/\sqrt{n}$ declines to zero in probability just as in Case 1. Furthermore, every other eigenvector of C is orthogonal to the largest one. Hence if $\sigma < |\mu|/2$, then with probability tending to 1, every other eigenvector acquires a mixture of positive and negative components in the large-n limit, including the bottom eigenvector of C, which is the top eigenvector of A. This establishes that in the case that $\mu < 0$ and $\sigma < |\mu|/2$, the system ends up in a state with two factions with probability converging to 1 for all finite n.

Numerical simulations of the case that $\mu < 0$ suggest the conjecture that the two factions are approximately equal in size for large n. Furthermore, the derivation of Eq. (2.11) is in fact valid for all μ, so each trajectory rapidly decays from $x_{ij}(0)$ toward $x_{ij}(0) - \mu$ on $[0, 1/K)$ (Fig. 2.4C). This transient decay appears to extend beyond $t = 1/K$ in numerical simulations. So, for example, if time is rescaled by $1/\sqrt{n}$ instead of $1/n$, we would hypothesize that (i) each trajectory makes a complete jump from $x_{ij}(0)$ to $x_{ij}(0) - \mu$ in the large-n limit, and that (ii) from this point onward, the system behaves like an initial configuration of the $\mu = 0$ case and so separates into two equal factions *en route* to its blow-up at $1/(2\sigma)$.

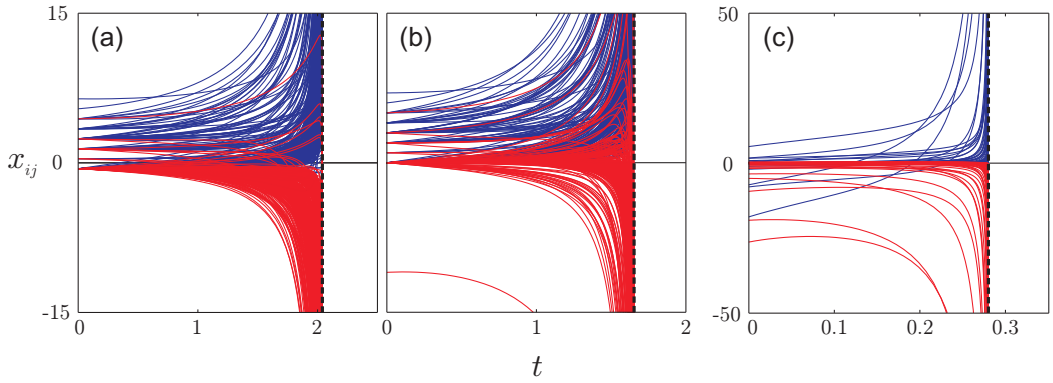

Figure 2.5: Tests of the model of Kułakowski et al. (Eq. (2.3) with a $t \to t/n$ rescaling of time) against two existing data sets. (a) The evolution of the model starting from Zachary's capacity matrix with the capacity of each relationship reduced by 0.58. This is the minimal downward displacement necessary (to two significant figures) for the resulting separation to be correct for all but 1 of the 34 club members. For reasons described by Zachary [89], this is basically the best separation we can expect. (b) The evolution of the model from Zachary's capacity matrix with the capacity of zero between the two club leaders replaced by -11; the resulting factions are identical to those in (a). Substituted values less than -11 yield the same two factions, while greater values produce less accurate divisions. (c) The evolution of the model starting from Axelrod and Bennett's 1939 propensity$(i, j) \cdot$ size$(i) \cdot$ size(j) matrix for the 17 countries involved in World War II (by Axelrod and Bennett's definition). The model finds the correct split into Allied and Axis powers with the exceptions of Denmark and Portugal. Axelrod and Bennett's own landscape theory of aggregation does slightly better—its only misclassification is Portugal.

Discussion

Our first result above was a demonstration that the model forms two factions in finite time across a broad set of initial conditions. As noted at the outset, similar demonstrations have not been possible for dynamic models of structural balance in earlier literature because these models contained so-called *jammed states* that could trap a social network before it reached a two-faction configuration [5, 50]. The model of Kułakowski et al. by contrast has no such jammed states for generic initial conditions and hence provides a robust means for a social network to balance itself.

The second major result of this section is the discovery and characterization of a transition from global polarization to global harmony as the initial mean friendliness of the network crosses from nonpositive to positive values. Similar transitions have been observed in other models of structural balance but so far none has been characterized at a quantitative level. For example, Antal et al. [5] found a nonlinear transition from two cliques of equal size to a single unified clique as the fraction of positively signed edges at $t = 0$ was increased from 0 to 1 (see Fig. 5 of Ref. [5]). The authors provided a qualitative argument for this transition, but left open the problem of its quantitative detail. Our results both confirm the generality of their observations and provide a quantitative account of a transition analogous to theirs.

To complement the theoretical nature of our work and get a better sense of how the model behaves in practice, we can numerically integrate it for several cases of empirical social network data where the real-life outcomes of the time-evolution are known. Our first example is based on a study by Zachary [89] who witnessed the break-up of a karate club into two smaller clubs. Prior to the separation, Zachary collected counts of the number of social contexts in which each pair of individuals interacted outside of the karate club, with the idea being that the more social contexts they shared, the greater the likelihood for information exchange. These counts, or *capacities* as Zachary called them, can be converted to estimates of friendliness and rivalry in many different ways. For a large class of such conversions, Eq. (2.3) predicts the same division that Zachary's method found, which misclassified only 1 of the 34 club members (Fig. 2.5a,b).

A second example can be constructed from the data of a study by Axelrod and Bennett [9] regarding the aggregation of Allied and Axis powers during World War

II. If we simply take the entries of their propensity$(i, j) \cdot \text{size}(i) \cdot \text{size}(j)$ matrix to be proportional to the friendliness felt between the various pairs of countries in the war, then running the model gives the correct Allied-Axis split for all countries except Denmark and Portugal (Fig. 2.5C).

Nevertheless, the model clearly contains several strong simplifications of the underlying social processes. The first of these is inherent to structural balance theory itself; it is a framework restricted to capture a particular kind of social situation, in which the need for consistency among one's friendships and rivalries brings about the emergence of two factions. Extensions of the theory have considered models in which it is possible to have multiple mutual enemies and hence more than two factions [15], and also networks that are not complete graphs [12]. However, our focus here has been on the basic theory, since as we have seen, obtaining a satisfactory dynamics even for this simplest form of structural balance has been an elusive challenge. Moreover, the basic version of structural balance that we have considered here, with a complete graph of relationships and constraints leading to two factions, is relevant to a range of different situations. These span the kinds of settings discussed earlier in this section, including clubs, classrooms, and small organizations [17], as well as international relations during crisis (where a large set of nations can all mutually maintain friendly or unfriendly diplomatic relations) [9, 52].

Another consequence of the particular model studied here that has no direct analogue in real social situations is the divergence to infinity of the the relationship strengths x_{ij}. However, since the purpose of the model is to study the pattern of signs that emerges, our main conclusions are based not on the actual magnitudes of these numbers but on the fact that the sign pattern eventually stabilizes

at a point before the divergence. This stabilization of the sign pattern is our primary focus, and one could interpret the subsequent singularity as simply the straightforward and unimpeded "ramping up" of values caused by the system once all inconsistencies have been worked out of the social relations—the divergence itself can be viewed as taking place beyond the window of time over which the system corresponds to anything real. Alternately, one can imagine that as the community completes its separation into two groups, other social processes take over. For example, individuals with differing ideological views or social preferences may self-segregate, breaking the all-to-all assumption of the model. In other cases, mounting tensions may erupt into violence, reflecting a sort of bound on the relationship intensity achievable for pairs of nodes in the network.

Finally, we note that there is a large body of work in social psychology that studies issues such as the formation and reconciliation of factions from a much more empirical basis; see for example Refs. [64, 65]. It is an interesting open problem to determine the extent to which the strictly mathematical development of the models here can be combined with the perspectives in this empirical body of literature, ultimately leading to a richer theory of these types of social processes.

CHAPTER 3

CONFORMISTS AND CONTRARIANS [1]

Systems of N identical phase oscillators with global sinusoidal coupling are known to display low-dimensional dynamics. Although this phenomenon was first observed about 20 years ago, its underlying cause has remained a puzzle. In Section 3.1, we expose the structure working behind the scenes of these systems by proving that the governing equations are generated by the action of the Möbius group, a three-parameter subgroup of fractional linear transformations that map the unit disc to itself. When there are no auxiliary state variables, the group action partitions the N-dimensional phase space into three-dimensional invariant manifolds (the group orbits). The $N-3$ constants of motion associated with this foliation are the $N-3$ functionally independent cross ratios of the oscillator phases. No further reduction is possible, in general; numerical experiments on models of Josephson junction arrays suggest that the invariant manifolds often contain three-dimensional regions of neutrally stable chaos.

After assembling a general framework for studying systems of identical coupled oscillators in Section 3.1, we consider in Section 3.2 a simple coupled oscillator model for the interaction between conformists and contrarians in a population. This model can be analyzed using the techniques demonstrated in Section 3.1. For the special case in which both the conformists and contrarians are distributed like Poisson kernels, we obtain a complete characterization of the long-time behavior of the system. This implies that when conformists are more numerous or intense, contrarians in general become more unified in their opposition to the conformist

[1] Much of the material in this chapter is drawn from S. A. Marvel, R. E. Mirollo, and S. H. Strogatz. Identical phase oscillators with global sinusoidal coupling evolve by Möbius group action. *Chaos*, 19:043104, 2009. and S. Marvel, H. Hong, and S. H. Strogatz. Stability of asynchrony among identical coupled oscillators. *Physical Review E*, in preparation.

position. Conversely when the conformists are either sufficiently sparse or sufficiently dispassionate, the state of complete asychrony (where both conformists and contrarians are uniformly spread around the complex unit circle) becomes stable.

This final observation is equivalent to the statement that the asynchronous state is stable just when the average of all conformist and contrarian coupling constants is negative. In Section 3.3, we show that this condition not only holds for the simple case in which the conformist and contarian subpopulations each have a single coupling constant, but also for the case of an *arbitrary* (integrable) distribution of coupling constants.

3.1 Identical oscillators and Möbius group action

When a nonlinear system shows unexpectedly simple behavior, it may be a clue that some hidden structure awaits discovery.

For example, recall the classic detective story [43] that began in the 1950s with the work of Fermi, Pasta, and Ulam [27, 86, 87]. In their numerical simulations of a chain of anharmonic oscillators, Fermi et al. were surprised to find the chain returning almost perfectly, again and again, to its initial state. The struggle to understand these recurrences led Zabusky and Kruskal [88] to the discovery of solitons in the Korteweg–de Vries equation, which in turn sparked a series of results showing that this equation possessed many conserved quantities—in fact, infinitely many [51]. Then several other equations turned out to have the same properties. At the time these results seemed almost miraculous. But by the mid-1970s the hidden structure responsible for all of them—the complete integrability of certain infinite-dimensional Hamiltonian systems [90]—had been made manifest by the inverse scattering transform [34, 1] and Lax pairs [47].

Something similar, though far less profound, has been happening again in nonlinear science. The broad topic is still coupled oscillators, but unlike the conservative oscillators studied by Fermi et al., the oscillators in question now are dissipative and have stable limit cycles. This latest story began around 1990, when a few researchers noticed an enormous amount of neutral stability and seemingly low-dimensional behavior in their simulations of Josephson junction arrays—specifically, arrays of identical, overdamped junctions arranged in series and coupled through a common load [79, 80, 74, 36, 57]. Then, just a year ago, Antonsen et al. [44] uncovered similarly low-dimensional dynamics in the periodically forced version of the Kuramoto model of biological oscillators [46, 70, 3]. This was particularly surprising because the oscillators in that model are non-identical.

As in the soliton story, these numerical observations then inspired a series of theoretical advances. For the case of identical coupled phase oscillators (the subject of this section), these included the discovery of constants of motion [83, 84], and of a pair of transformations that established the low-dimensionality of the dynamics [83, 84, 35, 59, 66, 60]. But what remained to be found was the final piece, the identification of the hidden structure. Without it, it was unclear why the transformations and constants of motion should exist in the first place.

In this section we show that the group of Möbius transformations is the key to understanding this class of dynamical systems. Our analysis unifies the previous treatments of Josephson arrays and the Kuramoto model, and clarifies the geometric and algebraic structures responsible for their low-dimensional behavior. One spin-off of our approach is a new set of constants of motion; these generalize the constants found previously, and hold for a wider class of oscillator arrays.

The section is organized as follows. To keep the treatment self-contained and

to establish notation, Subsection 3.1 reviews the relevant background about coupled oscillators and the Möbius group. In Subsection 3.1 we show how to use Möbius transformations to reduce the dynamics of identical oscillators with global sinusoidal coupling, the type of coupling that appears in both the Josephson and Kuramoto models. The reduced flow lives on a set of invariant three-dimensional manifolds, arising naturally as the so-called group orbits of the Möbius group. The results obtained in this way are then compared to previous findings (Subsection 3.1) and used to generate new constants of motion via the classical cross ratio construction (Subsection 3.1). We explore the dynamics on the invariant manifolds in Subsection 3.1, and show that the phase portraits for resistively coupled Josephson arrays are filled with chaos and island chains, reminiscent of the pictures encountered in Hamiltonian chaos and KAM theory.

Background

Reducible systems with sinusoidal coupling. The theory developed here was originally motivated by simulations of the governing equations for a series array of N identical, overdamped Josephson junctions driven by a constant current and coupled through a resistive load. As shown in Tsang et al. [79], the dimensionless circuit equations for this system can be written as

$$\dot{\phi}_j = \Omega - (b+1)\cos\phi_j + \frac{1}{N}\sum_{k=1}^{N}\cos\phi_k \tag{3.1}$$

for $j = 1, \ldots, N$. The physical interpretation need not concern us here; the important point for our purposes is that this set of N ordinary differential equations (ODEs) displayed low-dimensional dynamics. The same sort of low-dimensional behavior was later found in other kinds of oscillator arrays [36] as well as in Josephson arrays with other kinds of loads [80, 74, 57].

Building on contributions from several teams of researchers [79, 80, 74, 36, 57], Watanabe and Strogatz [84] showed that the system Eq. (3.1) could be reduced from N ODEs to three ODEs, in the following sense. Consider a time-dependent transformation from a set of constant angles θ_j to a set of functions $\phi_j(t)$, defined via

$$\tan\left[\frac{\phi_j(t) - \Phi(t)}{2}\right] = \sqrt{\frac{1+\gamma(t)}{1-\gamma(t)}}\tan\left[\frac{\theta_j - \Theta(t)}{2}\right] \tag{3.2}$$

for $j = 1, \ldots, N$. By direct substitution, one can check that the resulting functions $\phi_j(t)$ simultaneously satisfy all N equations in Eq. (3.1) as long as the three variables $\Phi(t), \gamma(t)$ and $\Theta(t)$ satisfy a certain closed set of ODEs [84].

Watanabe and Strogatz also noted that the same transformation can be used to reduce any system of the form

$$\dot{\phi}_j = f e^{i\phi_j} + g + \bar{f} e^{-i\phi_j} \tag{3.3}$$

for $j = 1, \ldots, N$, where f is any smooth, complex-valued, 2π-periodic function of the phases $\phi_1, \ldots, \phi_N$. (Here the overbar denotes complex conjugate. Also, note that g has to be real-valued since $\dot{\phi}_j$ is real.) The functions f and g are allowed to depend on time and on any other auxiliary state variables in the system, for example, the charge on a load capacitor or the current through a load resistor for certain Josephson junction arrays. The key is that f and g must be the same for all oscillators, and thus do *not* depend on the index j. We call such systems *sinusoidally coupled* because the dependence on j occurs solely through the first harmonics $e^{i\phi_j}$ and $e^{-i\phi_j}$.

Soon after the transformation Eq. (3.2) was reported, Goebel [35] observed that it could be related to fractional linear transformations, and he used this fact to simplify some of the calculations in Ref. [84]. At that point, research on the reducibility of Josephson arrays paused for more than a decade. The question

of *why* this particular class of dynamical systems Eq. (3.3) should be reducible by fractional linear transformations was not pursued at that time, but will be addressed in the subsection *Möbius Group Reduction*.

Ott-Antonsen ansatz. Ott and Antonsen [59, 60] recently reopened the issue of low-dimensional dynamics, with their discovery of an ansatz that collapses the infinite-dimensional Kuramoto model to a two-dimensional system of ODEs.

To illustrate their ansatz in its simplest form, let us apply it to the class of identical oscillators governed by Eq. (3.3), in the limit $N \to \infty$. (Note that this step involves two simplifying assumptions, namely, that N is infinitely large and that the oscillators are identical. The Ott-Antonsen ansatz applies more generally to systems of non-identical oscillators with frequencies chosen at random from a prescribed probability distribution—indeed, this generalization was one of Ott and Antonsen's major advances—but it is not needed for the issues that we wish to address.) In the limit $N \to \infty$, the evolution of the system Eq. (3.3) is given by the continuity equation

$$\frac{\partial \rho}{\partial t} + \frac{\partial (\rho v)}{\partial \phi} = 0 \tag{3.4}$$

where the phase density $\rho(\phi, t)$ is defined such that $\rho(\phi, t)\mathrm{d}\phi$ gives the fraction of phases that lie between ϕ and $\phi + \mathrm{d}\phi$ at time t, and where the velocity field is the Eulerian version of Eq. (3.3):

$$v(\phi, t) = f e^{i\phi} + g + \bar{f} e^{-i\phi}. \tag{3.5}$$

Our earlier assumptions about the coefficient functions f and g now take the form that f and g may depend on t but not on ϕ. The time-dependence of f and g can arise either explicitly (through external forcing, say) or implicitly (through the time-dependence of the harmonics of ρ or any auxiliary state variables in the

system).

Following Ott and Antonsen [59], suppose ρ is of the form

$$\rho(\phi,t) = \frac{1}{2\pi}\left\{1 + \sum_{n=1}^{\infty}\left(\bar{\alpha}(t)^n e^{in\phi} + \alpha(t)^n e^{-in\phi}\right)\right\} \tag{3.6}$$

for some unknown function α that is independent of ϕ. (Our definition of α is, however, slightly different from that in Ott and Antonsen [59]; our α is their $\bar{\alpha}$.) Note that Eq. (3.6) is just an algebraic rearrangement of the usual form for the Poisson kernel:

$$\rho(\phi) = \frac{1}{2\pi}\frac{1-r^2}{1-2r\cos(\phi-\Phi)+r^2} \tag{3.7}$$

where r and Φ are defined via

$$\alpha = re^{i\Phi}. \tag{3.8}$$

In geometrical terms, the ansatz Eq. (3.6) defines a submanifold in the infinite-dimensional space of density functions ρ. This *Poisson submanifold* is two-dimensional and is parametrized by the complex number α, or equivalently, by the polar coordinates r and Φ.

The intriguing fact discovered by Ott and Antonsen is that the Poisson submanifold is invariant: if the density is initially a Poisson kernel, it remains a Poisson kernel for all time. To verify this, we substitute the velocity field Eq. (3.5) and the ansatz Eq. (3.6) into the continuity equation Eq. (3.4), and find that the amplitude equations for each harmonic $e^{in\phi}$ are simultaneously satisfied if and only if $\alpha(t)$ evolves according to

$$\dot{\alpha} = i\left(f\alpha^2 + g\alpha + \bar{f}\right). \tag{3.9}$$

This equation can be recast in a more physically meaningful form in terms of the complex order parameter, denoted by $\langle z\rangle$ and defined as the centroid of the

phases ϕ regarded as points $e^{i\phi}$ on the unit circle:

$$\langle z \rangle = \int_0^{2\pi} e^{i\phi} \rho(\phi, t) \mathrm{d}\phi. \tag{3.10}$$

By substituting Eq. (3.6) into Eq. (3.10) we find that $\langle z \rangle = \alpha$ for all states on the Poisson submanifold. Hence, $\langle z \rangle$ satisfies the Riccati equation

$$\dot{\langle z \rangle} = i(f\langle z \rangle^2 + g\langle z \rangle + \bar{f}). \tag{3.11}$$

When f and g are functions of $\langle z \rangle$ alone, as in mean-field models, Eq. (3.11) constitutes a closed two-dimensional system for the flow on the Poisson submanifold. More generally, the system will be closed whenever f and g depend on ρ only through its Fourier coefficients. We will show this explicitly in Subsubsection 3.1, by finding formulas for all the higher Fourier coefficients in terms of α, and hence in terms of $\langle z \rangle$. (However, as we will see, things become more complicated for states lying off the Poisson submanifold. Then $\langle z \rangle$ no longer coincides with α and the closed system becomes three dimensional, involving ψ as well as α.)

The work of Ott and Antonsen [59] raises several questions. Why should the set of Poisson kernels be invariant? What is the relationship, if any, between the ansatz Eq. (3.6) and the transformation Eq. (3.2) studied earlier? Why does Eq. (3.2) reduce equations of the form Eq. (3.3) to a three-dimensional flow, whereas Eq. (3.6) reduces them to a two-dimensional flow?

As we shall see, the answers have to do with the properties of the group of conformal mappings of the unit disc to itself. Before showing how this group arises naturally in the dynamics of sinusoidally coupled oscillators, let us recall some of its relevant properties.

Möbius group. Consider the set of all fractional linear transformations $F : \mathbb{C} \to \mathbb{C}$ of the form

$$F(z) = \frac{az + b}{cz + d}, \tag{3.12}$$

where a, b, c and d are complex numbers, and the numerator is not a multiple of the denominator (that is, $ad - bc \neq 0$). This family of functions carries the structure of a group. The group operation is composition of functions, the identity element is the identity map, and inverses are given by inverse functions.

Of most importance to us is a subgroup G—which we refer to as the *Möbius group*—consisting of those fractional linear transformations that map the open unit disc $\mathbb{D} = \{z \in \mathbb{C} : |z| < 1\}$ onto itself in a one-to-one way. These transformations and their inverses are analytic on $\mathbb{D}$ and map its boundary (the unit circle $S^1 = \{z \in \mathbb{C} : |z| = 1\}$) to itself. All such automorphisms of the disc can be written [69] in the form

$$F(z) = e^{i\varphi} \frac{\alpha - z}{1 - \bar{\alpha} z}, \tag{3.13}$$

for some $\varphi \in \mathbb{R}$ and $\alpha \in \mathbb{D}$. The Möbius group G is in fact a three-dimensional Lie group, with real parameters φ, $\mathrm{Re}(\alpha)$, and $\mathrm{Im}(\alpha)$.

However, it turns out that a different parametrization of G will be more notationally convenient in what follows, in the sense that it simplifies comparisons between our results and those in the prior literature. Specifically, we will view a typical element of G as a mapping M from the unit disc in the complex w-plane to the unit disc in the complex z-plane, with parametrization given by

$$z = M(w) = \frac{e^{i\psi} w + \alpha}{1 + \bar{\alpha} e^{i\psi} w} \tag{3.14}$$

where $\alpha \in \mathbb{D}$ and $\psi \in \mathbb{R}$. Note that the inverse mapping

$$w = M^{-1}(z) = e^{-i\psi} \frac{z - \alpha}{1 - \bar{\alpha} z} \tag{3.15}$$

has an appearance closer to that of the standard parametrization Eq. (3.13).

A word about terminology: our definition of the Möbius group is not the conventional one. Usually this term denotes the larger group of all fractional linear transformations (or bilinear transformations, or linear fractional transformations), whereas we reserve the adjective Möbius for the subgroup G and its elements. Thus, from now on, when we say *Möbius transformation* we specifically mean an element of the subgroup G consisting of analytic automorphisms of the unit disc.

Möbius Group Reduction

In this subsection we show that if the equations for the oscillator array are of the form Eq. (3.3), then the oscillators' phases $\phi_j(t)$ evolve according to the action of the Möbius group on the complex unit circle:

$$e^{i\phi_j(t)} = M_t(e^{i\theta_j}), \tag{3.16}$$

for $j = 1, \ldots, N$, where M_t is a one-parameter family of Möbius transformations and θ_j is a constant (time-independent) angle. In other words, the time-t flow map for the system is always a Möbius map.

Incidentally, this result is consistent with a basic topological fact: we know that different oscillators cannot pass through each other on S^1 under the flow, so we expect the time-t flow map to be an orientation-preserving homeomorphism of S^1 onto itself—and indeed any Möbius map is.

We begin the analysis with an algebraic method similar to that in Goebel [35]. Then, in Subsections 3.1 and 3.1, we adopt a geometrical perspective and show that it answers several questions left open by the first method.

Algebraic method. Parametrize the one-parameter family of Möbius transformations as

$$M_t(w) = \frac{e^{i\psi}w + \alpha}{1 + \bar{\alpha}e^{i\psi}w} \tag{3.17}$$

where $|\alpha(t)| < 1$ and $\psi(t) \in \mathbb{R}$, and let

$$w_j = e^{i\theta_j}. \tag{3.18}$$

To verify that Eq. (3.17) gives an exact solution of Eq. (3.3)—subject to the constraint that the Möbius parameters $\alpha(t)$ and $\psi(t)$ obey appropriate ODEs, to be determined—we compute the time-derivative of $\phi_j(t) = -i \log M_t(w_j)$, keeping in mind that w_j is constant:

$$\dot{\phi_j} = \frac{\dot{\psi}e^{i\psi}w_j - i\dot{\alpha}}{e^{i\psi}w_j + \alpha} + \frac{(i\dot{\bar{\alpha}} - \bar{\alpha}\dot{\psi})e^{i\psi}w_j}{1 + \bar{\alpha}e^{i\psi}w_j}. \tag{3.19}$$

From Eq. (3.15), we get

$$e^{i\psi}w_j = \frac{e^{i\phi_j} - \alpha}{1 - \bar{\alpha}e^{i\phi_j}} \tag{3.20}$$

which when substituted into Eq. (3.19) yields

$$\dot{\phi_j} = Re^{i\phi_j} + \frac{\dot{\psi} + i\bar{\alpha}\dot{\alpha} - \alpha(i\dot{\bar{\alpha}} - \bar{\alpha}\dot{\psi})}{1 - |\alpha|^2} + \bar{R}e^{-i\phi_j} \tag{3.21}$$

where $R = (i\dot{\bar{\alpha}} - \bar{\alpha}\dot{\psi})/(1 - |\alpha|^2)$.

Note that Eq. (3.21) falls precisely into the algebraic form required by Eq. (3.3). Thus, to derive the desired ODEs for $\alpha(t)$ and $\psi(t)$, we now subtract Eq. (3.21) from Eq. (3.3) to obtain N equations of the form $0 = C_1e^{i\phi_j} + C_0 + C_{-1}e^{-i\phi_j}$, for $j = 1, \ldots, N$. If the system contains at least three distinct oscillator phases, then C_1, C_0, and C_{-1} must generically be zero. Explicitly,

$$f = \frac{i\dot{\bar{\alpha}} - \bar{\alpha}\dot{\psi}}{1 - |\alpha|^2}, \quad g = \frac{\dot{\psi} + i\bar{\alpha}\dot{\alpha} - \alpha(i\dot{\bar{\alpha}} - \bar{\alpha}\dot{\psi})}{1 - |\alpha|^2}. \tag{3.22}$$

Eq. (3.22) can be algebraically rearranged to give

$$\dot{\alpha} = i(f\alpha^2 + g\alpha + \bar{f}) \tag{3.23a}$$

$$\dot{\psi} = f\alpha + g + \bar{f}\bar{\alpha}. \tag{3.23b}$$

Eqs. (3.23a) and (3.23b) have been derived previously; they appear as Eqs.(10) and (11), respectively, in Pikovsky and Rosenblum's work [66], where they were derived by applying the transformation Eq. (3.2). Both their approach and the one above are certainly quick and clean, but they require us to guess the transformation ahead of time, and reveal little about why this transformation works.

Incidentally, observe that under the change of variables $z_j = e^{i\phi_j}$, Eq. (3.3) becomes

$$\dot{z_j} = i(fz_j^2 + gz_j + \bar{f}). \tag{3.24}$$

Eq. (3.24) is a Riccati equation with the form of Eq. (3.23a)—another coincidence that seems a bit surprising when approached this way. In the following subsubsection, we will see how these Riccati equations emerge naturally from the infinitesimal generators of the Möbius group.

Geometric method of finding $\dot{\alpha}$. Now we change our view of Möbius maps slightly. Instead of thinking of M as a map from the w-plane to the z-plane, we view it as a map from the z-plane to itself. This requires a small and temporary change in notation, but it makes things clearer, especially when we start to discuss differential equations on the complex plane.

We begin by recalling some basic facts and definitions. Suppose the coupled oscillator system contains just three distinct phases among its N oscillators. Then by a property of Möbius transformations, there exists a unique Möbius transfor-

mation from any point $\boldsymbol{z}_1 = (e^{i\theta_1}, e^{i\theta_2}, e^{i\theta_3})$ to any other point $\boldsymbol{z}_2 = (e^{i\phi_1}, e^{i\phi_2}, e^{i\phi_3})$ in the phase space $S^1 \times S^1 \times S^1$. If the system instead contains only one or two distinct phases, many Möbius transformations will take $\boldsymbol{z}_1$ to $\boldsymbol{z}_2$, so we can still reach every point of the phase space from every other point. However, if the system contains more than three distinct phases, say N, then there is not in general a Möbius transformation that transforms $\boldsymbol{z}_1 = (e^{i\theta_1}, e^{i\theta_2}, e^{i\theta_3}, \ldots, e^{i\theta_N})$ to $\boldsymbol{z}_2 = (e^{i\phi_1}, e^{i\phi_2}, e^{i\phi_3}, \ldots, e^{i\phi_N})$; only some points are accessible from $\boldsymbol{z}_1$, while others are not.

In the language of group theory, we say that $\boldsymbol{z}_2$ is in the *group orbit* of $\boldsymbol{z}_1$ if there exists a Möbius map M such that $\boldsymbol{z}_2 = M(\boldsymbol{z}_1)$. Then, as a direct consequence of the fact that Möbius maps form a three-parameter group G under composition, the group orbits of G partition the phase space into three-dimensional manifolds (when the phase space is at least three dimensional).

To compute infinitesimal generators for G, we compute the time derivatives of the three one-parameter families of curves corresponding to the three parameters of G: ψ, $\mathrm{Re}(\alpha)$ and $\mathrm{Im}(\alpha)$. Each of the three families is obtained from the Möbius transformation by setting two of the three parameters to zero, and leaving the remaining parameter free. For example, if we set $t = 0$ at $\boldsymbol{z} = (z_1, \ldots, z_N)$, these three families may be written as

$$\begin{aligned} M_1(\boldsymbol{z}) &= e^{it}\boldsymbol{z} \\ M_2(\boldsymbol{z}) &= \frac{\boldsymbol{z} - t}{1 - t\boldsymbol{z}} \\ M_3(\boldsymbol{z}) &= \frac{\boldsymbol{z} + it}{1 - it\boldsymbol{z}} \end{aligned} \tag{3.25}$$

where $M_1(\boldsymbol{z})$ is written in place of $(M_1(z_1), \ldots, M_1(z_N))$ and likewise for $M_2(\boldsymbol{z})$ and $M_3(\boldsymbol{z})$. We continue using this shorthand in subsequent equations, writing $h(\boldsymbol{z})$ in place of $(h(z_1), \ldots, h(z_N))$ for any one-parameter function h.

The time derivatives of the curves in Eq. (3.25) evaluated at $t = 0$ then give a set of infinitesimal generators for G:

$$\begin{aligned} \boldsymbol{v}_1 &= i\boldsymbol{z} \\ \boldsymbol{v}_2 &= \boldsymbol{z}^2 - 1 \\ \boldsymbol{v}_3 &= i\boldsymbol{z}^2 + i. \end{aligned} \tag{3.26}$$

Note that these three generators point out into the full N-dimensional complex space $\mathbb{C}^N$, as expected.

Meanwhile, if we substitute $f = -ih_1 + h_2$ (where h_1 and h_2 are real functions) into the original Riccati dynamics Eq. (3.24), we can rewrite this equation of motion in terms of the three infinitesimal generators:

$$\dot{\boldsymbol{z}} = i\boldsymbol{z}g + (\boldsymbol{z}^2 - 1)h_1 + (i\boldsymbol{z}^2 + i)h_2. \tag{3.27}$$

The implication of the rewritten form Eq. (3.27) is then given by a theorem from Lie theory: if L is a Lie group acting on a submanifold with linearly independent infinitesimal generators $\boldsymbol{v}_1, \ldots, \boldsymbol{v}_n$, and $\boldsymbol{v}$ is a vector field of the form $\boldsymbol{v} = c_1\boldsymbol{v}_1 + \cdots + c_n\boldsymbol{v}_n$ where the coefficients c_k depend only on time t, then the trajectory of the dynamics $\dot{\boldsymbol{z}} = \boldsymbol{v}$ from any initial condition $\boldsymbol{z}_0$ can be expressed in the form $\{A_t(\boldsymbol{z}_0)\}$ for a unique family $\{A_t\} \subset L$ parameterized by t. Since the Möbius group is a complex Lie group, this result can be applied directly to conclude Eq. (3.27) has the solution $\boldsymbol{z}(t) = M_t(\boldsymbol{z}_0)$ where $\{M_t\}$ is a unique one-parameter family of Möbius transformations.

Although we have so far assumed that the components z_k of $\boldsymbol{z}$ lie on the complex unit circle, both Eq. (3.17) and Eq. (3.27) extend naturally to all of $\mathbb{C}^N$. This implies that $z_0 = 0$ must evolve as $z(t) = M_t(0)$ for some family $\{M_t\}$. However, Eq. (3.17) shows that $M(0) = \alpha$ for all $M \in G$. So $z(t) = M_t(0) = \alpha$ for all

t, meaning that $\alpha(t)$ satisfies Eq. (3.27). Since Eq. (3.27) is just a rewriting of Eq. (3.24), the dynamics Eq. (3.23a) for α that we derived earlier are now placed in a geometrical context. This approach reveals that $\alpha(t)$ is just the image of the origin under a one-parameter family of Möbius maps, applied to any one complex plane of $\mathbb{C}^N$.

It is even more illuminating to compute the infinitesimal generators within the N-fold torus $\mathbb{T}^N$ of phase values, i.e., the quantities $\boldsymbol{u}_k = -i\frac{d}{dt}\log M_k(e^{i\boldsymbol{\phi}})|_{t=0}$. These turn out to be

$$\begin{aligned} \boldsymbol{u}_1 &= (1, \ldots, 1) \\ \boldsymbol{u}_2 &= 2\sin\boldsymbol{\phi} \\ \boldsymbol{u}_3 &= 2\cos\boldsymbol{\phi}. \end{aligned} \tag{3.28}$$

When expressed in terms of these infinitesimal generators, the equation of motion Eq. (3.27) becomes

$$\dot{\boldsymbol{\phi}} = g + (2\sin\boldsymbol{\phi})h_1 + (2\cos\boldsymbol{\phi})h_2 \tag{3.29}$$

which is precisely what we earlier referred to as a sinusoidally coupled system Eq. (3.3), and whose solution must therefore be of the form $\boldsymbol{\phi}_t = -i\log M_t(e^{i\boldsymbol{\theta}})$ for some $M_t \in G$.

This calculation finally clarifies what is so special about sinusoidally coupled systems Eq. (3.3): they are induced naturally by a flow on the Möbius group. This fact underlies their reducibility and all their other beautiful (but non-generic) properties.

Geometric method of finding $\dot{\psi}$. We turn next to the dynamics of ψ. As we will show in the next section, the action of the Möbius transformation involves a clockwise rotation of the oscillator phase density $\rho(\phi, t)$ by $\arg(\alpha) - \psi$ and a

counterclockwise rotation by $\arg(\alpha)$. Hence, $\psi(t)$ may be viewed as the overall counterclockwise rotation of the distribution at time t relative to the initial distribution at $t = 0$.

To support this interpretation, we show here that $\dot{\psi}$ equals the average value of the vector field on the circle, given by

$$\langle \dot{\phi} \rangle = \frac{1}{2\pi} \int_{S^1} \dot{\phi} \, d\theta. \tag{3.30}$$

Observe the right side of the integrand Eq. (3.19) has two terms:

$$\begin{aligned} R_1(w) &= \frac{\dot{\psi} e^{i\psi} w - i\dot{\alpha}}{e^{i\psi} w + \alpha} \\ R_2(w) &= \frac{(i\dot{\bar{\alpha}} - \bar{\alpha}\dot{\psi}) e^{i\psi} w}{1 + \bar{\alpha} e^{i\psi} w}. \end{aligned} \tag{3.31}$$

By Cauchy's formula,

$$\frac{1}{2\pi i} \int_{S^1} R_2(w) \frac{dw}{w} = R_2(0) = 0. \tag{3.32}$$

So $\langle \dot{\phi} \rangle$ simplifies to

$$\langle \dot{\phi} \rangle = \frac{1}{2\pi i} \int_{S^1} R_1(w) \frac{dw}{w}. \tag{3.33}$$

Note that $R_1(w)$ has a pole in the unit disc, so we make the change of variables $w \to w^{-1}$ to move this pole outside the circle. Evaluating the resulting integral yields

$$\frac{1}{2\pi i} \int_{S^1} R_1(w) \frac{dw}{w} = \frac{1}{2\pi i} \int_{S^1} \frac{\dot{\psi} - i\dot{\alpha} e^{-i\psi} w}{1 + \alpha e^{-i\psi} w} \frac{dw}{w} = \dot{\psi} \tag{3.34}$$

which completes the demonstration that $\langle \dot{\phi} \rangle = \dot{\psi}$.

We can now go back and evaluate the average vector field in a different way to find the differential equation that governs $\psi(t)$. Differentiating $\phi = -i \log M_t(w)$ with respect to time and substituting the result into $\dot{\psi} = \frac{1}{2\pi} \int_{S^1} \dot{\phi} \, d\theta$, we obtain

$$\dot{\psi} = \frac{1}{2\pi i} \int_{S^1} \frac{\dot{M}_t(w)}{M_t(w)} \frac{dw}{iw}. \tag{3.35}$$

Since M_t obeys the Riccati equation, we can eliminate $\dot{M}_t$ in the numerator above to get

$$\dot{\psi} = \frac{1}{2\pi i}\int_{S^1}(fM_t(w) + g + \bar{f}M_t(w)^{-1})\frac{dw}{w}. \tag{3.36}$$

There are three integrals to evaluate here. The third one involves a term $M_t(w)^{-1}$ which has a pole inside the unit circle, so we do the same change of variables as before, $w \to w^{-1}$, to move the pole outside. The corresponding integral then simplifies to

$$\frac{1}{2\pi i}\int_{S^1} M_t(w)^{-1}\frac{dw}{w} = \frac{1}{2\pi i}\int_{S^1}\frac{e^{-i\psi}w + \bar{\alpha}}{1 + \alpha e^{-i\psi}w}\frac{dw}{w} = \bar{\alpha} \tag{3.37}$$

where the final integration follows from Cauchy's formula. Similiarly, we use Cauchy's formula to integrate the first and second terms of the integrand in Eq. (3.36), and thereby obtain the desired differential equation for ψ, thus rederiving Eq. (3.23b) found earlier.

Connections to Previous Results

Relation to the Watanabe-Strogatz transformation. It is natural to ask how the trigonometric transformation Eq. (3.2) used in earlier studies [83, 84, 66] relates to the Möbius transformation Eq. (3.17) used above. As we will see, Eq. (3.2) may be viewed as a restriction of Eq. (3.17) to the complex unit circle.

First, by trigonometric identities, we have

$$\tan\left[\frac{\phi - \Phi}{2}\right] = i\frac{1 - e^{i(\phi-\Phi)}}{1 + e^{i(\phi-\Phi)}}. \tag{3.38}$$

To connect this to Möbius transformations, consider what happens when we apply the map defined by Eq. (3.17) to a point $w = e^{i\theta}$ on the unit circle. Since the image is also a point on the unit circle, it can be written as $M(e^{i\theta}) = e^{i\phi}$ for some

angle ϕ. Next let $\alpha = re^{i\Phi}$ and divide both sides of Eq. (3.17) by $e^{i\Phi}$. Thus

$$e^{i(\phi-\Phi)} = \frac{e^{i(\theta-\Theta)} + r}{1 + re^{i(\theta-\Theta)}} \tag{3.39}$$

where $\Theta = \Phi - \psi$. Substitution of Eq. (3.39) into the right side of Eq. (3.38) gives

$$\tan\left[\frac{\phi-\Phi}{2}\right] = \frac{1-r}{1+r}\left(i\frac{1-e^{i(\theta-\Theta)}}{1+e^{i(\theta-\Theta)}}\right). \tag{3.40}$$

By the identity Eq. (3.38), Eq. (3.40) is equivalent to Eq. (3.2) with $\gamma = -2r/(1+r^2)$.

We can now see how the Möbius parameters α and ψ operate on the set of $e^{i\theta}$ in $\mathbb{C}$. From the relationships between Θ, γ, Φ and the Möbius parameters, the initial phase density is first rotated clockwise around S^1 by $\arg(\alpha) - \psi$, then squeezed toward one side of the circle as a function of $|\alpha|$, and afterwards rotated counterclockwise by $\arg(\alpha)$. The squeeze, which takes uniform distributions to Poisson kernels, can be thought of as a composition of inversions, dilations and translations in the complex plane.

Invariant manifold of Poisson kernels. In the subsection *Ott-Antonsen ansatz*, we used the Ott-Antonsen ansatz Eq. (3.6) to show that systems of identical oscillators with global sinusoidal coupling contain a degenerate two-dimensional manifold among the three-dimensional leaves of their phase space foliation. This two-dimensional manifold, which we called the Poisson submanifold, consists of phase densities $\rho(\phi, t)$ that have the form of a Poisson kernel. We now rederive these results within the framework of Möbius transformations.

Let T denote one instance of the transformation Eq. (3.2); in other words, fix the parameters Φ, γ and Θ and let $\phi = T(\theta)$. Let μ denote the normalized uniform

measure on S^1; thus

$$d\mu(\theta) = \frac{1}{2\pi} d\theta. \tag{3.41}$$

The transformation T maps μ to the measure $T_*\mu$, and, by the usual formula for transformation of single-variable measures, we have $d(T_*\mu)(\phi) = \frac{1}{2\pi} T^{-1}(\phi)' d\phi$, where the prime denotes differentiation by ϕ. From this equation it follows that $d(T_*\mu)(\phi)$ has the form of the Poisson kernel, because the inverse of the Möbius transformation Eq. (3.17) is

$$M^{-1}(z) = e^{-i\psi} \frac{z - \alpha}{1 - \bar{\alpha} z} \tag{3.42}$$

which implies

$$T^{-1}(\phi) = -\psi - i \log(e^{i\phi} - \alpha) + i \log(1 - \bar{\alpha} e^{i\phi}). \tag{3.43}$$

Then by differentiation and algebraic rearrangement, we obtain

$$T^{-1}(\phi)' = \frac{1 - r^2}{1 - 2r \cos(\phi - \Phi) + r^2}. \tag{3.44}$$

The integral of $T^{-1}(\phi)'$ over $[0, 2\pi)$ is 2π, so $d(T_*\mu)(\phi)$ is indeed a normalized Poisson kernel.

Finally, if the phase distribution $d(T_*\mu)(\phi)/d\phi$ ever takes the form of a Poisson kernel with parameters $r = r_0$ and $\Phi = \Phi_0$, then we can set $r(0) = r_0$, $\Phi(0) = \Phi_0$ and $d\mu(\theta) = \frac{1}{2\pi} d\theta$, and the above calculation shows that $d(T_*\mu)(\phi)/d\phi$ remains a Poisson kernel for all future and past times. Hence, the set of normalized Poisson kernels constitutes an invariant submanifold of the infinite-dimensional phase space.

The above demonstration also reveals that the Poisson submanifold has dimension $k + 2$ where k is the number of state variables besides α, ψ and the oscillator

phases. More concretely, it implies that when the system lies on the Poisson submanifold, we can write $\dot{\alpha}$ as depending only on α; it is not possible to require $\dot{\alpha}$ to depend on ψ in any real coupling scheme.

To see this, we first consider the case in which the system is closed and there are no additional state variables. Suppose $\dot{\alpha}$ does *not* depend only on α. Then some of the phase space trajectories cross when projected onto the unit disc of α values. At the point of any crossing, the phase density $\rho(\phi, t)$ has multiple $\dot{\alpha}$ values. But by Eq. (3.44), the phase density depends only on α, so there is nothing in the phase space that can distinguish between the different $\dot{\alpha}$ values at that point. Hence, $\dot{\alpha}$ must be expressible in terms of α alone. By an analogous argument, $\dot{\alpha}$ is also independent of ψ on the Poisson submanifold when there are k other state variables besides the oscillator phases and Möbius parameters.

On the other hand, if the time-dependence of $\dot{\alpha}$ arises only via a dependence on α, then r and Φ decouple from ψ and the dynamics are two dimensional regardless of whether the system is evolving on the Poisson submanifold or not. Observe that we can always force ψ-independence for $\dot{\alpha}$ by throwing away enough information about the locations of the other phases. For instance, in the extreme, we may simply make f and g constant.

Finally, even when $\dot{\alpha}$ does not depend solely on α, the dynamics still may be two dimensional. For example, in the case of completely integrable systems [83], the variables r and $\Phi - \psi$ decouple from Φ to foliate the phase space with two-dimensional tori.

Characteristics of the Motion

Cross ratios as constants of motion. The reduction of Eq. (3.3) by the three-parameter Möbius group suggests that the corresponding system of coupled oscillators should have $N-3$ constants of motion. As we will see, these conserved quantities are given by the cross ratios of the points $z_j = e^{i\phi_j}$ on S^1. Recall from complex analysis [14] that the *cross ratio* of four distinct points $z_1, z_2, z_3, z_4 \in \mathbb{C} \cup \{\infty\}$ is

$$(z_1, z_2, z_3, z_4) = \frac{z_1 - z_3}{z_1 - z_4} \cdot \frac{z_2 - z_4}{z_2 - z_3} \tag{3.45}$$

This quantity is conserved under Möbius transformations: for all α and ψ, $(M(z_1), M(z_2), M(z_3), M(z_4)) = (z_1, z_2, z_3, z_4)$. Hence, the $N!/(N-4)!$ cross ratios of the N oscillator phases remain constant along the trajectories in phase space. We denote the constant value of (z_1, z_2, z_3, z_4) as λ_{1234}. Of course, we could have defined the cross ratio for four-tuples of *non-distinct* points as well, but these quantities are trivially conserved regardless of the dynamics and hence do not reduce the dimension of the phase space.

To show that exactly $N-3$ of the cross ratios are independent, consider the sequence: $\{(z_1, z_2, z_3, z_4), (z_2, z_3, z_4, z_5), \ldots, (z_{N-3}, z_{N-2}, z_{N-1}, z_N)\}$. Each cross ratio in the sequence includes a new point not in the cross ratios preceding it and therefore must be independent of them. Hence, there are at least $N-3$ independent cross ratios. With a bit more work (see Appendix B), we can also confirm that the rest of the cross ratios are functionally dependent on these $N-3$ integrals.

Since the phase space of the phases is an N-fold torus of real variables, we expect that each of the constants of motion can be expressed in terms of real functions and variables. Indeed, if z_1, z_2, z_3, z_4 lie on the unit circle, then the cross ratio (z_1, z_2, z_3, z_4) lies on $\mathbb{R} \cup \{\infty\}$. We see this explicitly by pulling out

$e^{\frac{i}{2}(\phi_1+\phi_3)}$ from the factor $(e^{i\phi_1} - e^{i\phi_3})$ of $(e^{i\phi_1}, e^{i\phi_2}, e^{i\phi_3}, e^{i\phi_4})$, and likewise for the other three factors, and then canceling the factors $e^{\frac{i}{2}(\phi_1+\phi_2+\phi_3+\phi_4)}$ in the numerator and denominator to find

$$(e^{i\phi_1}, e^{i\phi_2}, e^{i\phi_3}, e^{i\phi_4}) = \frac{S_{13}S_{24}}{S_{14}S_{23}} \tag{3.46}$$

where

$$S_{ij} = \sin\left[\frac{\phi_i - \phi_j}{2}\right]. \tag{3.47}$$

This way of writing the cross ratio also suggests a relationship with the constants of motion reported by Watanabe and Strogatz [83, 84] for completely integrable systems (those with $f = \frac{1}{2}e^{i\delta}\overline{\langle z\rangle}$ and $g = 0$, where $\langle z\rangle$ is the phase centroid Eq. (3.10)). These constants of motion, which we will call *WS integrals*, take the form

$$I = S_{12}S_{23}\cdots S_{(N-1)N}S_{N1} \tag{3.48}$$

where any permutation of the indices generates another WS integral. As previously demonstrated [84], exactly $N - 2$ of the $N!$ index permutations of Eq. (3.48) are functionally independent.

As we might anticipate, the WS integrals imply that the cross ratios are constants of motion: consider two distinct WS integrals $I = S_{ik}S_{kl}S_{lj}\Pi$ and $I' = S_{il}S_{lk}S_{kj}\Pi$, where Π denotes the remaining product of factors. Assume Π is the same for both I and I'. Then $I/I' = -\lambda_{ijkl}$. Since i, j, k, l are arbitrary, we can generate all cross ratios via this procedure.

Additionally, if a single WS integral holds for a system in which the cross ratios are invariant, then *all* WS integrals hold, since we can arbitrarily permute the indices of the first WS integral by sequences of transpositions of the form $I = -\lambda_{ijkl}I'$ in which l and k are interchanged.

Fourier coefficients of the phase distribution. When we introduced f and g in Subsection 3.1, we required that they depend on the phases *only* through the Fourier coefficients of the phase density $\rho(\phi, t)$. Since the centroid Eq. (3.10) is the Fourier coefficient corresponding to the first harmonic $e^{-i\phi}$, this condition is met by standard Kuramoto models, Josephson junction series arrays, laser arrays and many other well-studied systems of globally coupled oscillators.

Our goal now is to show that this condition implies the closure of Eq. (3.23), in the sense that $\dot{\alpha}$ and $\dot{\psi}$ depend only on α and ψ. To do so, we will show that the Fourier coefficient of all higher harmonics $e^{-im\phi}$ for any integer m may be expressed in terms of α and ψ.

For a fixed measure $\mu(\theta)$ on $[0, 2\pi)$ and a transformation $T(\theta) = -i \log M(\theta)$ of this measure via the Möbius map M, the Fourier coefficient of $e^{-im\phi}$ is given by

$$\langle z^m \rangle = \int_{S^1} e^{im\phi} d(T_* \mu)(\phi) = \int_{S^1} M(e^{i\theta})^m d\mu(\theta). \tag{3.49}$$

We use the notation $\langle z^m \rangle$ as a reminder that $\langle z \rangle$ is the phase centroid.

We assume that we can take a Fourier expansion of $\mu(\theta)$, so

$$d\mu(\theta) = \frac{1}{2\pi} \sum_{n=-\infty}^{\infty} c_n e^{in\theta} d\theta \tag{3.50}$$

where the constants c_n are independent of θ. Since the phase distribution must be real and normalized, we know that $c_{-n} = \bar{c}_n$ and $c_0 = 1$, so we can write

$$d\mu = \frac{1}{2\pi i} \left(1 + P(w) + \overline{P(w)} \right) \frac{dw}{w} \tag{3.51}$$

where $w = e^{i\theta}$ and $P(w) = \sum_{n=1}^{\infty} c_n w^n$. The formula for $\langle z^m \rangle$ then becomes:

$$\langle z^m \rangle = \frac{1}{2\pi i} \int_{S^1} M(w)^m \left(1 + P(w) + \overline{P(w)} \right) \frac{dw}{w}. \tag{3.52}$$

Now, $M(w)^m(1+P(w))$ is analytic on the open disc $\mathbb{D}$ and $M(0)^m(1+P(0)) = \alpha^m$. Meanwhile, the remaining term of the integrand of Eq. (3.52) has the complex conjugate

$$\frac{\overline{M(w)}^m P(w)}{w} = \left(\frac{1+\bar{\alpha}e^{i\psi}w}{e^{i\psi}w+\alpha}\right)^m \frac{P(w)}{w} \tag{3.53}$$

which features an order-1 pole at $w = 0$ and an order-m pole at $w = -e^{-i\psi}\alpha$. The first residue evaluates to zero, while the second is given by

$$\frac{e^{-im\psi}}{(m-1)!}\frac{d^{m-1}}{dw^{m-1}}\left[(1+\bar{\alpha}e^{i\psi}w)^m \frac{P(w)}{w}\right]\Bigg|_{w=-e^{-i\psi}\alpha.} \tag{3.54}$$

Therefore, $\langle z^m \rangle$ is equal to α^m added to the complex conjugate of this second residue:

$$\langle z^m \rangle = \alpha^m + \sum_{k=0}^{m-1} \frac{(1-|\alpha|^2)^{k+1}}{k!} \sum_{n=0}^{\infty} (-1)^n \frac{(n+k)!}{n!} \bar{c}_{n+k+1} e^{i(m+n)\psi} \bar{\alpha}^n. \tag{3.55}$$

For example, the centroid may be written in terms of α and ψ as

$$\langle z \rangle = \alpha + (|\alpha|^2 - 1) \sum_{n=1}^{\infty} (-1)^n \bar{c}_n e^{in\psi} \bar{\alpha}^{n-1}. \tag{3.56}$$

This calculation reveals what is so special about the Poisson submanifold. Recall from Subsection 3.1 that Poisson kernels arise when we take μ to be the uniform measure. Then $c_n = 0$ for all $n \neq 0$ and $\langle z \rangle = \alpha$. In this exceptional case, the centroid simply evolves according to the Riccati equation (3.11) and the dynamics of α and ψ decouple in Eqs. (3.23a), (3.23b). (A similar observation about the crucial role of the uniform measure here was made by Pikovsky and Rosenblum [66]. The centroid evolution equation Eq. (3.23a) on the Poisson submanifold was first written down by Ott and Antonsen; see Eq.(6) in Ref. [59].)

But for the generic case of states lying off the Poisson submanifold, $\langle z \rangle$ is no longer equal to α and the reduced dynamics become fully three dimensional, due to the coupling between α and ψ induced by Eq. (3.56) and the dependence of f

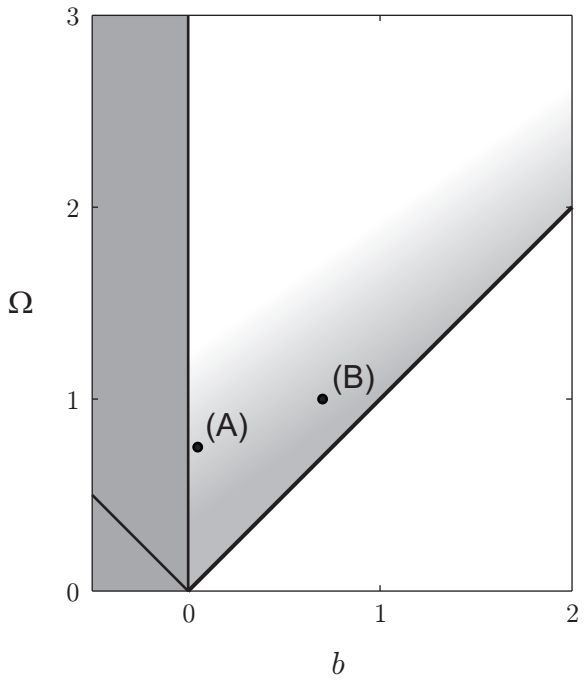

Figure 3.1: The qualitative trend of chaos observed in the first quadrant of the b-Ω parameter plane is indicated by the shaded gradient. As the shade darkens near the bifurcation curve $\Omega = b$, chaos fills increasingly larger regions of the submanifolds containing the sinusoidal initial distributions. Points (A) and (B) are chosen as (1/20, 3/4) and (17/10, 1), respectively. Representative Poincaré sections for these points are shown in Fig. 3.2 and Fig. 3.3. The region $b < 0$ is grayed out to represent that negative values of b are not physical.

and g on $\langle z \rangle$ and the higher Fourier coefficients. In the next subsection we will explore some of the possibilities for such three-dimensional flows.

Chaos in Josephson Arrays

Although the leaves of the foliation imposed by the Möbius group action are only three dimensional, they often contain chaos for commonly studied f and g [36, 84]. In this section, we showcase this phenomenon by specializing to the case of a resistively-loaded series array of overdamped Josephson junctions.

In several previous studies of sinusoidally coupled oscillators in the continuum

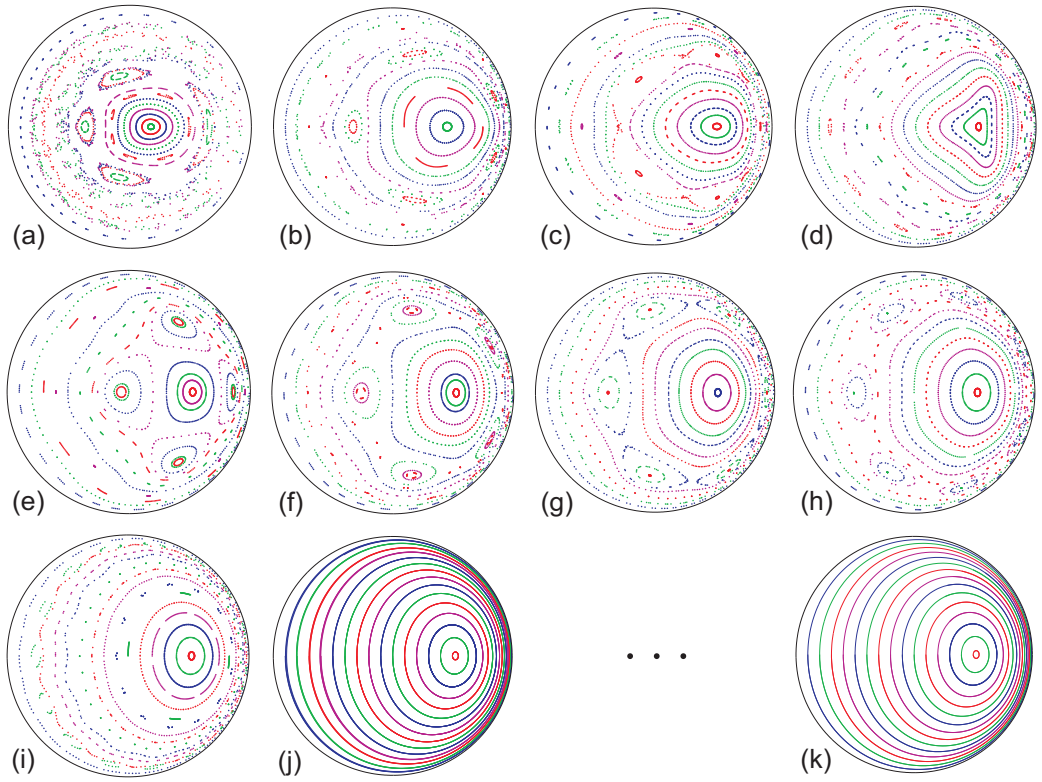

Figure 3.2: Poincaré sections of α at $\psi \,(\mathrm{mod}\, 2\pi) = 0$ for a resistively-loaded series array of Josephson junctions with $b = 1/20, \Omega = 3/4$ (pt. (A) in Fig. 3.1). The initial distributions are sinusoidal with wavenumber n, where n is (a) 1, (b) 2, (c) 3, (d) 4, (e) 5, (f) 6, (g) 7, (h) 8, (i) 16, (j) 32, and (k) ∞, i.e. on the Poisson submanifold. In (j) and (k), the complete trajectories are plotted instead of the intersections with the plane $\psi \,(\mathrm{mod}\, 2\pi) = 0$.

limit, it was found that under certain conditions, the Fourier harmonics of the phase density $\rho(\phi, t)$ evolved as if they were decoupled, at least near certain points in phase space [72, 36, 73]. In the spirit of these observations, we can get a sense for how individual harmonics contribute to the chaos by starting the system Eq. (3.23) from sinusoidal phase densities with different wavenumbers n.

To be more precise, we choose an initial density

$$\rho(\phi, 0) = \frac{1}{2\pi}(1 + \cos n\phi). \tag{3.57}$$

At $t = 0$, we choose $\alpha = \psi = 0$ so that M_t in Eq. (3.17) is simply the identity

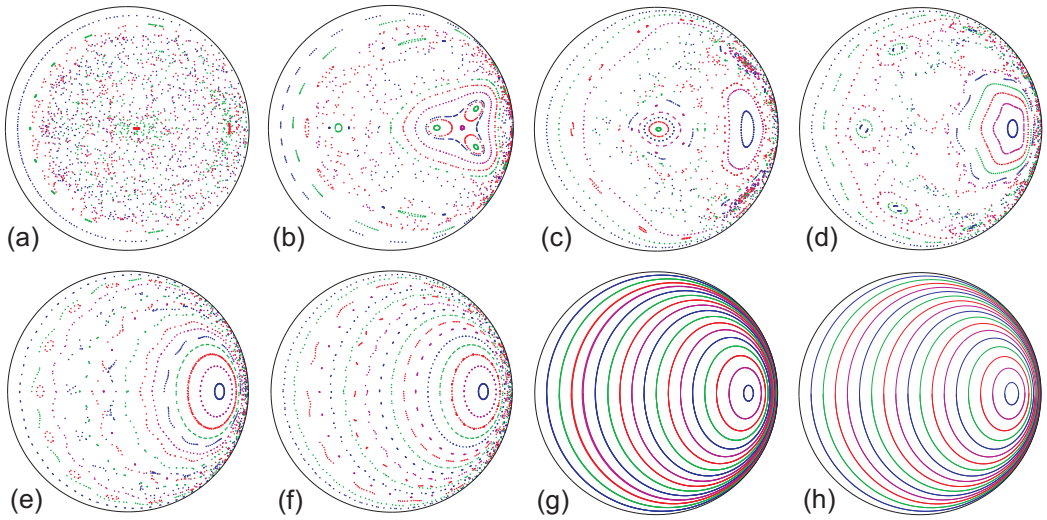

Figure 3.3: Poincaré sections of α at $\psi \pmod{2\pi} = 0$ for a resistively-loaded series array of Josephson junctions with $b = 17/10, \Omega = 1$ (pt. (B) in Fig. 3.1). The initial distributions are sinusoidal with wavenumber n, where n is (a) 1, (b) 2, (c) 4, (d) 8, (e) 16, (f) 32, (g) 64, and (h) ∞, i.e. on the Poisson submanifold. In (g) and (h), the full trajectories are plotted.

map, and the time-dependent change of variables $e^{i\phi} = M_t(e^{i\theta})$ reduces to $\phi = \theta$, initially. Thus, the corresponding density of θ is

$$\sigma_n(\theta) = \frac{1}{2\pi}(1 + \cos n\theta). \tag{3.58}$$

This density is independent of time, just as the angles θ_j were in the finite-N case.

Next we flow the density forward by $e^{i\phi} = M_t(e^{i\theta})$, where the Möbius parameters $\alpha(t), \psi(t)$ satisfy the reduced flow Eq. (3.23). Then, by our earlier results, the resulting density $\rho(\phi, t)$ automatically satisfies Eq. (3.4) and Eq. (3.5). The three-dimensional plot of $\mathrm{Re}(\alpha(t))$, $\mathrm{Im}(\alpha(t))$ and $\psi(t)$ indicates how such a single-harmonic density evolves in time, revealing for example whether it exhibits chaos, follows a periodic orbit, or approaches a fixed point.

To ease the notation, from now on we write α in Cartesian coordinates as

$$\alpha = x + iy. \tag{3.59}$$

Then the reduced flow Eq. (3.23) becomes

$$\begin{aligned}\dot{x} &= -uy + \mathrm{Im}(f)(1 - x^2 - y^2) \\ \dot{y} &= ux + \mathrm{Re}(f)(1 - x^2 - y^2) \\ \dot{\psi} &= u\end{aligned} \tag{3.60}$$

where

$$u = 2x\,\mathrm{Re}(f) + g - 2y\,\mathrm{Im}(f). \tag{3.61}$$

We immediately see that for every fixed point of this system, $|\alpha| = 1$ and ψ is arbitrary. If for some change of state variables $\zeta(x, y, \psi)$, $\eta(x, y, \psi)$, and $\xi(x, y, \psi)$, the ODEs $\dot{\zeta}$ and $\dot{\eta}$ constitute a closed two-dimensional system and $\dot{\xi}$ receives all of its t-dependence through ζ and η, then there could be other fixed points for the physical system, namely where $\dot{\zeta} = \dot{\eta} = 0$ but $\dot{\xi} \neq 0$. Examples of the second type of fixed point include the splay states found on the Poisson submanifold [79, 73].

As discussed in Subsection 3.1, series arrays of Josephson junctions with a resistive load have dynamics given by Eq. (3.1), Eq. (3.4), and Eq. (3.5), with $f = -(b + 1)/2$ and $g = \Omega + \mathrm{Re}\langle z\rangle$, where b and Ω are dimensionless combinations of certain circuit parameters [79, 49] and $\langle z\rangle$ is the complex order parameter Eq. (3.10). The dynamics of x, y and ψ are given by substitution into Eq. (3.60):

$$\begin{aligned}\dot{x} &= -uy \\ \dot{y} &= ux - \frac{b+1}{2}(1 - x^2 - y^2) \\ \dot{\psi} &= u\end{aligned} \tag{3.62}$$

with $u = \Omega + \mathrm{Re}\langle z\rangle - (b + 1)x$. From Eq. (3.56) and Eq. (3.58), $\mathrm{Re}\langle z\rangle = x + (-1)^n \frac{1}{2}(x^2 + y^2 - 1)(x^2 + y^2)^{(n-1)/2} \cos[n\psi - (n - 1)\tan^{-1}(y/x)]$.

We can now plot the phase portrait for Eq. (3.62) on the cylinder $\{(x, y, \psi) |\, x, y, \psi \in \mathbb{R}, x^2 + y^2 \leq 1\}$. In the simple case where α decouples from ψ, trajectories can

be projected down onto the α-disc without intersecting themselves or each other. However, in the more typical case that α and ψ are interdependent, we use Poincaré sections at $\psi \,(\mathrm{mod}\, 2\pi) = 0$ to sort out the structure. In these Poincaré sections, quasiperiodic trajectories (ideally) appear as closed curves or island chains, periodic trajectories appear as fixed points or period-p points of integer period, and chaotic trajectories fill the remaining regions of the unit disc.

First, however, we must choose an appropriate b and Ω. To do so, we consider their definitions in terms of the original circuit parameters: $b = R/(NR_J)$ and $\Omega = bI_b/I_c$, where N is the number of junctions, I_b the source current, R the load resistance, I_c the critical current of each Josephson junction, and R_J the intrinsic Josephson junction resistance [79, 49]. Because the resistances must be positive in the physical system, we examine only $b > 0$ in our simulations. Additionally, I_c represents a positive current magnitude, while I_b reflects both a source current magnitude and direction. Since the circuit is symmetric with respect to reversal of the source circuit (see Fig. 1 of [49]), the corresponding dynamical system is left unchanged by the reflection $\Omega \to -\Omega, x \to -x$. Hence, we also restrict our study to positive values of Ω.

If $b/\Omega > 1$, Eq. (3.62) implies there are fixed points at $x^* = \Omega/b$, $y^* = \pm\sqrt{1 - \Omega^2/b^2}$ for arbitrary ψ. In numerical experiments, the negative-y^* line of fixed points appears to attract distributions, while the positive-y^* line repels them. Along the bifurcation curve $\Omega = b$, the two rows of fixed points merge at $x = 1$, and we find computational evidence that a splay state (for which $\dot{x} = \dot{y} = 0$) emerges from their union and moves inside the unit disc along the x-axis toward the origin as b is decreased or Ω is increased. We can see from Eq. (3.62) that any such state must lie on the x-axis for all parameter values, as it did in previous

characterizations of the Poisson submanifold [49].

For the submanifolds we examined, chaos only appeared in the portion of the first quadrant in the b-Ω plane that did not contain the fixed points, and the chaos became more widespread as $b/\Omega \to 1$. This is illustrated schematically in Fig. 3.1; the gradient of increasing darkness represents increasingly pervasive chaos. In submanifolds where the chaos was not widespread, the dynamics on the Poincaré sections were reminiscent of a Kolmogorov-Arnold-Moser Hamiltonian system with hierarchies of islands enclosing nested sets of closed orbits. Alternatively, the sections had the appearance of "quasi-Hamiltonian" dynamics [78], and reflected the time reversibility common to such systems: under the transformation $t \to -t, y \to -y, \psi \to -\psi$, Eq. (3.62) remains unchanged. Nevertheless, we do not have an explicit Hamiltonian for Eq. (3.1) as we do for its averaged counterpart [83].

The increase in chaotic behavior is clearly visible in Figs. 3.2 and Fig. 3.3, which show sequences of Poincaré sections corresponding to the points (A) and (B) in Fig. 3.1. Point (A) lies at $(b, \Omega) = (1/20, 3/4)$, about $1/2$ unit from the bifurcation curve $\Omega = b$, while point (B) lies at $(b, \Omega) = (17/10, 1)$, about $1/3$ unit from $\Omega = b$. As an example of the pattern of escalating chaos, observe that Figs. 3.3(a),(b),(c) have larger, more dramatically overlapping chaotic regions than the corresponding plots (a),(b),(d) of Fig. 3.2.

Although not shown, the chaotic trajectories that produced the scattered points in the Poincaré sections are phase coherent: they cycle smoothly and unidirectionally around the splay states throughout each period of ψ. When the splay states are moved toward the edge of the unit disc by increasing b or decreasing Ω, these trajectories appear increasingly less prone to return to the same neighborhoods in the Poincaré sections, resulting in the observed amplification of chaotic behavior.

It is also possible to interpret the association between the parameter values and the intensity of the chaos in terms of the underlying physical parameters. In terms of these parameters, the limit $b/\Omega \to 1^-$ translates to $I_c/I_b \to 1^-$ or $I_b \to I_c^+$, which predicts that chaos should appear in real series arrays of Josephson junctions if the source current is reduced to near the critical current of the junctions.

Even though the Poincaré sections in Fig. 3.2 and Fig. 3.3 show differing degrees of chaos, both series of plots depict a trend of decreasing chaotic behavior with increasing n. This stems from the dependence of g on the phase centroid $\langle z \rangle$, which in turn arises because the oscillators are coupled only through their effect on the first harmonic of the phase density. For a coupling of this type, a sinusoidal phase density with a very short period and rapid oscillations (high n) "looks" nearly identical (in the Riemann-Lebesgue sense) to a uniform density. Hence, in the limit of large n, we see α decoupling from ψ, just as it does on the Poisson submanifold (recall that the Poisson submanifold corresponds to a uniform density in θ, as shown in Subsection 3.1). From this perspective, then, chaos becomes increasingly dominant as we move "away" from the Poisson submanifold, down toward small n.

Finally, we point out a surprising feature in the Poincaré sections of (A) that was common in other simulations we performed. Starting at $n = 5$, we see prominent sets of period-$(n-1)$ islands which appear for n up to 8 in Fig. 3.2. This ring of islands appears for higher n as well and forms an increasingly larger and thinner band as n is increased. Inside the dilating band, a set of nested orbits resembling the corresponding neutrally stable cycles of the Poisson submanifold grows, filling the unit disc and approaching coincidence with the trajectories on the Poisson submanifold. We are currently unclear on why exactly $(n-1)$ islands

emerge from the Möbius group action on Eq. (3.58), but pose this as an open question for future study.

Although it is tempting to try to extrapolate our numerical results to the case of non-identical oscillators, Ott and Antonsen [60] have recently demonstrated that such systems contain a two-dimensional submanifold (the generalization of the simpler Poisson submanifold studied here) that carries all the long-term dynamics of the phase centroid $\langle z \rangle$. Their results hold for the common case in which g is a time-independent angular frequency with some distribution of values among the oscillators, and f is a function of time, independent of oscillator variability. Our numerical experiments, together with this new result, indicate that the widespread neutral stability in systems of identical, sinusoidally-coupled phase oscillators is a consequence of their special symmetries and underlying group-theoretic structure.

3.2 Conformists and contrarians: a simple case

While achieving synchrony is a critical function for many biological oscillators (pacemaker cells, snowy tree crickets, smooth muscle cells during peristalsis, etc.), achieving *asynchrony* is just as critical for many others. For example it would be maladaptive to have synchronized mitosis, and synchrony in the brain to the point of epileptic seizure is not biologically acceptable. Similarly, synchrony along wildlife corridors could exaccerbate swings in population density which could lead to species extinctions [24].

Examples like these motivate the general problem of understanding better the conditions necessary and sufficient for stable asynchrony. In this section, we consider a system of coupled oscillators with a mix of attractive and repulsive inter-

actions with the mean field. In the context of a complete characterization of the fixed points of this system, we determine when the incoherent state is stable. We finish with a natural generalization to the case of arbitrary coupling.

The specific model we consider in this section is

$$\dot{\phi}_j = \omega + \frac{K_s}{N}\sum_{k=1}^{N}\sin(\phi_k - \phi_j), \quad j = 1, \ldots, N \tag{3.63}$$

where $\phi_j(t)$ is the phase of the jth oscillator at time t and ω is its natural frequency. K_s is the coupling constant of this oscillator, which is a positive constant K_1 if the oscillator is conformist and a negative constant K_2 if it is contrarian. N is the total count of oscillators in the system.

Eq. (3.63) is just the classic Kuramoto model with individual natural frequencies ω_j replaced by a unanimous natural frequency ω and the single positive coupling constant K replaced by a two-valued coupling constant K_s. A recent paper considered the case in which ω_j was kept heterogeneous [42]. As we will see here however, the long-time dynamics are actually more complicated for the homogeneous case (see Refs. [59, 60] for more about this).

The average phase of the system at any time is given by the centroid of the phases:

$$Z = Re^{i\Phi} = \frac{1}{N}\sum_{k=1}^{N} e^{i\phi_k}. \tag{3.64}$$

R is the magnitude (on $[0, 1]$) and Φ is the phase. Stepping into a rotating frame of angular speed ω, we can simplify Eq. (3.63) using the centroid variables R and Φ:

$$\dot{\phi}_j = K_s R\sin(\Phi - \phi_j), \quad j = 1, \ldots, N. \tag{3.65}$$

This rewriting indicates that all oscillators are at equilibrium if and only if either $R = 0$ or $\Phi - \phi_j = 0, \pi$. Furthermore, from the phase diagrams of Eq. (3.65), we

can see that the latter condition is only stable if $\phi_j = \Phi$ for the conformists and $\phi_j = \Phi + \pi \pmod{2\pi}$ for the contrarians. If we define p as the fraction of oscillators that are conformist, then from the definition of Z we have that $Z = pe^{i\Phi} - (1-p)e^{i\Phi}$, or $R = 2p - 1$. So the π-state can only be stable for $p \geq 1/2$. This however is not the only requirement for π-state stability, as we will soon see.

Reduction via Möbius Group Action

We jump from these preliminary observations to a complete solution of Eq. (3.63) using the framework presented in Section 3.1. This will provide us with a high-level understanding of the overall structure of the system. As shown in Section 3.1, the dynamics of Eq. (3.63) can be reduced to a six-dimensional system by the group action of the Möbius transformation. To explain how this is done, suppose the pN conformists are indexed first and rewrite Eq. (3.65) as

$$\begin{aligned} \dot{\phi}_j &= F_1 e^{i\phi_j} + \bar{F}_1 e^{-i\phi_j}, \quad j = 1, \ldots, pN, \\ \dot{\phi}_j &= F_2 e^{i\phi_j} + \bar{F}_2 e^{-i\phi_j}, \quad j = pN+1, \ldots, N, \end{aligned} \tag{3.66}$$

where $F_1 \equiv iK_1\bar{Z}/2$ and $F_2 \equiv iK_2\bar{Z}/2$. If we now parameterize the Möbius transformation as

$$M_s(w) = \frac{e^{i\psi_s} w + \alpha_s}{1 + \bar{\alpha}_s e^{i\psi_s} w} \tag{3.67}$$

with α_s on the (closed) complex unit disk and ψ_s real, then Eq. (3.65) is solved by

$$\begin{aligned} e^{i\phi_j(t)} &= M_1(e^{i\phi_j(0)}), \quad j = 1, \ldots, pN, \\ e^{i\phi_j(t)} &= M_2(e^{i\phi_j(0)}), \quad j = pN+1, \ldots, N, \end{aligned} \tag{3.68}$$

where α_1, α_2, ψ_1, ψ_2 are all set to zero at $t = 0$ and evolved according to

$$\dot{\alpha}_s = i(F_s \alpha_s^2 + \bar{F}_s), \quad s = 1, 2, \tag{3.69a}$$

$$\dot{\psi}_s = F_s \alpha_s + \bar{F}_s \bar{\alpha}_s, \quad s = 1, 2, \tag{3.69b}$$

for future and past times (see Ref. [48] for a verification of this). In addition to expressing a deep mathematical connection between Eq. (3.63) and group action, this solution foliates the N-dimensional phase space into six-dimensional invariant submanifolds.

Although the foliation provides a conceptual simplification, the behavior of Eq. (3.69) is still complicated, with regions of quasiperiodic orbits interspersed with regions of chaos. The quasiperiodicity resembles that of Kolmogorov-Arnold-Moser Hamiltonian systems, with Poincaré sections showing a fractal-like hierarchy of island chains separating nested sets of closed orbits from chaotic domains (see Ref. [48] for pictures of a related system and Ref. [41] for an informal description of the fractal formed by the quasiperiodic orbits). Even trajectories perturbed slightly off the Poisson submanifold do not in general converge back to it or imitate its behavior after long times. Rather their behavior is consistent with the analogy to perturbed systems of neutral stability.

The Poisson Submanifold

There is however a special degenerate leaf of the foliation that is only four-dimensional and has tractable dynamics. Within this leaf, the conformists and contrarians are each distributed like Poisson kernels. Thus the oscillator density on this invariant submanifold has the form

$$f(\phi) = pf_1(\phi) + qf_2(\phi), \tag{3.70}$$

where $q \equiv 1 - p$ and

$$f_s(\phi) = \frac{1}{2\pi} \frac{1 - r_s^2}{1 - 2r_s \cos(\phi - \varphi_s) + r_s^2} \tag{3.71}$$

for both the conformists ($s = 1$) and contrarians ($s = 2$). The presence of this manifold is suggested by recent work of Ott and Antonsen [59, 60] showing that if the distribution of oscillators in the Kuramoto model initially has the form of a Poisson kernel, then it will continue to be so distributed for all time. In our system here, we call this invariant set of states the *Poisson submanifold*.

The normalized Poisson kernel, Eq. (3.71), is 2π-periodic, unimodal and symmetric about its one peak. The parameters r_s and φ_s give the magnitude and phase respectively of the centroid of its density, so r_s reflects the pointedness of the peak and φ_s its angle around the complex unit circle. Even though the densities of conformists and contrarians remain Poisson kernels for all time on the Poisson submanifold, the parameters r_1, r_2, φ_1, φ_2 may vary widely in time.

We now find the four-dimensional dynamics on the Poisson submanifold in terms of these variables, r_1, r_2, φ_1, φ_2. Eq. (3.69) above gives the six-dimensional dynamics on any one leaf of the foliation, so we might expect some reduction of this system on the Poisson submanifold. Indeed, it turns out that only the equation for α_s is necessary to describe the state of the system in this region.

To show this, we start by considering the large-N (or continuum) limit of Eq. (3.64):

$$Z(t) = \int_0^{2\pi} e^{i\phi} f(\phi, t) d\phi. \tag{3.72}$$

On the Poisson submanifold, each density function f_s is a Poisson kernel, which has the Fourier expansion

$$f_s = \frac{1}{2\pi}\left\{1 + \sum_{k=1}^{\infty}\left[\bar{\alpha}_s^k e^{ik\phi} + \alpha_s^k e^{-ik\phi}\right]\right\} \tag{3.73}$$

where $\alpha_s \equiv r_s e^{i\varphi_s}$. Substitution of Eq. (3.70) and then Eq. (3.73) into Eq. (3.72)

yields

$$Z = p\alpha_1 + q\alpha_2. \tag{3.74}$$

We can then substitute our definition of F_s (that is, $F_s \equiv iK_s\bar{Z}/2$) into Eq. (3.69a) to obtain

$$\dot{\alpha}_s = \frac{K_s}{2}(Z - \bar{Z}\alpha_s^2) \quad s = 1, 2, \tag{3.75}$$

and proceed with a substitution of Eq. (3.74) to conclude that

$$\dot{\alpha}_s = \frac{K_s}{2}[p\alpha_1 + q\alpha_2 - (p\bar{\alpha}_1 + q\bar{\alpha}_2)\alpha_s^2] \quad s = 1, 2. \tag{3.76}$$

Eq. (3.76) gives the complete dynamics on the Poisson submanifold. The equation of motion for ψ_s is not necessary to identify the system state in this subregion because the state anywhere on the Poisson submanifold can be uniquely identified by r_1, r_2, φ_1, φ_2, and α_1, α_2 specify these values uniquely through $\alpha_1 = r_1 e^{i\varphi_1}$ and $\alpha_2 = r_2 e^{i\varphi_2}$. (For a more extensive mathematical explanation of this issue, consult §V.B. of Ref. [48].)

By substituting $\alpha_1 = r_1 e^{i\varphi_1}$ and $\alpha_2 = r_2 e^{i\varphi_2}$ into Eq. (3.76), we can write this system in terms of real variables as

$$\begin{aligned}
\dot{r}_1 &= C(1 - r_1^2)(pr_1 + qr_2\cos\delta), \\
\dot{r}_2 &= -D(1 - r_2^2)(pr_1\cos\delta + qr_2), \\
\dot{\varphi}_1 &= qC\sin\delta\left(\frac{r_2}{r_1} + r_1 r_2\right), \\
\dot{\varphi}_2 &= pD\sin\delta\left(\frac{r_1}{r_2} + r_1 r_2\right),
\end{aligned} \tag{3.77}$$

where we have rescaled time by $t \to 2t/(K_1 + |K_2|)$ and let $\delta \equiv \varphi_2 - \varphi_1$, $C \equiv K_1/(K_1 + |K_2|)$ and $D \equiv 1 - C$. We can further reduce the dimension of the

dynamics by considering only relative phase:

$$\begin{aligned}
\dot{r}_1 &= C(1-r_1^2)(pr_1 + qr_2\cos\delta), \\
\dot{r}_2 &= -D(1-r_2^2)(pr_1\cos\delta + qr_2), \\
\dot{\delta} &= \sin\delta\left[pD\Big(\frac{r_1}{r_2} + r_1 r_2\Big) - qC\Big(\frac{r_2}{r_1} + r_1 r_2\Big)\right].
\end{aligned} \tag{3.78}$$

Note that since φ_1 and φ_2 appear only through δ in $\dot{\varphi}_1$ and $\dot{\varphi}_2$, any fixed point of Eq. (3.78) that is not a fixed point of Eq. (3.77) will have constant $\dot{\varphi}_1$ and $\dot{\varphi}_2$ and hence move around the complex unit circle at constant speed. As we will demonstrate, the only state of this kind is a traveling wave state.

Preview of Stable States

As we will see, a fixed point analysis of Eq. (3.78) uncovers four possible equilibrium states (Fig. 3.4):

(a) the *incoherent state*, in which both the conformists and contrarians are uniformly distributed around the complex unit circle (i.e. $r_1 = r_2 = 0$),

(b) the *π-state*, in which the conformists and contrarians are completely synchronized into two antipodal delta functions (i.e. $r_1 = r_2 = 1$),

(c) a *blurred π-state* in which the conformists and contrarians are each only partially synchronized with peaks separated by a phase of π, and

(d) a *traveling wave state* in which the conformists and contrarians exhibit full and partial synchrony respectively and are offset by an angle less than π.

Per our discussion following Eq. (3.65), the oscillators in the incoherent state and π-state must be at equilibrium. As we will see, $pr_1 = qr_2$ for the blurred π-states, so for them, $Z = pr_1 e^{i\varphi_1} - qr_2 e^{i\varphi_1}$, or $R = 0$. So the oscillators in this state

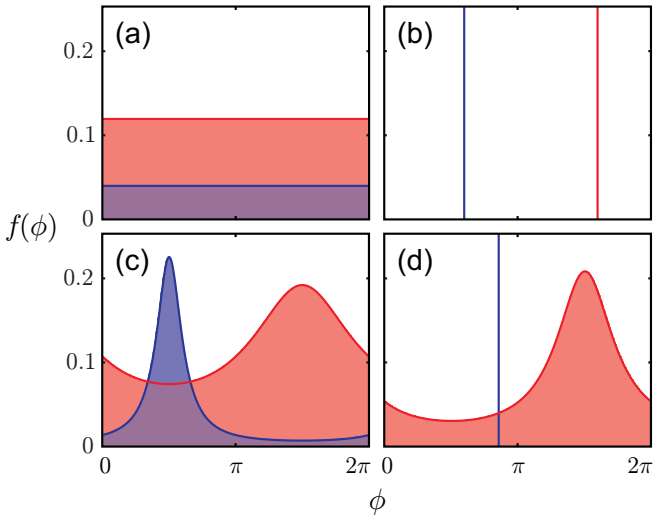

Figure 3.4: Oscillator phase densities that lie on the Poisson submanifold and are stable (unchanging in time up to a constant rotation). Conformists are shown in blue and contrarians in red. By name, the states are the (a) incoherent state, (b) π-state, (c) blurred π-state and (d) traveling wave state.

are also at rest. However the conformists in the traveling wave state cannot remain at a fixed phase as neither $R = 0$ nor $\phi_j = \Phi$ for them. So this configuration must be in a perpetual state of revolution around the complex unit circle.

Fixed Point Analysis

Each of the three equations in Eq. (3.78) has two factors on the left-hand side that may be zero, so there are at most eight types of fixed points that we need to consider. Three of these possibilities end up being special cases of a fourth, so

Eq. (3.78) has just five types of fixed points:

$$r_1 = r_2 = 1; \delta = 0, \pi, \tag{3.79a}$$

$$r_1 = r_2 = 1; C = p, \tag{3.79b}$$

$$pr_1 = qr_2; \delta = \pi, \tag{3.79c}$$

$$r_1 = 1; r_2 = (2V - 1)^{-1/2}; \cos\delta = -qr_2/p, \tag{3.79d}$$

$$r_1 = (2/V - 1)^{-1/2}; r_2 = 1; \cos\delta = -pr_1/q, \tag{3.79e}$$

where $V \equiv (q/p)(C/D)$. We can see immediately that the first type is the π-state, the second is a special case that lies only on the line $C = p$, the third must include both the incoherent state and the blurred π-states, and the fourth and fifth must be traveling wave states. We now determine where these five classes of fixed points exist and are stable on the p-C unit square.

For each fixed point, we can analyze its form to determine where it exists and its Jacobian to determine where it is stable (with r_1, r_2, δ treated as Cartesian coordinates). This yields the following information: The π-state (which exists for all p and C) is stable for $\delta = \pi$ when $p > \max\{C, 1/2\}$ and unstable otherwise. The special line of fixed points along $C = p$ is stable on the segment with endpoints given by $\cos\delta = -q/p$ when $p > 1/2$ and unstable elsewhere. With respect to the blurred π-states, which exist along the line $pr_1 = qr_2$, all are stable when both $p < 1/2$ and $C < 1 - 2pq$ and some are stable when $C < q$. Specifically, in the region $1 - 2pq < C < q$ the stable blurred π-states are found from $r_1 = 0$ to

$$r_1 = \sqrt{\frac{Dq/p - C}{C - Dp/q}}, \tag{3.80}$$

and in the region $1/2 < p < D$ the stable blurred π-states are located between $r_2 = 0$ and

$$r_2 = \sqrt{\frac{D - Cp/q}{D - Cq/p}}. \tag{3.81}$$

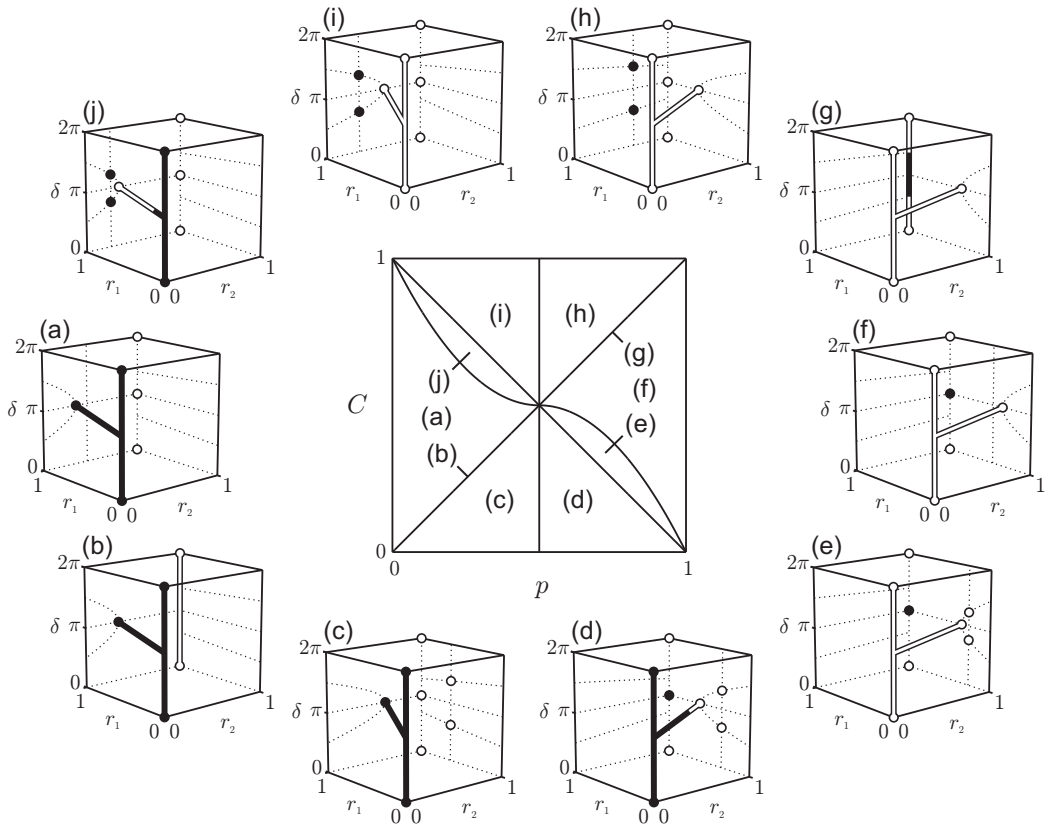

Figure 3.5: The p-C parameter plane partitioned into the ten regions with qualitatively distinct three-dimensional phase portraits, together with these ten phase portraits. Black and white points and lines denote fixed points and lines of fixed points of Eq. (3.78). Isolated fixed points are colored black when they are stable—i.e. when all of their eigenvalues have negative real parts. The black lines of fixed points are also stable; they have one zero eigenvalue and two eigenvalues with negative real parts. All other fixed points are unstable. The dotted lines indicate either back edges of the unit cube or important nullclines, or both. The (p, C) points for the shown phase portraits are (a) (1/4,1/2), (b) (1/4,1/4), (c) (3/8,1/4), (d) (5/8,1/4), (e) (3/4,8/31), (f) (3/4,1/2), (g) (3/4,3/4), (h) (5/8,3/4), (i) (3/8,3/4), and (j) (1/4,23/31).

These observations suggest that the incoherent state ($r_1 = r_2 = 0$) is stable when $C < q$, which can be verified by rewriting Eq. (3.76) in terms of Cartesian coordinates and diagonalizing the Jacobian. A less obvious and more elegant calculation is given in the next section. Lastly, the traveling wave state (3.79d) exists and is stable on $C \geq \max\{p, 1 - 2pq\}$, while the traveling wave state (3.79e) exists and is *unstable* on $C < \min\{p, 2pq\}$.

Combining the results of this analysis, we obtain Fig. 3.5. This figure suggests a variety of conclusions. For instance, it appears that the the traveling wave states are born in a pitchfork bifurcation and die when they merge with the line at $r_1 = r_2 = 1$. This can be confirmed with a center manifold calculation. The collective picture also indicates that the central point $(p, C) = (1/2, 1/2)$ is an organizing center for the dynamics; it is a point of intersection for the boundaries of all ten qualitatively unique regions of the parameter space.

3.3 Stability of complete asynchrony for arbitrary coupling

As an additional conclusion, Fig. 3.5 implies that the incoherent state ($r_1 = r_2 = 0$) is stable for $C < q$ and unstable otherwise. The $C < q$ condition is interesting because we can rewrite it as $\langle K \rangle < 0$ where $\langle K \rangle$ is the mean K ($K = pK_1 + qK_2$). This raises the question of whether it might be true that the incoherent state is stable when $\langle K \rangle < 0$ for an arbitrary density $\Gamma(K)$.

To prepare for the general calculation, let us first see how it might work for our current system. Suppose $|\alpha_1| \ll 1$ and $|\alpha_2| \ll 1$, where $|\cdot|$ denotes the complex modulus. Then Eq. (3.76) approaches the linear system

$$\dot{\alpha}_s = \frac{K_s}{2}(p\alpha_1 + q\alpha_2) \quad s = 1, 2. \tag{3.82}$$

Multiplying $\dot{\alpha}_1$ by p and $\dot{\alpha}_2$ by q, and summing corresponding sides of Eq. (3.82) for $s = 1, 2$, gives by Eq. (3.74)

$$\dot{Z} = \frac{1}{2}\langle K \rangle Z, \tag{3.83}$$

where $\langle K \rangle \equiv pK_1 + qK_2$, i.e. $\langle K \rangle$ is the mean coupling strength. In polar coordi-

nates, Eq. (3.83) is the system

$$\begin{aligned} \dot{R} &= \frac{1}{2}\langle K\rangle R, \\ \dot{\Phi} &= 0. \end{aligned} \tag{3.84}$$

So if $\langle K\rangle < 0$, then R vanishes exponentially fast, while if $\langle K\rangle > 0$, R grows rather than vanishing.

The above reasoning can be generalized to any continuous distribution of coupling constants $\Gamma(K)$ as follows. To do so, we start by considering Z for the case of both a continuous distribution of oscillator phases and a continuous distribution of coupling constants:

$$Z(t) = \int_{-\infty}^{\infty}\left(\int_0^{2\pi} e^{i\phi} f(\phi, K, t)d\phi\right)\Gamma(K)dK. \tag{3.85}$$

Here f is the continuous joint probability distribution of ϕ and K as a function of time t (that f is continuous for all times is an assumption). If for each t and K, f has the form of a Poisson kernel, then we can write it as

$$f = \frac{1}{2\pi}\left\{1 + \sum_{k=1}^{\infty}\left[\bar{\alpha}(K,t)^k e^{ik\phi} + \alpha(K,t)^k e^{-ik\phi}\right]\right\}. \tag{3.86}$$

Substituting this into Eq. (3.85) yields

$$Z(t) = \int_{-\infty}^{\infty}\alpha(K,t)\Gamma(K)dK. \tag{3.87}$$

By a method introduced by Ott and Antonsen [59],

$$\dot{\alpha}(K) = \frac{K}{2}(Z - \bar{Z}\alpha^2), \tag{3.88}$$

which is the continuous-K analog of Eq. (3.75). For $|\alpha| \ll 1$, this has the linear approximation, $\dot{\alpha} = KZ/2$. We can compute $\dot{Z}$ for this approximation by taking a time derivative of both sides of Eq. (3.87) and then substituting in $\dot{\alpha} = KZ/2$ to obtain

$$\dot{Z} = \frac{1}{2}\langle K\rangle Z, \tag{3.89}$$

where $\langle K \rangle$ is now the mean of $\Gamma(K)$: $\langle K \rangle \equiv \int_{-\infty}^{\infty} K\Gamma(K)dK$. In terms of this generalization, our preliminary calculation simply considers the special case of $\Gamma(K) = p\delta(K - K_1) + q\delta(K - K_2)$.

Although these results are, strictly speaking, only applicable to the Poisson submanifold of sinusoidally coupled identical oscillators, there might be ways of generalizing them to the case of nonidentical oscillators, perhaps even to the case of nonsinusoidal coupling. Recent work by Ott and Antonsen [60] has shown that for a Lorenzian distribution of natural frequencies for the oscillators (that is, for nonidentical oscillators of a particular type), all trajectories approach the equivalent of our Poisson submanifold in long time. Thus a statement regarding the stability of the incoherent state on this submanifold for this case of nonidentical oscillators would apply to all trajectories, not just those starting on the Poisson submanifold. Whether such generalizations exist remains an open problem for future work.

CHAPTER 4

PAIR FORMATION

At school, students may often find themselves pairing off for a formal dance or laboratory course. However in cultures where monogamy is the norm, the process of pair formation is frequently of more than minor consequence: it can be critical for social or reproductive success. Outside of social contexts, matching processes occur naturally in many fields, including organic chemistry, statistical physics, and computer science. In Section 4.1, we give a brief overview of the corresponding literature and its main results.

In Section 4.2, we examine the classic derivations of Flory and Page to illustrate how matching processes can be studied mathematically. The techniques used in these calculations are generally useful only for the case of a simple path and several other idealizations. However they help to provide an indication of why it is challenging to accurately analyze more realistic network topologies.

To address the challenge of studying pair formation on a broader class of networks, we introduce a new model for matching on the two-dimensional grid graph in Section 4.3. This model involves heterogeneous agents distinguished from each other by a "quality factor." We show that this model has an approximative analysis that is substantially simpler than that needed for the current two-dimensional lattice models, and we perform simulations to demonstrate the accuracy of our derived estimates. We conclude by providing a short proof of a new upper bound on the maximum possible fraction of isolated nodes on the grid graph. To our knowledge this bound is better than all previous bounds in literature.

4.1 Many fields, a common problem

The first analysis of the pair formation problem was provided by Flory in 1939 [30]. He began his paper with a description of a chemistry experiment by Carl Shipp Marvel (this author's second cousin three times removed) involving aldol condensation between pairs of adjacent side chains on a long polymer of methyl vinyl ketone. After 24 hours, 15% of the substituents remained unreacted. By formulating the problem in terms of difference equations, Flory was able to show that the expected fraction of isolated substituents was e^{-2}, or about 13.53%.

The next appearance in literature of a related problem came with Alfred Rényi's statement and analysis of the parking problem [67]: if cars are parked uniformly at random in the available space along a curb, what is the fraction of unoccupied space remaining when no more cars can be parked? Rényi's original solution involved an integral which could be solved numerically to yield a fraction of about 25.2%. Alternative approaches that reach the same percentage have since been proposed by Gonzalez et al. [37], Hemmer [40], and Evans [26].

More recently, matching algorithms have been analyzed in computer science literature. The earliest of this literature focuses on algorithms for obtaining maximal or near maximal matchings (see for example Mulmuley et al. [54] and Galil [33]). This work was followed by studies of randomized greedy matching, with results including a tight lower bound on the expected fraction of matched nodes in trees [22], and a demonstration that for an arbitrary graph there exists an $\epsilon > 0$ such that the expected fraction of matched nodes is at least $1/2 + \epsilon$ of the maximum possible [7]. Dyer et al. [23] and Aronson et al. [8] have also characterized the asymptotic behavior of randomized greedy matching on sparse random graphs.

In physics literature, pair formation has been studied as random sequential adsorption and its cooperative generalizations [26]. This has applications for chemisorption in one- and two-dimensional systems, as well as for other reaction and deposition processes. There is also a substantial body of literature on "sphere parking" in which a space of given dimension is partially filled by inserting balls of the same dimension uniformly at random into spaces where they will fit. The analytical methods used here rely heavily on recursion techniques, hierarchical rate equations, and dynamical Markov formulations [58]. Evans [26] provides an exhaustive review of the literature prior to 1993.

More recent work has been focused in several specialized areas. Mathematical papers such as Penrose and Yukich [63] analyze sphere parking with tools from probability. In physics literature, D'Orsogna et al. [19] has examined the successive binding of two particle types onto a single one-dimensional lattice, and D'Orsogna et al. [20] has analyzed a molecular ratchet driven by random sequential absorption (perhaps the main biophysical mechanism for driven translocation of polymers through pores). Variants of the conventional models involving reversible deposition, size effects of deposited particles, and particle sliding have also been explored.

4.2 Randomized greedy matching on a line

The one-dimensional case of randomized greedy matching (or dimer deposition, or discrete sphere parking) is particularly instructive and can—unlike randomized greedy matching in higher-dimensional cases—be solved exactly. The standard randomized greedy matching algorithm on a graph $G = (V, E)$ is as follows [22]:

begin

$M \leftarrow \emptyset$;

while $E(G) \neq \emptyset$ **do**

begin

A: Choose $e = \{u, v\} \in E$ uniformly at random

$G \leftarrow G \backslash \{u, v\}$;

$M \leftarrow M \cup \{e\}$

end;

Output M

end

Here we initialize M, the set of matchings, to be the empty set $\emptyset$. We then select an edge from E uniformly at random, remove its nodes from V and all edges involving them from E, and add the selected edge to M. We repeat these steps until E is empty, and finish by returning the final matching M.

When G is a simple path of n nodes, we can calculate that this process leaves an average of e^{-2} single nodes in the large-n limit [30]. To do this, we start by observing that the probability of any one edge being chosen as the first edge is $1/(n-1)$, and no matter which edge is chosen, the algorithm will separate the path into two disjoint paths of k and $(n-2-k)$ nodes each, where k may range from 0 to $(n-2)$. Hence if we let I_n represent the expectation of the final number of the single nodes for the path of length n, I_n satisfies the recurrence relation:

$$I_n = \frac{1}{n-1} \sum_{k=0}^{n-2} (I_k + I_{n-2-k}) \tag{4.1}$$

with initial conditions $I_0 = 0$ and $I_1 = 1$ obtained directly from the definition of I_n. Formally, this equation follows from a general property of the expectation of

random variables:

$$E(X) = \sum_{y \in \mathcal{Y}} E(X|Y = y)P(Y = y), \tag{4.2}$$

where $\mathcal{Y}$ is the set of all possible values for y. Returning to Eq. (4.1), we have by reindexing,

$$(n-1)I_n = 2\sum_{k=0}^{n-2} I_k. \tag{4.3}$$

If we replace n in Eq. (4.3) with $(n-1)$ and subtract the result from the original Eq. (4.3), we obtain

$$(n-1)I_n - (n-2)I_{n-1} = 2I_{n-2}. \tag{4.4}$$

In simplify this recurrence relation, let $J_n = I_n - I_{n-1}$ and $J_0 = I_0$, so $I_n = \sum_{k=0}^{n} J_k$. We can then rewrite Eq. (4.4) as

$$(n-1)J_n = -J_{n-1} + \sum_{k=0}^{n-2} J_k. \tag{4.5}$$

If we again replace n in Eq. (4.5) with $(n-1)$ and subtract the result from the original Eq. (4.5), we find

$$(n-1)J_n - (n-2)J_{n-1} = -J_{n-1} + 2J_{n-2}. \tag{4.6}$$

By rearrangement, this becomes $(n-1)(J_n - J_{n-1}) = -2(J_{n-1} - J_{n-2})$, so by defining $K_n = J_n - J_{n-1}$ and $K_0 = J_0$, we have that $K_n = -2K_{n-1}/(n-1)$, or

$$K_n = \frac{(-2)^{n-1}}{(n-1)!}. \tag{4.7}$$

Retracing our steps, $J_n = \sum_{k=0}^{n} K_k$ and so $I_n = \sum_{k=0}^{n} \sum_{j=0}^{k} K_j$, which by a triangle summation is $I_n = \sum_{k=0}^{n}(n+1-k)K_k$. Further rearrangement yields $I_n = nJ_n + 2J_{n-1}$. So by the usual expansion of e^a: $\sum_{k=0}^{\infty} a^k/k!$, the fraction of isolated single nodes in the large-n limit (or the *singles fraction* as we will call it from now on) is just

$$\lim_{n\to\infty} \frac{I_n}{n} = e^{-2}. \tag{4.8}$$

Although this approach works well for the path, one dimension turns out to be special; calculating singles fractions for randomized greedy matching in higher dimensions is generally infeasible [26]. This is due to the loss of a shielding property that is present in one dimension but incomplete in higher dimensions. To illustrate the property with a calculation of Page [61], consider the related problem of computing the probability $P(k,n)$ that the kth node in a path of n nodes is single. This is equivalent to the probability that the kth node is single for both the path of nodes $1,\ldots,k$ and the path of nodes $k,\ldots,n$, which are two *independent* conditions in one dimension. So we may write $P(k,n)$ as

$$P(k,n) = P(k,k)P(n-k+1,n-k+1). \tag{4.9}$$

This reduces our work to computing $P(1,n)$. To do the latter, we first observe that

$$P(1,n) = \frac{1}{n-1}\sum_{k=1}^{n-2} P(1,k). \tag{4.10}$$

We can then replace n by $(n-1)$ in this equation and subtract the result from the original to obtain

$$(n-1)(P(1,n) - P(1,n-1)) = -(P(1,n-1) - P(1,n-2)). \tag{4.11}$$

This implies

$$P(1,n) - P(1,n-1) = \frac{(-1)^{n-1}}{(n-1)!}, \tag{4.12}$$

which tells us that

$$P(1,n) = \sum_{k=0}^{n-1} \frac{(-1)^k}{k!}. \tag{4.13}$$

So

$$P(k,n) = \sum_{r=0}^{k-1} \frac{(-1)^r}{r!} \sum_{s=0}^{n-k} \frac{(-1)^s}{s!}. \tag{4.14}$$

As expected, this is consistent with the e^{-2} result in the double limit that both k and n are taken to infinity.

The above derivation works because the probabilities that a node is single in the two paths on either side of it are independent of each other. In higher dimensions, individual nodes do not break down the space into statistically independent regions in the same way. As explained by Evans [26], this lies at the heart of the analytical intractability of dimer filling on higher-dimensional grids. For two- and three-dimensional problems, for example, the best available method for approximating the singles fraction involves truncation of large systems of equations; see the references in Evans [26] for the details of this approach.

4.3 Pair formation on a grid

Since we are concerned with social systems, we have an interest in network topologies with higher connectivity than the simple path or cycle. Yet as Evans [26] describes, exact analysis of random greedy matching on such networks is generally infeasible (and even good approximations challenging). Moreover, individuals in real social networks are heterogeneous, and this heterogeneity plays an important role in matching processes. For example, certain individuals are sometimes viewed as more desirable partners than others and this influences the choice of who partners with whom. Yet the standard algorithm for randomized greedy matching treats nodes as distinguishable only by their location in the network if at all.

Motivated by these concerns, we introduce a model of pair formation that offers a solution to both problems at once: it allows for the assignment of different "quality factors" to different nodes, with matchings restricted by these quality factors, and it affords an easy method of deriving estimates for many of the quantities of interest in the model, including the singles fraction. Although we will consider only

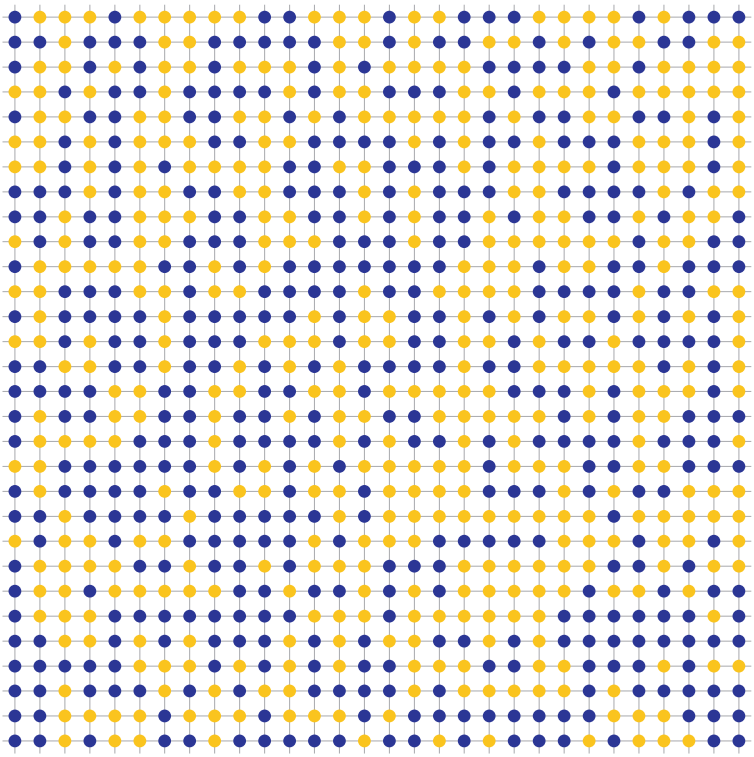

Figure 4.1: The matching process that we propose takes place on an $m \times n$ grid with helical boundary conditions, meaning that the kth rightward pointing endpoint is attached to the $(k+1)$th leftward pointing endpoint. Here $m = n = 30$, but m and n are usually larger. We assign a quality factor of high (H) or low (L) to each of the nodes independently and with equal probability. These assignments are shown in gold and blue respectively. We then proceed through the nodes in dictionary order, matching each node with an adjacent node of like quality if one is available. (If more than one is available, we choose a partner for the node uniformly at random.)

the case of two quality factors and the topology of a two-dimensional grid graph, our analysis generalizes to an arbitrary set of quality factors and potentially any regular graph topology.

We start with the two-dimensional $m \times n$ grid graph with helical boundary conditions: the right end of the kth row is contiguous with the left end of the $(k+1)$th row for all $k = 1, \ldots, n-1$ (Fig. 4.1). This allows us to index the nodes in a natural way from 1 to mn, starting at the leftmost node of the top row (node

1) and proceeding left-to-right across the rows and down the spiral until we reach the rightmost node in the mth row (node mn). We assign to each node a high (H) or low (L) quality factor to represent an objective score of the individual's desirability as a partner or mate. (We assume that such a score is a meaningful quantity.) Each assignment is statistically independent of other assignments, and each value has an equal probability of being assigned to any given node.

The pair formation process then consists of running through the nodes in dictionary order (1 through mn) and pairing each unpaired node with an adjacent node having the same quality factor if any are available. If none is available then the node remains unpaired, and if more than one is available then a partner is chosen from the available options uniformly at random. We assume m is long enough that boundary effects in the column direction are negligible.

It is worth noting that this model is essentially a combination of site percolation and greedy matching. A current estimate for the site percolation threshold p_c on the grid graph (the $\mathbb{Z}^2$ lattice in percolation parlance) is $p_c \in [0.592, 0.593]$ with 99.9999% confidence [11]. Hence both the high and the low quality nodes are below percolation threshold if the H and L assignments are made with equal probability.

Simulation Results

Monte Carlo simulations of this matching process were performed for $m = n = 10^4$. A patch from a typical run is shown in Fig. 4.2. The singles fraction from 10 such runs, where nodes 1 through 10^7 were discarded as an initial transient, was 0.19424 ± 0.00004 (where the error corresponds to one standard deviation from the mean). This singles fraction was almost identical for runs with $m = n = 10^3$ where the first 10^5 nodes were discarded, although of course more runs were necessary to

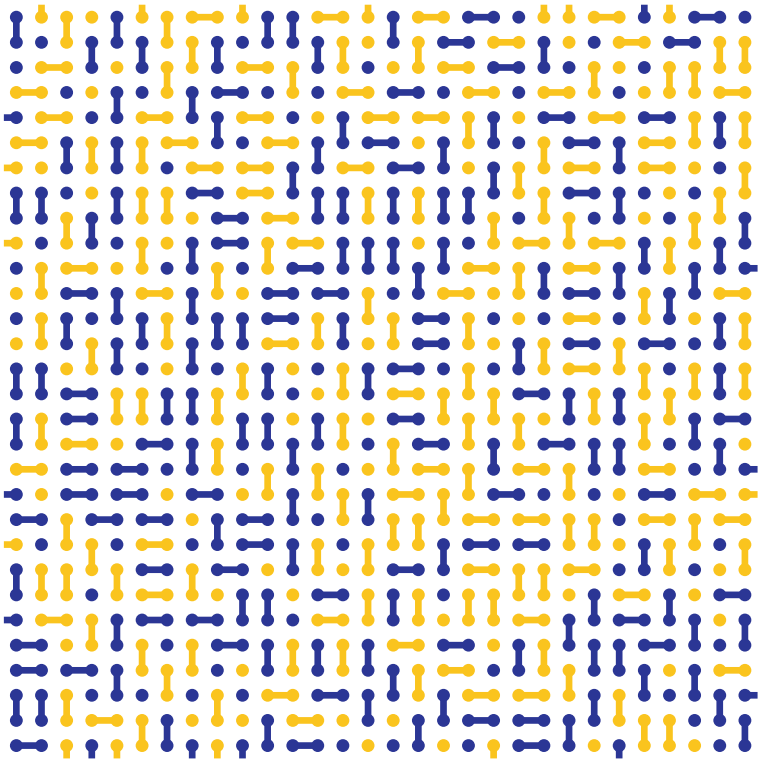

Figure 4.2: A 30×30 node square from a $10^4 \times 10^4$ node Monte Carlo simulation of the matching process described. High quality nodes and pairs are shown in gold, while low quality nodes and pairs are shown in blue. The resulting singles fraction is 0.19424 ± 0.00004 for both quality factors. Since the nodes are gold or blue with equal probability, about 6.25% of the nodes remain single simply because none of the four nodes to which they are connected have their same quality factor. The balance are single because other nodes of equal quality paired with their potential partners before they could.

achieve the same error.

Further testing indicated that discarding an initial transient as described was enough to essentially eliminate boundary effects, and that the singles fraction and other measured parameters were insensitive to changes in n over a wide range. Furthermore, we performed the simulations using both the default pseudo-random number generator provided in the MATLAB software suite and the Mercenne Twister generator developed by Matsumoto and Nishimura. The results were nearly identical, with all numerical values reported here taken from the Mercenne

Twister simulations.

As we will see in the following subsection, the value from the analysis is a little lower, at $5 - 2\sqrt{29/5}$, or about 0.18336. This is due to a single (clearly marked) approximation made in the course of the analysis. Refining this approximation could potentially increase the accuracy of the method arbitrarily, but here we keep our treatment as simple as possible to demonstrate the approach.

Derivation of Singles Fraction

Suppose we have considered for matching nodes 1 through $(v-1)$ and are preparing to consider node v for matching. At this point, the nodes of the helical grid graph may be partitioned into four regions: (1) nodes that have neither been considered directly for matching nor as partners to other nodes directly considered (this region is composed of nodes $(v+n)$ and beyond), (2) nodes that have been considered as a potential partner once before (nodes $(v+1)$ through $(v+n-1)$), (3) nodes that have been considered *twice* as a potential partner (node v only), and (4) nodes that have been considered twice as a potential partner and also directly for matching (nodes preceding node v).

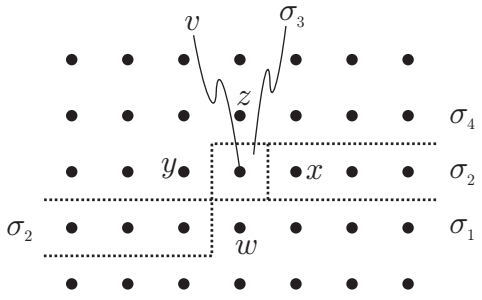

Figure 4.3: The nodes of the grid graph (with helical boundary conditions) may be partitioned into four regions of fixed probabilistic density, as indicated by the dotted lines. The σ's denote the probabilities that the nodes in the corresponding regions are single, and the v, w, x, y and z label the indicated nodes.

If we assume that the probability that any one node in these regions is at equilibrium, then we can denote these fixed probabilities of being single for the regions (1), (2), (3) and (4) as σ_1, σ_2, σ_3 and σ_4, respectively. Clearly, $\sigma_1 = 1$ and our remaining task is determine the values of the other three σ's.

First, we make a key observation: when v is in region (3) and single, it cannot be matched with y or z, because this would require that y or z be single, in which case they would have paired with v if they could when they were in region (3). Thus we only need to consider w and x as potential partners for v. Letting u denote either w of x, we introduce several definitions:

f : the probability that u has the same quality factor as v

p_u : the probability that u and v can bond, assuming v is single (i.e. that u is single and u and v have the same quality factor)

b_u : probability that u and v do bond, assuming v is single

By the pair bonding algorithm, we pick uniformly at random between w and x if both are single and have the same quality factor as v. So we can write b_w and b_x in terms of p_w and p_x as follows:

$$b_w = p_w(1 - p_x) + p_w p_x/2, \tag{4.15a}$$

$$b_x = (1 - p_w)p_x + p_w p_x/2. \tag{4.15b}$$

Using the fact that σ_3 is the probability that v is single, and b_w and b_x are conditional on this probability, we can use these quantities to relate the σ's to each

other:

$$\sigma_2 = \sigma_1 - \sigma_3 b_w, \tag{4.16a}$$

$$\sigma_3 = \sigma_2 - \sigma_3 b_x, \tag{4.16b}$$

$$\sigma_4 = \sigma_3 - \sigma_3(b_w + b_x). \tag{4.16c}$$

Finally, since $\sigma_1 = 1$, we know that $p_w = f$, and for equal assignment of H and L quality factors, $f = 1/2$. This leaves us with five equations and six unknowns: p_x, b_w, b_x, σ_2, σ_3 and σ_4. We solve this system for σ_4, the singles fraction, in terms of p_x. After doing so, we will discuss approximations for relating p_x to f and σ_1 in order to obtain a numerical value for σ_4.

First we add the corresponding sides of Eq. (4.16a) and Eq. (4.16b) to obtain

$$\sigma_3 = \sigma_1 - \sigma_3(b_w + b_x). \tag{4.17}$$

By rearranging this to be an expression of σ_3 and substituting into Eq. (4.16c) for σ_3, we obtain an expression of σ_4 in terms of b_w and b_x:

$$\sigma_4 = \sigma_1 \frac{1 - b_w - b_x}{1 + b_w + b_x}. \tag{4.18}$$

Second, adding the corresponding sides of Eq. (4.15a) and Eq. (4.15b) gives

$$b_w + b_x = p_w(1 - p_x) + (1 - p_w)p_x + p_w p_x. \tag{4.19}$$

The right-hand side of this equation is just $1 - (1 - p_w)(1 - p_x)$, so Eq. (4.18) reduces to

$$\sigma_4 = \sigma_1 \frac{(1 - p_w)(1 - p_x)}{2 - (1 - p_w)(1 - p_x)} \tag{4.20}$$

or, for our constants ($\sigma_1 = 1$ and $p_w = f = 1/2$),

$$\sigma_4 = \frac{1 - p_x}{3 + p_x}. \tag{4.21}$$

This is an exact expression without approximations for the singles fraction. For example, if we substitute in the value for p_x found in the Monte Carlo simulations described above: $p_x = 0.34944 \pm 0.00008$, we obtain 0.19423 ± 0.00002, consistent with the Monte Carlo singles fraction of $\sigma_4 = 0.19424 \pm 0.00004$. The challenge, though, is to express p_x in terms of the unknowns that we already have, and determining how to do so is a nontrivial problem that we will not fully address here.

However, there is a natural two-step approximation that we do want to explore. Observe that we can write p_x without approximation as

$$p_x = \Pr(A|B \cap C) \Pr(B|C) \tag{4.22}$$

where $A = \{v \text{ and } x \text{ have the same quality factor}\}$, $B = \{v \text{ is single}\}$ and $C = \{x \text{ is single}\}$. If we then assume that B is approximately independent of C, i.e. that $\Pr(B|C) \approx \Pr(B)$, and that A is approximately independent of B and C, i.e. $\Pr(A|B \cap C) \approx \Pr(A)$, then we can write

$$p_x \approx f\sigma_2 \tag{4.23}$$

since $\Pr(A) = f$ and $\Pr(B) = \sigma_2$. We emphasize that neither of these approximations is exact: from simulation we find that $\Pr(B|C) = 0.77456 \pm 0.00005$ while $\Pr(B) = 0.75360 \pm 0.00004$, and from the same numerical data we can compute that $\Pr(A|B \cap C) = p_x / \Pr(B|C) = 0.4511 \pm 0.0002$, compared with the exact value for $\Pr(A)$ of 0.5.

Yet if we adopt this approximation, we can solve the above equations in closed form for the singles fraction σ_4: first observe again that the right side of Eq. (4.19) is $1 - (1 - p_w)(1 - p_x)$. This reduces Eq. (4.16c) to

$$\sigma_4 = \sigma_3(1 - p_w)(1 - p_x). \tag{4.24}$$

In parallel, we subtract Eq. (4.17) from Eq. (4.16c) to obtain

$$2\sigma_3 = \sigma_1 + \sigma_4 \tag{4.25}$$

and then substitute this into Eq. (4.24) to obtain

$$2\sigma_4 = (\sigma_1 + \sigma_4)(1 - p_w)(1 - p_x). \tag{4.26}$$

Third, by substituting Eq. (4.15a) into Eq. (4.16a) and then substituting the result into our approximation Eq. (4.23), we find that

$$p_x \approx f(\sigma_1 - \sigma_3(p_w(1 - p_x) + p_w p_x/2)). \tag{4.27}$$

By rearrangement, Eq. (4.27) is

$$p_x \approx \frac{p_w(1 - f\sigma_3)}{1 - p_w f\sigma_3/2}. \tag{4.28}$$

If we then substitute Eq. (4.25) into Eq. (4.28), and substitute the result into Eq. (4.26), we arrive at

$$2\sigma_4 \approx (\sigma_1 + \sigma_4)(1 - p_w)\left(1 - \frac{p_w(1 - f(\sigma_1 + \sigma_4)/2)}{1 - p_w f(\sigma_1 + \sigma_4)/4}\right). \tag{4.29}$$

Simplifying this equation gives a quadratic in σ_4: $a\sigma_4^2 + b\sigma_4 + c \approx 0$, with coefficients

$$a = p_w f(3 - p_w)/4 \tag{4.30a}$$

$$b = -1 - 2p_w + 2p_w^2 - p_w^3/2 \tag{4.30b}$$

$$c = (1 - p_w)(1 - p_w + p_w^2/4) \tag{4.30c}$$

Our estimate of the singles fraction σ_4 is then given by the root

$$\sigma_4 \approx \frac{-b - \sqrt{b^2 - 4ac}}{2a}. \tag{4.31}$$

since only this root lies on in the unit interval. For $\sigma_1 = 1$ and $f = 1/2$, the estimate of σ_4 is $5 - 2\sqrt{29/5}$ or about 0.18336.

While the accuracy of this estimate is modest, the derivation is significantly simplier than comparable calculations of dimer filling on the two-dimensional lattice. In particular, the confinement of the approximation to the single question of how to approximate p_x leaves open the possibility of improving the accuracy of the estimate while keeping the calculation manageable.

New Upper Bound for Worse Case Matching on the Grid

As one looks, one encounters many interesting and (to our knowledge) unsolved problems regarding pair formation on graphs. One of the simplest regards the maximum possible value of the singles fraction for dimer filling on the two-dimensional grid. It is clear that there are configurations in which the singles fraction is zero—e.g. forming pairs end-to-end in each row. And it is also clear that the singles fraction can be as large as 1/3—see Fig. 4.4a for an example of such a scheme. However it is unclear whether 1/3 is the true maximum.

In this section we make progress on this question by giving a simple proof that the maximum singles fraction can be no more than 5/12, and so must lie on the interval $[4/12, 5/12]$. To our knowledge, this new bound beats all previous bounds in literature, and it is conceivable that our method could be expanded with computer automation to achieve increasingly better bounds.

To demonstrate this new upper bound, consider the cross-shaped tile shown in Fig. 4.4b. We can see by inspection that, up to rotation, the four nodes at the center of this tile may be either single (s) or matched (m) in three configurations:

$$\begin{matrix} m & m \\ m & m \end{matrix} \quad (4.32a) \qquad \begin{matrix} s & m \\ m & m \end{matrix} \quad (4.32b) \qquad \begin{matrix} s & m \\ m & s \end{matrix} \quad (4.32c)$$

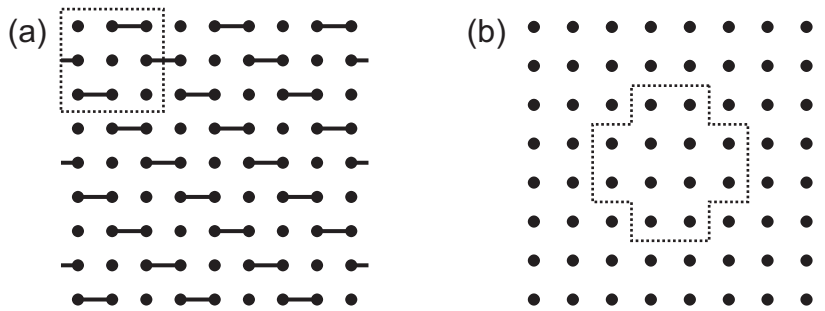

Figure 4.4: (a) A dimer filling that achieves a singles fraction of 1/3. The 3×3 box shown tessellates the plane. (b) A cross-shaped tile used to demonstrate an upper bound of 5/12 for the maximum singles fraction on the grid graph.

However now consider the four pairs of edge nodes of the cross-shaped tile. Any one pair can contain at most one single node—otherwise the two single nodes could form a match with each other, so the first and second configurations, Eq. (4.32a) and Eq. (4.32b), cannot exceed a singles fraction of 5/12. For the third configuration, Eq. (4.32c), each of the two central matched nodes must have a match among the edge nodes, and the two central single nodes must have all matched neighbors, so this tile has a maximum singles fraction of 1/3.

Now index the set of crosses in the plane with k (e.g. such that they spiral out from the origin) and rewrite the singles fraction of the plane (S) as the mean of the singles fractions of these crosses (S_k):

$$S = \lim_{n\to\infty} \frac{1}{n} \sum_{k=1}^{n} S_k. \tag{4.33}$$

Since none of the S_k are greater than 5/12, neither can be the mean. Hence, the maximum of the singles fraction for a two-dimensional grid topology lies on $[4/12, 5/12]$.

Although the question appears to remain open, we conjecture that the true maximum singles fraction is 1/3. Hopefully future studies will provide the answer.

APPENDIX A

PROOFS REGARDING $\dot{X} = X^2$

In Section 2.3, we assert that a variant of the dynamics proposed by Kułakowski et al. [45] generically balances an isolated triangle. We explain what we mean here.

Theorem 1. The system $\dot{x}_{12} = x_{13}x_{23}$, $\dot{x}_{13} = x_{12}x_{23}$, $\dot{x}_{23} = x_{12}x_{13}$ achieves balance when the initial values $x_{12}(0)$, $x_{13}(0)$ and $x_{23}(0)$ are all unequal.

Proof. Multiplying each $\dot{x}_{ij}$ by x_{ij} yields $x_{12}\dot{x}_{12} = x_{13}\dot{x}_{13} = x_{23}\dot{x}_{23}$. Integrating these equalities gives the constraints $x_{12}^2 - x_{13}^2 = C_1$ and $x_{12}^2 - x_{23}^2 = C_2$ which partition the three-dimensional space of (x_{12}, x_{13}, x_{23}) into trajectories (with the direction of flow given by the original dynamical system). Examination of this flow reveals that each initial condition $(x_{12}(0), x_{13}(0), x_{23}(0))$ with distinct coordinates flows into one of the four octants on which Heider balance holds, that is where $x_{12}x_{13}x_{23} > 0$. Furthermore, these octants each act as separate trapping regions: once a trajectory enters, it cannot leave. Hence, the theorem follows. □

The next theorem regards the main system of Section 2.3 with a rescaling of time: $\dot{X} = n^{-1}X^2$, where X is a real symmetric $n \times n$ matrix. Recall that $x_{ij}(t)$ denotes the (i,j)th element of the solution matrix $X(t)$ subject to the initial condition $X(0)$. In the following, we will abbreviate $X(0)$ as A and $x_{ij}(0)$ as a_{ij}. Suppose that the a_{ij}, $i \leq j$, are drawn independently from distributions F_{ij} with zero mass outside $[-K, K]$, and the off-diagonal distributions F_{ij} have common expectation μ and variance σ^2.

Theorem 2. $\lim_{n\to\infty} x_{ij}(t) = a_{ij} - \mu + \mu/(1-\mu t)$ with probability 1 for $t \in [0, 1/K)$.

Proof. Regard each step of the limit $n \to \infty$ as a selection and concatenation of elements $\{a_{in}\}_{1\le i\le n-1}, \{a_{nj}\}_{1\le j\le n-1}, a_{nn}$ to the elements $\{a_{ij}\}_{1\le i,j\le n-1}$ selected in preceding steps. Now consider the partial sum of the Taylor series expansion of $x_{ij}(t)$:

$$x_{ijnN}(t) = \sum_{k=0}^{N} \alpha_{kn} t^k \quad \text{where} \quad \alpha_{kn} = \frac{1}{k!} \frac{d^k x_{ij}}{dt^k}\bigg|_{t=0}. \tag{A.1}$$

The first step of the proof of Theorem 2 consists of proving that $\lim_{N\to\infty} \lim_{n\to\infty} x_{ijnN}(t)$ converges to $a_{ij} - \mu + \mu/(1-\mu t)$ with probability 1 on $[0, 1/|\mu|)$ (see Lemma 1). The second step of the proof consists of proving that $\lim_{N\to\infty} \lim_{n\to\infty} x_{ijnN}(t) = \lim_{n\to\infty} x_{ij}(t)$ with probability 1 on $[0, 1/K)$ (see Lemma 2). Since we can write $\lim_{n\to\infty} x_{ij}(t)$ as $\lim_{n\to\infty} \lim_{N\to\infty} x_{ijnN}(t)$, this amounts to showing that the two limits can be exchanged on $[0, 1/K)$. The above theorem then follows trivially by a union bound. □

Lemma 1. Under the assumptions of Theorem 2, $\lim_{N\to\infty} \lim_{n\to\infty} x_{ijnN} = a_{ij} - \mu + \mu/(1-\mu t)$ with probability 1 for $t \in [0, 1/|\mu|)$.

Proof. For the sake of generality, we present a proof with more mild assumptions than those of Theorem 2: we only require that the moments of the F_{ij} distributions be finite (and off-diagonal distributions to have mean μ), not that the a_{ij} values be bounded by K with probability 1.

Define $\alpha_{k\infty} = \lim_{n\to\infty} \alpha_{kn}$ (merely shorthand—we do not assume the limit

exists). By a union bound, we have

$$\Pr\Big(\bigcap_{k=1}^{\infty}[\alpha_{k\infty} = \mu^{k+1}]\Big) \geq 1 - \sum_{k=1}^{\infty}[1 - \Pr(\alpha_{k\infty} = \mu^{k+1})]. \tag{A.2}$$

So if we can show that $\Pr(\alpha_{k\infty} = \mu^{k+1}) = 1$ for all $k \geq 1$, then $\Pr(\bigcap_{k=1}^{\infty}[\alpha_{k\infty} = \mu^{k+1}]) = 1$. In this case, $\lim_{N\to\infty}\lim_{n\to\infty} x_{ijnN}$ has the convergent Taylor series $a_{ij} + \sum_{k=1}^{\infty}\mu^{k+1}t^k$ on $[0, 1/|\mu|)$ with probability 1, which proves the lemma.

So our task reduces to showing that $\Pr(\alpha_{k\infty} = \mu^{k+1}) = 1$ for each $k \geq 1$. In order to do this, we need to compute the leading behavior of α_{kn} in n. To calculate the k time derivatives of x_{ij} in the formula for α_{kn} (see Eq. (A.1)), we alternate between applying the chain rule of differential calculus and substituting in the right-hand side of $\dot{x}_{ij} = n^{-1}\sum_k x_{ik}x_{kj}$ (our system $\dot{X} = n^{-1}X^2$ written in element-wise fashion). This gives

$$\alpha_{kn} = n^{-k}\sum_{m_1=1}^{n}\sum_{m_2=1}^{n}\cdots\sum_{m_k=1}^{n} a_{im_1}a_{m_1m_2}\cdots a_{m_kj} \tag{A.3}$$

where the factor n^{-k} comes from the k factors of n^{-1} introduced by the k derivatives, and the factor $1/k!$ in the formula for α_{kn} cancels with a factor $k!$ that arises from repeated applications of the chain rule. In Eq. (A.3), the dominant term is a sum of the edge value products of all simple length-$(k+1)$ paths between i and j. This sum contains $(n-2)!/(n-2-k)!$ terms. All other paths include fewer immediate nodes and thus have at least a factor of n fewer terms in their sums.

Our goal then for the remainder of the proof is to show that the first term of Eq. (A.3) is the only term that remains after taking n to infinity, and that it converges to μ^{k+1} with probability 1. To simplify notation, let ℓ denote the product of the edge values a_{ij} along a particular path of length $k+1$ (not necessarily simple) from i to j, and let L denote the set of all such products on paths with the same configuration, or pattern of connectivity. Denote the set of all L by $\{L\}$, and let

S denote the one L in $\{L\}$ consisting of simple paths of length $k+1$ from i to j.

Now observe that $\cap_L[\lim_{n\to\infty} n^{-k}\sum_{\ell\in L}\ell = 0] \cap [n^{-k}\sum_{\ell\in S}\ell = \mu^{k+1}] \subset [\alpha_{k\infty} = \mu^{k+1}]$. So by another union bound,

$$\Pr(\alpha_{k\infty} = \mu^{k+1}) \geq 1 - \Pr\left(\lim_{n\to\infty} n^{-k}\sum_{\ell\in S}\ell \neq \mu^{k+1}\right) - \sum_{\{L\}\setminus S}\Pr\left(\lim_{n\to\infty} n^{-k}\sum_{\ell\in L}\ell \neq 0\right). \quad \text{(A.4)}$$

Hence, we are done if we can show that (i) $\Pr(\lim_{n\to\infty} n^{-k}\sum_{\ell\in S}\ell = \mu^{k+1}) = 1$ for S and (ii) $\Pr(\lim_{n\to\infty} n^{-k}\sum_{\ell\in L}\ell = 0) = 1$ for all other L. Although $\sum_{\ell\in L}\ell$ is in general a sum of correlated random variables, it is possible to adapt a standard proof of the strong law of large numbers for uncorrelated random variables to prove both items. We do this next.

Let's prove (ii) first. For brevity, let $S_n = \sum_{\ell\in L}\ell$ and choose v to denote the number of nodes in the path configuration of L. For any positive ϵ and $r = 1, 2, \ldots,$ Markov's inequality gives $\Pr(|S_n| \geq (n\epsilon)^k) \leq E(|S_n|^r)/(n\epsilon)^{kr}$. So if we can find an r such that $E(|S_n|^r)/(n\epsilon)^{kr} \leq C/n^2$ for some constant C (dependent on ϵ), then $\sum_n \Pr(|S_n| \geq (n\epsilon)^k)$ converges, and by the first Borel-Cantelli lemma, $\Pr(|n^{-k}\sum_{\ell\in L}\ell| \geq \epsilon \text{ i.o.}) = 0$ for all $\epsilon > 0$ (where i.o. stands for infinitely often). Careful reflection reveals that $\cup_\epsilon[|n^{-k}\sum_{\ell\in L}\ell| \geq \epsilon \text{ i.o.}]$ (for, say, all rational ϵ) is the complementary event of $[\lim_{n\to\infty} n^{-k}\sum_{\ell\in L}\ell = 0]$, and so we have arrived at the desired result (ii).

Hence, in order to actually show (ii), we need to find an r such that $E(|S_n|^r)$ $/(n\epsilon)^{kr} \leq C/n^2$. Consider $r = 2$: $E(S_n^2) = \sum E(\ell_x\ell_y)$, where each index of the sum ranges independently over L. There are $(n-2)!/(n-2-v)!$ paths ℓ in L, so there are fewer than n^{2v} terms in $\sum E(\ell_x\ell_y)$, and $E(S_n^2) \leq Dn^{2v}$ for some constant D. Since $v < k$ for all L other than S, we have $E(|S_n|^2)/(n\epsilon)^{2k} \leq Dn^{2v}/(n\epsilon)^{2k} \leq C/n^2$

where $C = D\epsilon^{-2k}$, and the proof of (ii) is complete.

Finally, to prove (i), start by replacing each factor a_{xy} in ℓ with $b_{xy} + \mu$, where $b_{xy} = a_{xy} - \mu$. Now expand the result and cancel μ^{k+1} from both sides of $n^{-k}S_n = \mu^{k+1}$ to obtain $n^{-k}S'_n = 0$, where S'_n is a sum over S of a polynomial Q with $2^{k+1} - 1$ terms, each of the form $\mu\mu\cdots\mu b_{uv}b_{wx}\cdots b_{yz}$ where at least one of the factors is a b_{xy} and the total number of factors in the term is $k+1$. Note that each place of Q corresponds to a particular set of b_{xy}'s from the original simple path, e.g. the 14th place of Q might have b_{xy}'s corresponding to the 1st, 4th, 5th, and 7th edges of the path, and μ's for the other edges. Now let m_q denote the number of nodes (excluding i and j) among the subscripts of the b_{xy}'s in a given term. The remaining $k - m_q$ nodes of the path not found in the term (supplanted by the μ's) can take any of $(n-2-m_q)!/(n-2-k)!$ permutations. Hence, there are no more than n^{k-m_q} identical copies of any one term in S'_n from the same place in Q.

Now consider one of the $(2^{k+1}-1)^4$ ways that terms in the $2^{k+1}-1$ places of Q can be multiplied together in S'^4_n. Note that this can produce no more than $n^{4k-\sum_{q=1}^4 m_q}$ identical copies of the same term. Second, since the b_{xy}'s each have expectation zero, every b_{xy} in the final term must appear to at least a power of two or the whole term has expectation zero. This implies that for each nonvanishing term, there must be some pattern of matching between the b_{xy}'s. The number of possible matchings is clearly a function of k and not n (it certainly is not more than the number of partitions of $4(k+1)$ edges), so consider one of these possible matchings. Now observe that if, as we stated above, we consider only one of the $(2^{k+1}-1)^4$ ways that terms in the $2^{k+1}-1$ places of Q can be multiplied together in S'^4_n, then no more than $n^{\sum_{q=1}^4 m_q/2}$ distinct nonvanishing terms can be constructed per matching for any such way of combining terms. This holds because each b_{xy}

needs at least one match, and so the number of free nodes cannot exceed half the total number of b_{xy}'s in the final term. Thus we have shown the highest order of n possible for $E(S_n'^4)$ is given by the maximum value of $n^{\sum_{q=1}^4 m_q/2} n^{4k-\sum_{q=1}^4 m_q}$. Since $m_q \geq 1$ for each $q = 1, \ldots, 4$, this can at most be n^{4k-2}, which by the above reasoning completes the proof of (i) and hence the full theorem. □

Lemma 2. Under the assumptions of Theorem 2, $\lim_{n\to\infty} \lim_{N\to\infty} x_{ijnN} = \lim_{N\to\infty} \lim_{n\to\infty} x_{ijnN}$ with probability 1 for $t \in [0, 1/K)$.

Proof. We need three ingredients for this proof. We will first describe the three ingredients and then show how they together prove Lemma 2. Throughout the following, all statements hold with probability 1 unless stated otherwise.

As we found in the course of the proof of Lemma 1, the limits $\lim_{n\to\infty} \alpha_{kn}$ exist for all k and are μ^{k+1} on $[0, 1/|\mu|)$, so $\lim_{n\to\infty} \sum_{k=0}^N \alpha_{kn} t^k$ exists under the same conditions, and we call it $x_{ij\infty N}(t)$. This gives us the first ingredient: (i) $\lim_{n\to\infty} x_{ijnN}(t) = x_{ij\infty N}(t)$ for $t \in [0, 1/|\mu|)$ and any N. Additionally, from Lemma 1 we know that $\lim_{N\to\infty} x_{ij\infty N}(t)$ exists and is $a_{ij} - \mu + \mu/(1 - \mu t)$ on $[0, 1/|\mu|)$. We call this limit $x_{ij\infty\infty}(t)$, and write the second ingredient as (ii) $\lim_{N\to\infty} x_{ij\infty N}(t) = x_{ij\infty\infty}(t)$ for $t \in [0, 1/|\mu|)$.

Finally, as we saw in the proof of Lemma 1, $\alpha_{kn} = n^{-k} \sum a_{im_1} a_{m_1 m_2} \cdots a_{m_k j}$ (by definition, not just with probability 1), where the k indices m_x each range independently from 1 to n. Since each $|a_{ij}| < K$, we must have that $|\alpha_{kn}| \leq K^{k+1}$, which implies $|x_{ijn\infty}(t) - x_{ijnN}(t)| \leq K(Kt)^{N+1}/(1 - Kt)$. So if $|Kt| < 1$, then for any $\epsilon > 0$, there is a sufficiently large N_1 independent of n such that $|x_{ijn\infty}(t) - x_{ijnN}(t)| \leq \epsilon$ for all $N \geq N_1$. This constitutes our third ingredient,

that $x_{ijnN}(t)$ converges uniformly to $x_{ijn\infty}(t)$: (iii) for every $\epsilon > 0$, there exists an N_1 such that for all $N \geq N_1$ and all n, $|x_{ijn\infty}(t) - x_{ijnN}(t)| < \epsilon$.

To complete the proof of Lemma 2, we need to show that $\lim_{n\to\infty} x_{ijn\infty}(t)$ exists and is just $x_{ij\infty\infty}(t)$ on $[0, 1/K)$. Start by picking an $\epsilon > 0$. Then by (iii), there exists an N_1 such that if $N > N_1$ then $|x_{ijn\infty}(t) - x_{ijnN}(t)| < \epsilon$ for all n. Similarly, (ii) implies that there exists an N_2 such that if $N \geq N_2$, then $|x_{ij\infty\infty}(t) - x_{ij\infty N}(t)| < \epsilon$. Finally, let $N_3 = \max\{N_1, N_2\}$. Then by (i), we may choose an n_1 such that if $n \geq n_1$, then $|x_{ij\infty N_3}(t) - x_{ijnN_3}(t)| < \epsilon$. Now define the following events:

$$\begin{aligned} E_1 &= [|x_{ij\infty\infty}(t) - x_{ij\infty N_3}(t)| < \epsilon], \\ E_2 &= [|x_{ij\infty N_3}(t) - x_{ijnN_3}(t)| < \epsilon], \\ E_3 &= [|x_{ijnN_3}(t) - x_{ijn\infty}(t)| < \epsilon], \\ E_4 &= [|x_{ij\infty\infty}(t) - x_{ijn\infty}(t)| < 3\epsilon]. \end{aligned} \tag{A.5}$$

Observe that, in similar form to Eq. (A.4), $(E_1 \cap E_2 \cap E_3) \subset E_4$, so $\Pr(E_4) \geq \Pr(E_1 \cap E_2 \cap E_3) = 1 - \Pr(E_1' \cup E_2' \cup E_3') \geq 1 - \Pr(E_1') - \Pr(E_2') - \Pr(E_3') = 1$ for all $n \geq n_1$. Thus, $|x_{ij\infty\infty}(t) - x_{ijn\infty}(t)| < 3\epsilon$ for all $n \geq n_1$ and $t \in [0, 1/K)$. $\square$

APPENDIX B

INTERDEPENDENCE OF CROSS RATIOS

We show that the $N!/(N-4)!$ cross ratios of the oscillator phases are functionally dependent on the $N-3$ cross ratios $\{\lambda_{1234}, \lambda_{2345}, \ldots, \lambda_{(N-3)(N-2)(N-1)N}\}$. To do so, we use the fact that the 4! cross ratios corresponding to the 4! permutations of z_i, z_j, z_k, z_l can be written as elementary functions of λ_{ijkl}:

$$\begin{aligned}
\lambda_{ijkl} &= \lambda_{jilk} = \lambda_{klij} = \lambda_{lkji}, \\
\lambda_{ijlk} &= 1/\lambda_{ijkl}, \\
\lambda_{iklj} &= 1/(1-\lambda_{ijkl}), \\
\lambda_{ikjl} &= 1-\lambda_{ijkl}, \\
\lambda_{ilkj} &= \lambda_{ijkl}/(1-\lambda_{ijkl}), \\
\lambda_{iljk} &= (\lambda_{ijkl}-1)/\lambda_{ijkl}.
\end{aligned} \tag{B.1}$$

Additionally, we can obtain new cross ratios from existing ones by multiplication:

$$\lambda_{ijkl}\lambda_{jmkl} = \lambda_{imkl}. \tag{B.2}$$

Using these facts, we need to show that we can write λ_{PQRS} for any distinct $P, Q, R, S \in \{1, 2, \ldots, N\}$ in terms of elements from $\{\lambda_{1234}, \lambda_{2345}, \ldots, \lambda_{(N-3)(N-2)(N-1)N}\}$. First, note that we can rewrite (B.2) as a function F_j which takes two cross ratios λ_{ijkl} and λ_{jklm} (with indices in order), permutes the indices as necessary to eliminate z_j, executes the multiplication and returns the product with its indices in order:

$$F_j(\lambda_{ijkl}, \lambda_{jklm}) = \lambda_{iklm} \tag{B.3}$$

Observe, however, that F_j is just short-hand for a composition of elementary functions from (B.1):

$$F_j(\lambda_{ijkl}, \lambda_{jklm}) = \frac{1}{1-\lambda_{ijkl}(\lambda_{jklm}-1)/\lambda_{jklm}}. \tag{B.4}$$

We can also define the analogous functions G_k and H_l:

$$\begin{aligned} G_k(\lambda_{ijkl}, \lambda_{jklm}) &= \lambda_{ijlm}, \\ H_l(\lambda_{ijkl}, \lambda_{jklm}) &= \lambda_{ijkm}. \end{aligned} \tag{B.5}$$

These functions have their own compositions like that of F_j in (B.4).

Let λ_{pqrs} correspond to the permutation of λ_{PQRS} in which the indices are in order. We can write λ_{PQRS} in terms of λ_{pqrs} using one of the functions in (B.1). Thus, the problem reduces to showing that we can obtain λ_{pqrs} from the elements of $\{\lambda_{1234}, \lambda_{2345}, \ldots, \lambda_{(N-3)(N-2)(N-1)N}\}$ by elimination of the indices between p, q, r, s using the operations F_j, G_k, H_l.

If there are one or more indices between i and j, we say there is a *gap* between i and j. Now observe that we can obtain the first gap between p and q using only λ_{ijkl} with no gaps; we grow this gap iteratively one index at a time by the operation: $F_k(\lambda_{pk(k+1)(k+2)}, \lambda_{k(k+1)(k+2)(k+3)}) = \lambda_{p(k+1)(k+2)(k+3)}$. We can then grow the second gap between q and r to its full size using only λ_{ijkl} that have no gaps between j and k or k and l (each of which could be made from λ_{ijkl} with no gaps) using the operation: $G_k(\lambda_{pqk(k+1)}, \lambda_{qk(k+1)(k+2)}) = \lambda_{pq(k+1)(k+2)}$. Finally, we can create the third gap between r and s using only λ_{ijkl} with no gaps between k and l (which could be made from λ_{ijkl} with fewer gaps) using the operation: $H_k(\lambda_{pqrk}, \lambda_{qrk(k+1)}) = \lambda_{pqr(k+1)}$.

Since each λ_{ijkl} (with $i < j < k < l$) can be built up from λ_{ijkl} with fewer gaps, the proof is complete: all $N!/(N-4)!$ cross ratios are dependent on the elements of $\{\lambda_{1234}, \lambda_{2345}, \ldots, \lambda_{(N-3)(N-2)(N-1)N}\}$.

BIBLIOGRAPHY

[1] M. J. Ablowitz and H. Segur. *Solitons and the Inverse Scattering Transform.* SIAM Studies in Applied Mathematics, Philadelphia, 1981.

[2] H. Abou-Kandil, G. Freiling, V. Ionescu, and G. Jank. *Matrix Riccati Equations in Control and Systems Theory.* Birkhäuser, Basel, 2003. See page 21.

[3] J. A. Acebrón, L. L. Bonilla, C. J. P. Vicente, F. Ritort, and R. Spigler. The Kuramoto model: a simple paradigm for synchronization phenomena. *Journal of Theoretical Biology*, 77:137, 2005.

[4] R. Albert and A.-L. Barabási. Statistical mechanics of complex networks. *Reviews of Modern Physics*, 74:47, 2002.

[5] T. Antal, P. L. Krapivsky, and S. Redner. Dynamics of social balance on networks. *Physical Review E*, 72:036121, 2005.

[6] L. Arnold. On Wigner's semicircle law for the eigenvalues of random matrices. *Probability Theory and Related Fields*, 19:191, 1971.

[7] J. Aronson, M. Dyer, A. Frieze, and S. Suen. Randomized greedy matching. ii. *Random Structures and Algorithms*, 6:55, 1995.

[8] J. Aronson, A. Frieze, and B. G. Pittel. Maximum matchings in sparse random graphs: Karp-Sipser re-visited. *Random Structures and Algorithms*, 12:111, 1998.

[9] R. Axelrod and D. S. Bennett. A landscape theory of aggregation. *British Journal of Political Science*, 23:211, 1993.

[10] B. Bollobás. *Random Graphs.* Cambridge University Press, Cambridge, UK, 2001.

[11] B. Bollobás and O. Riordan. *Percolation.* Cambridge University Press, Cambridge, UK, 2006. See pages 165-166.

[12] D. Cartwright and F. Harary. Structural balance: A generalization of Heider's theory. *The Psychological Review*, 63:277, 1956.

[13] C. Castellano, S. Fortunato, and V. Loreto. Statistical physics of social dynamics. *Reviews of Modern Physics*, 81:591, 2009.

[14] J. B. Conway. *Functions of One Complex Variable*. Springer, New York, 1973.

[15] J. A. Davis. Clustering and structural balance in graphs. *Human Relations*, 20:181, 1967.

[16] C. De Dominicis, M. Gabay, T. Garel, and H. Orland. White and weighted averages over solutions of TAP equations for the SK spin glass. *Journal de Physique (France)*, 41:922, 1980.

[17] P. Doreian and A. Mrvar. A partitioning approach to structural balance. *Social Networks*, 18:149, 1996.

[18] S. N. Dorogovtsev and J. F. F. Mendes. *Evolution of Networks*. Oxford University Press, 2003.

[19] M. R. D'Orsogna and T. Chou. Interparticle gap distributions on one-dimensional lattices. *Journal of Physics A: Mathematical and General*, 38:531, 2005.

[20] M. R. D'Orsogna, T. Chou, and T. Antal. Exact steady-state velocity of ratchets driven by random sequential adsorption. *Journal of Physics A: Mathematical and Theoretical*, 40:5575, 2007.

[21] S. N. Durlauf and H. P. Young. *Social Dynamics*. Economic Learning and Social Evolution. The MIT Press, Cambridge, MA, 2001.

[22] M. Dyer and A. Frieze. Randomized greedy matching. *Random Structures and Algorithms*, 2:29, 1991.

[23] M. Dyer, A. Frieze, and B. Pittel. The average performance of the greedy matching algorithm. *The Annals of Applied Probability*, 3:526, 1993.

[24] D. J. D. Earn, S. A. Levin, and P. Rohani. Coherence and conservation. *Science*, 290:1360, 2000.

[25] D. Easley and J. Kleinberg. *Networks, Crowds, and Markets: Reasoning About a Highly Connected World*. Cambridge University Press, New York, 2010. See pages 119-152.

[26] J. W. Evans. Random and cooperative sequential adsorption. *Reviews of Modern Physics*, 65:1281, 1993.

[27] E. Fermi, J. Pasta, and S. Ulam. Studies of nonlinear problems: I. *Los Alamos Report LA-1940*, 1955.

[28] T. Filk. Random graph gauge theories as toy models for non-perturbative string theories. *Classical and Quantum Gravity*, 17:4841, 2000.

[29] K. H. Fischer and J. A. Hertz. *Spin Glasses*. Cambridge University Press, Cambridge, UK, 1991.

[30] P. J. Flory. Intramolecular reaction between neighboring substituents of vinyl polymers. *Journal of the American Chemical Society*, 61:1518, 1939.

[31] S. Franz, M. Mzard, F. Ricci-Tersenghi, M. Weigt, and R. Zecchina. A ferromagnet with a glass transition. *Europhysics Letters*, 55:465, 2001.

[32] Z. Füredi and J. Komlós. The eigenvalues of random symmetric matrices. *Combinatorica*, 1:233, 1981.

[33] Z. Galil. Efficient algorithms for finding maximum matching in graphs. *Computing Surveys*, 18:23, 1986.

[34] C. S. Gardner, J. M. Greene, M. D. Kruskal, and R. M. Miura. Method for solving the Korteweg-de Vries equation. *Physical Review Letters*, 19:1095, 1967.

[35] C. J. Goebel. Comment on constants of motion for superconductor arrays. *Physica D*, 80:18, 1995.

[36] D. Golomb, D. Hansel, B. Shraiman, and H. Somopolinsky. Clustering in globally coupled phase oscillators. *Physical Review A*, 45:3516, 1992.

[37] J. J. González, P. C. Hemmer, and J. S. Høye. Cooperative effects in random sequential polymer reactions. *Chemical Physics*, 3:228, 1974.

[38] F. Heider. Attitudes and cognitive organization. *The Journal of Psychology*, 21:107, 1946.

[39] F. Heider. *The Psychology of Interpersonal Relations*. John Wiley and Sons, New York, 1958.

[40] P. C. Hemmer. The random parking problem. *Journal of Statistical Physics*, 57:865, 1989.

[41] M. Hénon. Numerical exploration of Hamiltonian systems. In *Chaotic Behavior of Deterministic Systems (Les Houches, 1981)*, pages 53–170. North-Holland, Amsterdam, 1983.

[42] H. Hong and S. H. Strogatz. Kuramoto model of coupled oscillators with positive and negative coupling parameters: An example of conformist and contrarian oscillators. *Physical Review Letters*, 106:054102, 2011.

[43] E. A. Jackson. *Perspectives of Nonlinear Dynamics, Volume 2*. Cambridge University Press, Cambridge UK, 1990.

[44] T. M. Antonsen Jr., R. T. Faghih, M. Girvan, E. Ott, and J. Platig. External periodic driving of large systems of globally coupled phase oscillators. *Chaos*, 18:037112, 2008.

[45] K. Kułakowski, P. Gawroński, and P. Gronek. The Heider balance - a continuous approach. *International Journal of Modern Physics C*, 16:707, 2005.

[46] Y. Kuramoto. *Chemical Oscillations, Waves, and Turbulence*. Springer, Berlin, 1984.

[47] P. Lax. Integrals of nonlinear equations of evolution and solitary waves. *Communications on Pure and Applied Mathematics*, 21:467, 1968.

[48] S. A. Marvel, R. E. Mirollo, and S. H. Strogatz. Identical phase oscillators with global sinusoidal coupling evolve by Möbius group action. *Chaos*, 19:043104, 2009.

[49] S. A. Marvel and S. H. Strogatz. Invariant submanifold for series arrays of Josephson junctions. *Chaos*, 19:013132, 2009.

[50] S. A. Marvel, S. H. Strogatz, and J. M. Kleinberg. Energy landscape of social balance. *Physical Review Letters*, 103:198701, 2009.

[51] R. M. Miura. The Korteweg-de Vries equation: A survey of results. *SIAM Review*, 18:412, 1976.

[52] M. Moore. An international application of Heider's balance theory. *European Journal of Social Psychology*, 8:401, 1978.

[53] M. Moore. Structural balance and international relations. *European Journal of Social Psychology*, 9:323, 1979.

[54] K. Mulmuley, U. V. Vazirani, and V. V. Vazirani. Matching is as easy as matrix inversion. *Combinatorica*, 7:105, 1987.

[55] M. E. J. Newman. The structure and function of complex networks. *SIAM Review*, 45:167, 2003.

[56] M. E. J. Newman. *Networks: An Introduction*. Oxford University Press, New York, 2010.

[57] S. Nichols and K. Wiesenfeld. Ubiquitous neutral stability of splay-phase states. *Physical Review A*, 45:8430, 1992.

[58] W. H. Olson. A Markov chain model for the kinetics of reactant isolation. *Journal of Applied Probability*, 15:835, 1978.

[59] E. Ott and T. M. Antonsen. Low dimensional behavior of large systems of globally coupled oscillators. *Chaos*, 18:037113, 2008.

[60] E. Ott and T. M. Antonsen. Long time evolution of phase oscillator systems. *Chaos*, 19:023117, 2009.

[61] E. S. Page. The distribution of vacancies on a line. *Journal of the Royal Statistical Society. Series B (Methodological)*, 21:364, 1959.

[62] R. E. A. C. Paley. On orthogonal matrices. *Journal of Mathematical Physics*, 12:311, 1933.

[63] M. D. Penrose and J. E. Yukich. Limit theory for random sequential packing and deposition. *The Annals of Applied Probability*, 12:272, 2002.

[64] T. F. Pettigrew. Intergroup contact theory. *Annual Review of Psychology*, 49:65, 1998.

[65] T. F. Pettigrew and L. R. Tropp. A meta-analytic test of intergroup contact theory. *Journal of Personality and Social Psychology*, 90:751, 2006.

[66] A. Pikovsky and M. Rosenblum. Partially integrable dynamics of hierarchical populations of coupled oscillators. *Physical Review Letters*, 101:264103, 2008.

[67] A. Rényi. On a one-dimensional problem concerning random space-filling. *Publications of the Mathematical Institute of the Hungarian Academy of Sciences*, 3:109, 1958.

[68] J. J. Seidel. A survey of two-graphs. In *Colloquio Internazionale sulle Teorie Combinatorie (Rome, 1973)*, number 17 in Atti dei Convegni Lincei, pages 481–511. Accad. Naz. Lincei, Rome, 1976.

[69] E. M. Stein and R. Shakarchi. *Complex Analysis*. Princeton University Press, Princeton, 2003.

[70] S. H. Strogatz. From Kuramoto to Crawford: exploring the onset of synchronization in populations of coupled oscillators. *Physica D*, 143:1, 2000.

[71] S. H. Strogatz. Exploring complex networks. *Nature*, 410:268, 2001.

[72] S. H. Strogatz and R. E. Mirollo. Stability of incoherence in a population of coupled oscillators. *Journal of Statistical Physics*, 63:613, 1991.

[73] S. H. Strogatz and R. E. Mirollo. Splay states in globally coupled Josephson arrays: analytical prediction of Floquet multipliers. *Physical Review E*, 47:220, 1993.

[74] J. W. Swift, S. H. Strogatz, and K. Wiesenfeld. Averaging of globally coupled oscillators. *Physica D*, 55:239, 1992.

[75] T. Tao and V. Vu. Smooth analysis of the condition number and the least singular value. *Mathematics of Computation*, 79:2333, 2010.

[76] D. E. Taylor. *Some topics in the theory of finite groups*. PhD thesis, Univ. Oxford, 1971.

[77] H. F. Taylor. *Balance in Small Groups*. Van Nostrand Reinhold, New York, 1970.

[78] D. Topaj and A. Pikovsky. Reversibility vs. synchronization in oscillator lattices. *Physica D*, 170:118, 2002.

[79] K. Y. Tsang, R. E. Mirollo, S. H. Strogatz, and K. Wiesenfeld. Dynamics of a globally coupled oscillator array. *Physica D*, 48:102, 1991.

[80] K. Y. Tsang and I. B. Schwartz. Interhyperhedral diffusion in Josephson-junction arrays. *Physical Review Letters*, 68:2265, 1992.

[81] V. Vu. Spectral norm of random matrices. *Combinatorica*, 27:721, 2007.

[82] S. Wasserman and K. Faust. *Social Network Analysis: Methods and Applications*. Structural Analysis in the Social Sciences. Cambridge University Press, New York, 1994. See pages 220-248.

[83] S. Watanabe and S. H. Strogatz. Integrability of a globally coupled oscillator array. *Physical Review Letters*, 70:2391, 1993.

[84] S. Watanabe and S. H. Strogatz. Constants of motion for superconducting Josephson arrays. *Physica D*, 74:194, 1994.

[85] F. Wegner. Duality in generalized Ising models and phase transitions without local order parameters. *Journal of Mathematical Physics*, 12:2259, 1971.

[86] T. P. Weissert. *The Genesis of Simulation in Dynamics: Pursuing the Fermi-Pasta-Ulam Problem*. Springer, New York, 1997.

[87] N. J. Zabusky. Fermi-Pasta-Ulam, solitons, and the fabric of nonlinear and computational science: History, synergetics, and visiometrics. *Chaos*, 15:015102, 2005.

[88] N. J. Zabusky and M. D. Kruskal. Interaction of "solitons" in a collisionless plasma and the recurrence of initial states. *Physical Review Letters*, 15:240, 1965.

[89] W. W. Zachary. An information flow model for conflict and fission in small groups. *Journal of Anthropological Research*, 33:452, 1977.

[90] V. E. Zakharov and L. D. Faddeev. Korteweg-de Vries equation: A completely integrable Hamiltonian system. *Functional Analysis and Its Applications*, 5:280, 1971.